5-2007

Design and Synthesis of Novel Sultams: A Family of Non-nucleoside Reverse Transcriptase Inhibitors and Modeling Studies of a Rhodium Catalyst

Riyam Kafri
University of Tennessee - Knoxville

To the Graduate Council:

I am submitting herewith a dissertation written by Riyam Kafri entitled "Design and Synthesis of Novel Sultams: A Family of Non-nucleoside Reverse Transcriptase Inhibitors and Modeling Studies of a Rhodium Catalyst." I have examined the final electronic copy of this dissertation for form and content and recommend that it be accepted in partial fulfillment of the requirements for the degree of Doctor of Philosophy, with a major in Chemistry.

David C. Baker, Major Professor

We have read this dissertation and recommend its acceptance:

John F. C. Turner, Michael Best, David Brian

Accepted for the Council:

Carolyn R. Hodges

Vice Provost and Dean of the Graduate School

(Original signatures are on file with official student records.)

To the Graduate Council:

I am submitting herewith a dissertation written by Riyam Kafri entitled “Design and Synthesis of Novel Sultams: A Family of Non-nucleoside Reverse Transcriptase Inhibitors. And Modeling Studies of a Rhodium Catalyst.” I have examined the final paper/electronic copy of this dissertation for form and content and recommend that it be accepted in partial fulfillment of the requirements for the degree of Doctor of Philosophy, with a major in Organic Chemistry.

David C. Baker
Major Professor

We have read this dissertation and recommend its acceptance:

Dr. John F. C. Turner

Dr. Michael Best

Dr. David Brian

Accepted for the Council:

Linda Painter
Interim Dean of Graduate Studies

Design and Synthesis of Novel Sultams, A Family of Non-nucleoside Reverse Transcriptase Inhibitors

And

Modeling Studies of a Rhodium Catalyst

A Dissertation Presented for the Doctor of Philosophy Degree

The University of Tennessee

Riyam Kafri

May 2007

Dedication

To my parents who have been there since my first steps.

To my father, the first scientist in my life, and to my mother a true inspiration to me and all women, and the perfect example of motherhood, unconditional love and sacrifice. Both of you have endured my absence for ten years, and this work would have not been done without you both.

And to my brother and sister you are my best friends, my source of humor and my rock. Thank you for keeping things in prospective. To all of you, my dearest family, I dedicate this work.

To my dearest Aunt Pat Stover whose friendship and support cannot be put to words. Thank you for the long phone conversations, the many shopping sprees, and most importantly the laughter. Thank you for giving me a home away from home.

And

In loving memory of my Uncle Connie Stover, the inventor in my life.

To past, present and future Arab women in Science

Acknowledgements

This work would have never been complete without the guidance and teaching of Dr. David C. Baker, my major professor. I am so thankful that he took the time to answer a college senior's e-mail. The impression that he left on me is eternal. I am thankful for the many things he have taught me in the lab, and I am always amazed at his vast knowledge and wide experience in chemistry. It felt as if there was never a question he could not answer. Dr. Baker, I know I was not the easiest student to mold into a scientist. Thank you for your patience as I grew up and matured. Thank you for the never ending faith in my abilities to do this. I enjoyed our many late night conversations about chemistry, politics, religion and the occasional jokes. I am deeply touched by your humility, and should I ever become half the chemist that you are, I will consider myself very lucky. You are the perfect example of a scientist. You are fair, concise and able to cut to the heart of the matter. I have said this often, and I will say it again here. Knowing all I know today, I would still choose UT for graduate school and I would choose you for my PhD advisor. Many times you were more than an advisor, much more like a father. I will miss you very much.

I would like to also mention my committee members, Dr. Michael Best, Dr. David Brian and Dr. John Turner. Dr. Best and Dr. Brian so kindly accepted my invitation to serve on my committee. And I enjoyed their presence, their questions, and the challenges they posed.

Dr. Turner, the passion you carry for chemistry is admirable. I am touched by the care you have shown me in my time here. You have always been

concerned, you always cared and you certainly wanted the best for me. It is very hard to imagine my career at the University of Tennessee without you. You have made many difficult situations bearable. Your vast knowledge of organic chemistry, literature, music, politics and religion will encourage me to never stop being a student. I am eternally grateful, and forever touched. Your friendship will always remain with me.

Dr. Charmaine Mamantov, thank you for taking me in as a young woman, and molding me into a good teacher. You are a wonderful woman in chemistry to look up to. I enjoyed our many long conversations. I will always look up to you, and I am deeply moved by your strength, compassion and intelligence.

I would like to now take a moment and thank the past and present members of the Baker group. From the past members, I would like to mention Dr. Sarah Headrick, Dr. Karen Welch, Dr. Sean Hamilton and Dr. Ambroise Akue for teaching me all the lab techniques, especially Dr. Karen Welch for helping me learn molecular modeling earlier in the project.

The current members of the Baker group, especially Medhanit Bahta, Julio Gutierrez and Samson Francis. Lunch hour will never be the same. The laughter, discussion and occasional arguments we shared make the best memories I have ever had. I am going to take a moment and mention each one of you personally. Julio, first of all thank you for the NMR help. The VT experiment would have never happened without you. But more importantly, your friendship is incredibly valuable. I love the sense of humor you have. You have constantly make me laugh. My memories of you will include “MMM’KKK,” “Tooo

mmucchh pprreesssuurree!!!" and many other catchy phrases. I will miss your story telling, because you definitely know how to make all of us laugh. Julio, when you are around it feels as if an older brother is around. And I thank you very much for listening to me in the moments of weakness I had, and thank you for your endless compassion. And thank you and Yolanda for opening your home to me, thank you for giving me a place to escape to. I wish you the best. Medhanit, it has been a pleasure to watch you transform from a young lady missing her homeland, to a strong, well spoken, and excellent synthetic organic chemist. I loved watching you handle your reactions and experiments. You have great talent, and I am sure you will have a bright future waiting for you. We have grown much closer in the last few months, and I am so happy I got an opportunity to get to know you not just as a colleague but as a friend as well. Thank you for feeding me, for reminding me that I can do this, and for standing by me at one the hardest times of my life. Samson, words cannot begin to express the admiration or respect I have for you. I think your talent is vast. I also think that no matter what you do in life after you get your PhD, you will do it well. You are a magnificent piece of work, an individual in every sense of the word. Thank you for sharing Cuban music and opera with me. I have enjoyed every discussion we had, including the arguments. And I certainly enjoyed your sense of humor and wit. Thank you for the food and the endless computer support that you provided so graciously without any complaint. And thank you very much for laughing at my jokes, although they were not always funny. Most important of all, I would like to simply thank you for listening to me and my endless complaints, and

tireless tirades. Thank you for lending me your ears. My dearest group members, it has been an absolute pleasure; you have taught me many things, made me laugh, and humbled me with your care and compassion. I am forever grateful for you, and I cannot express how much I will miss you. This work will not be done without you.

Dr. Samia and Dr. Wahid Hanna (Tante Samia and Uncle Wahid), I believe I have been blessed by meeting you. You have opened your hearts and home to me and made me a member of your wonderful family. Thank you for everything. Tante Samia, I found in you a wonderful friend. I will never forget the long hours we spent putting together seating arrangements for the gala. That was fun!!! I really will miss you dearly. You are generous, sweet, and very kind. I look up to you and hope that I will always make you proud.

I also would like to mention the Stover family, Mark, Karin, Jenny, Guillermo, Sarah, the kids and Aunte Pat, who has become my family in this country. Thank you for the Christmases, the thanksgivings, the phone calls and most importantly the love you have provided me. I want to especially mention Karin Stover Corea for her undying support, open mind and friendship.

I had many colleagues who contributed to this work, and I would like to thank them for their help. I would like to especially thank Dr. Megan Bragg for the rhodium catalyst cycle NMR studies, Dr. Cara Nygren who helped in the crystal structure identification of earlier sultams. Michael Blanchard for teaching me what a glove box is. Bill Gurley for the endless hours of installing, updating and maintaining SYBYL, and for the many interesting conversations we had

while we waited for updates to finish. I also would like to thank Dr. Mark Wahle and Dr. Mike Dolan at Tripos Inc. for their endless supportive services with SYBYL. They are always a phone call away and on the ready to solve all of my problems.

I also would like to mention the Arab-American community in Knoxville for providing me with a sense of belonging. And I especially like to thank Lina Shatara for her friendship and support. Thank you for give a place to come to, and for the dinners especially on the nights I did not have time to cook. And I also would like to mention the board members of the Arab-American Club members, for their support, sense of humor and endless lighthearted teasing.

One more friend I would like to mention is Mary Antone. Mary, thank so much for the infinite amount of hours we spent on the phone. And for the cooking and baking sessions we had, and the spontaneous but oh so secret road trips. Your friendship, grace and kindness will continue to touch me.

I have to mention my high school chemistry teacher Jiryes Abu El-Etham, because that is where it all started. If it was not for organic chemistry in eleventh grade, I am not sure I would have become a chemist. And I would like to also mention Dr. Thomas Ruttledge for the inspiration to become a chemist and for his friendship over the last ten years.

Last but certainly not least, I would like to thank the Department of Chemistry at the University of Tennessee for giving me the opportunity to pursue my PhD work here. Thank you.

I promised myself to keep this short, but I would have never been able to finish this work without the love, support and faith of so many people. It takes a village to raise a child and in my case it took two countries.

Abstract

3-Phenyl-2,3-dihydro-1,2-benzisothiazole 1,1 dioxide (NSC108406), identified as an HIV-1 reverse transcriptase inhibitor, is chosen for lead optimization. A series of analogues are docked using SYBYL FlexiDock into both wild-type (wt) reverse transcriptase (RT) and Tyr181→Cys181 (Y181C) RT, from the dataset of efavirenz (Sustiva®) bound to the enzyme. Minimizations using genetic algorithms are performed, and the lowest energy conformations are evaluated. Five structures emerge as good fits either in both enzymes or only in Y181C RT. 3-(*m*-Cyclopropylphenyl)- and 3-(isopropylfuranyl)-2-methyl-2,3-dihydro-1,2-benzisothiazole 1,1-dioxides do not exhibit improved binding in wt RT over efavirenz. In the Y181C pocket, the furanyl ring oxygen is oriented towards Cys181, and the cyclopropyl group on the phenyl ring makes a strong contact with Tyr183. Three 3-(alkylethynyl)-2,3-dihydro-2-methyl-1,2-benzisothiazole 1,1-dioxides (ethynyl sultams) make very good contacts in both wt and Y181C RT.

Synthesis of the ethynyl sultams is attempted using the appropriate alkylethynyllithium reagents with saccharin, but 3,3-bisalkylethynyl-2,3-dihydro-1,2-benzisothiazole 1,1-dioxides are the principal products. These are methylated to give the bisalkylated sultams. When docked into wt RT, they are consistently placed outside the pocket. In Y181C RT they make similar contacts to nevirapine, a first-generation NNRTI.

3-Chloro-1,2-benzisothiazole 1,1-dioxide is then coupled to the alkylethynyllithium reagents to give the desired monosubstituted products. (*R,R*)-*N*-(*p*-tolunesulfonyl)-1,2-diphenylethylenediamine-rhodium-(pentamethycycopentadienyl)-Cl [(*R,R*)-TSDPEN-Rh-Cl], an enantioselective catalyst for the reduction of imines, is used in an attempt to produce optically active sultams; however, the products are not optically active. The cyclopropyl- and cyclobutylethynyl bonds are reduced to the corresponding alkanes. These new cycloalkylethyl sultams, when docked into RT, exhibit a better fit in Y181C than wt RT, similar to that of efavirenz.

In a study on the mechanism of the enantioselective reduction of 3-alkyl- or aryl-imines by (*R,R*)-TSDPEN-Rh-Cl, a number of imines are docked into the catalyst cavity in two different approaches using the “original” approach that gives the observed enantioselectivity and the “reverse” approach, which is thought to give the opposite enantiomer. Molecular dynamic studies are carried out. In all 3-(aryl/alkyl)imine sultams, an average of at least 10 kcal/mol energy difference is observed between both approaches, showing probable structures for the intermediate complex in the catalytic cycle that accounts product stereochemistry.

Table of Contents

List of Tables

List Figures

List of Schemes

Abbreviations

Acquired Immunodeficiency Syndrome	AIDS
Human Immunodeficiency Virus 1/2	HIV-1/2
Interleukin-2	IL-2
Center for disease control	CDC
Scan electron microscope	SEM
Azidothymidine	AZT
Simian immunodeficiency virus	SIV
Ribonucleic acid	RNA
Deoxyribonucleic Acid	DNA
Cystine	Cys
Fusion peptide	FP
Heptad repeat	HR
Reverse Transcriptase	RT
Arginine	Arg
Leucine	Leu
Reverse Transcription Initiation Complex	RTIC
Phenylalanine	Phe
Double stranded DNA	dsDNA
Non-nucleoside reverse transcriptase inhibitors	NNRTI

Primer binding site	PBS
Barrier-to-autointegration factor	BAF
High-mobility-group	HMG
Histytdine	His
Nuclear magnetic resonance	NMR
Glutamine	Glu
Magnesium	Mg
Manganese	Mn
Glycine	Gly
Threonine	Thr
Cyclotriazadisulfonamide	CADA
Nucleoside reverse transcriptase inhibitors	NRTI
Nucleotide reverse transcriptase inhibitors	NtRTI
Protease Inhibitors	PI
2′,3′-dideoxycytidine	DDC
2′,3′-dideoxyinosine	DDI
2′,3′-didehydro-2′,3′-dideoxythymidine	D4T
2′,3′-dideoxy-3′-thia-5-fluorocytidine	(–)-FTC
Federal drug administration	FDA
1-[(2-Hydroxyethoxy)methyl]-6-(phenylsulfanyl)thymine	HEPT
4,5,6,7-Tetrahydroimidazole[4,5,1-jk][1,4] benzodiazepine-2(1H)-one	TIBO
Herpes simplex virus	HSV

Reverse transcriptase	RT
2-alkoxy-6-benzyl-3,4-dihydro-4-oxopyrimidines	DABO
2-(cyclohexylsulfanyl)-3,4-dihydro-5-mehtyl-6-(3-methylbenzyl)-4-oxopyrimidines	S-DABO
Non-nucleoside inhibitor binding pocket	NNIBP
Tyrosine	Tyr
Tryptophan	Trp
Lysine	Lys
Valine	Val
Proline	Pro
Glutamine	Glu
Nevirapine	NEV
Deliviradine	DLV
Efavirenz	EFV
National cancer institute	NCI
n-Butyl lithium	*n*-BuLi
Hydrochloric acid	HCl
Sodium hydroxide	NaOH
Sulfuric acid	H_2SO_4
Sodium hydride	NaH
Iodomethane	MeI
Cesium carbonate	Cs_2CO_3
Dimethylformamide	DMF

(1*R*,2*R*)-*N*-*p*-toluenesulfonyl)-1,2	
-diphenylethylenediamine	(*1R,2R*)-TSDPEN
Wild type	wt
Tripos force field	Tripos ff
Triethyl amine	TEA/Et_3N
Formic acid	HCOOH
Distortionless Enhancement of Polarization	DEPT
High resolution mass spectrometry	HRMS
Atmospheric pressure photoionization	APPI
Acetonitrile	CH_3CN
Phosphoruspentachloride	PCl_5
Ethanol	EtOH
Ammonium Chloride	NH_4Cl
Aqueous	aq
Saturated	sat
Anhydrous	anhyd
Thin layer chromatography	TLC
Carbon dioxide	CO_2
Variable temperature	VT
Ruthenium	Ru
Substrate-to-catalyst ratio	S/C
Cambridge Crystal Structure Database	CCSD
Dichloromethane	CH_2Cl_2

I. Introduction

A. AIDS—The Disease

Eighty million people are currently HIV (human immunodeficiency virus) positive or living with acquired immunodeficiency syndrome (AIDS), and 20 million lives have already been lost to one of the deadliest diseases known to man. Since its discovery, HIV has spread among 80 million people worldwide. A total 900,000 of these reside in the US, while the rest live in Europe, Asia or Africa, where the disease is rampant.[1]

In its early days, HIV was thought to target specific communities, such as homosexuals and drug abusers. But now it is known that HIV does not discriminate between woman, man or child, and it infects and causes AIDS using the same mechanism of action across all races, cultures, classes and political ranks. AIDS is not "a gay disease," as it was dubbed earlier. It is largely a sexually transmitted disease that has caused a widespread epidemic and a vast public health problem that needs to be taken seriously on all levels. The war against AIDS must continue on all battlefields from global and local political legislation that provides prevention programs, health care, tests and medication to all patients, to scientific research that facilitates the discovery and development of new therapeutic candidates.

B. A Virus Discovered

Robert Gallo's work on interleukin-2 (IL-2) growth factor paved the way for his discovery of Human T-Cell Leukemia Virus Type 1 (HTLV-1). His work at the

time was unique and came along when there was a general misguided opinion that human retroviruses do not exist and therefore do not cause cancer in humans.[2] After he isolated HTLV-1, independent studies out of Japan supported his results and reported that HTLV-1 caused a leukemia endemic in Japan. Gallo's work in this field changed the view on human retroviruses, and in a way played an important role in setting the stage for the discovery of the human immunodeficiency virus (HIV).[2]

In the meantime, Luc Montagnier was leading a small virology division in the Pasteur Institute in Paris. Montagnier and co-workers were also interested in retroviruses that caused cancer. In 1982, using Gallo's IL-2 growth factor technique, they were able to isolate a viral DNA sequence from a breast cancer patient biopsy, as well as from the patient's T-cells. This viral DNA was also similar to a sequence isolated from a mouse mammary cancer cell.[3]

In 1981 a report in the *Morbidity and Mortality Weekly Report* appeared describing patients with no immunological response suffering from pneumocystic pneumonia.[1] Their blood samples showed no helper T-cells or CD4+ T-cells. As more physicians across the US and the world became aware of this disease, more reports of such patients came into the Center for Disease Control (CDC).[1] By the summer of 1981 over 100 cases had been identified in the US, and all were gay men. The new disease was dubbed "the gay disease." Initially as the CDC gathered epidemiological data, it was thought that lifestyle played a roll in an individual's susceptibility to contracting AIDS. Even a report from a physician in Florida were both men and women of Haitian descent displayed similar

symptoms did not get rid of the lifestyle notion. Reports from France by Dr. Rozenbaum and from Belgium by Dr. Piot of more AIDS patients started emerging.[1] Most interesting was the report of some Congolese patients in Belgium exhibiting the same symptoms. In 1983 the CDC sent a team to the Congo to look for patients with AIDS. There they found that men, women and children were suffering from the disease. It was clear now that AIDS is not necessarily a new disease, but a newly discovered one, and that this was a worldwide health problem. Many questions needed to be answered. What causes this disease? Where did it come from? And more importantly, where was it going?

In the US more patients were being diagnosed with AIDS, but the patient profile had changed. It was no longer gay men only who came in with the symptoms, as intravenous drug users were exhibiting suppressed immune response. Then a hemophiliac baby, who had several blood transfusions, displayed loss of immune response and inability to breathe due to pneumonia.[1] With this report, the CDC was now certain that AIDS is caused by a virus, because a virus is the only particle small enough to pass through the different filters used when donated blood is collected from different donors. They were also sure that the blood supply was contaminated. More reports of hemophilia patients developing AIDS started emerging. About 35,000 Americans had been infected from contaminated blood and blood products.[1]

It is important to note here that by the time the first American patient was diagnosed with AIDS, 250,000 more Americans were already infected. And by

the time the first African patient was diagnosed, millions of Africans across the continent were infected.[1]

Robert Gallo firmly believed that AIDS was caused by a human retrovirus similar to HTLV. So his group decided to look for a retrovirus in blood cell cultures. The problem was that their cell cultures died after a few days. They were being consumed by the virus.[2]

In 1982 Francois Brun-Vezeinet, a former student of Montagnier and then a member of the virology group in the Pasteur Institute initiated a collaborative effort with Montagnier to find the cause of AIDS. Montagnier's laboratory was well equipped to hunt for lymphotropic retroviruses, so they obtained a lymph node biopsy from a young gay man (a patient of Dr. Rozenbaum) and used it to grow T-Cell cultures.[3] Two weeks later, the cultures tested positive for reverse transcriptase (RT) activity. At the time the only human retrovirus known was HTLV, but the virus in Montagnier's cell cultures tested negative for HTLV antibody recognition and could not be precipitated. They were able to precipitate it by using the patient's own serum. More samples from different patients were tested. Those with full-blown AIDS had a more aggressive form of the virus that replicated rapidly and unlike HTLV killed the T-cell cultures. Finally they isolated the virus and provided the first scanning electron microscopy (SEM) picture of the human immunodeficiency virus (HIV).[3] Montagnier and his colleagues knew immediately that this virus was not the same as HTLV. Its morphology was totally different. It had a cone-shaped center different than that of HTLV. The

new virus pictures matched those of animal lentiviruses, which further confirmed that this new virus does not belong to the HTLV genus.[3]

In the meantime Gallo's team was still looking for an HTLV-related virus in AIDS patients. SEM images of T-cell lines showed that AIDS patients had two viruses. Gallo initially thought that one was a "mature" form of HTLV, the other an "aberrant" form. However, with Montagnier's publication of SEM images of HIV, Gallo now knew that the reason many of his cell lines tested negative for HTLV is because they were infected with a completely different virus, and that the 5–10% HTLV-positive results came from patients infected with both HIV and HTLV. In 1984 Gallo and co-workers submitted four papers that provided further evidence that HIV is the causative agent of AIDS.[2] Their work laid the groundwork for the development of blood tests that could detect HIV. This halted infection through blood transfusion and shed light on how much of the world's blood supply had been tainted by HIV-positive blood samples.

In 1987 azidothymidine (AZT) was the first anti-HIV drug to be approved by the FDA for use by HIV patients.[4] Today twenty different HIV drugs are present on the market.[5]

C. The Origins of HIV: A Short Overview

HIV belongs to the lentivirus genus of which simian immunodeficiency virus (SIV) is a part. There are five different lentiviurs lineages. HIV-1 and HIV-2 come from two different lineages. In genetic studies HIV-1 clusters with chimpanzee SIV (SIV_{CPZ}).[6] Recent evidence suggests that the source of HIV-1 is the chimpanzee subspecies *P.t. troglodytes*.[7] HIV-2 clusters with Sooty

Mangabeys SIV (SIV_{SM}) and SIV_{MAC} from macaques. Although SIV_{MAC} was one of the first SIV strains isolated, it was later discovered that all macaque infections took place in captivity. Evolutionary evidence suggests that sooty mangabeys are naturally infected by SIV and that they are the source of HIV-2.[6] Other SIV strains are African Green monkeys SIV (SIV_{AGM}), Sykes monkeys SIV (SIV_{SYK}), l'Hoest monkeys SIV (SIV_{LHOEST}), and Sun monkeys SIV (SIV_{SUN}). All of these SIV strains have cross-species transmissions as well.

Both HIV-1 and HIV-2 have genetic diversity. HIV-1 has three major groups, M, N, O, and the M group has seven subtypes A–J. HIV-2 on the other hand has six subtypes A–F. At least four independent cross-species transmissions caused the formation of these subtypes.[8, 9] The origins of HIV-1 and HIV-2 are still a highly debated topic. Initially the origins for both viruses were estimated to date back as early as 1951,[10] but other estimates suggested that these viruses may have diverged as primates evolved putting the origin of the lentivirus that infected the common ancestor of all apes and Old World monkeys at 25 million years ago.[11]

A molecular clock model puts all three viruses, HIV-1, HIV-2 and SIV_{AGM}, with a common ancestor 150 years ago. A molecular clock model uses information from different viruses isolated at various times. By comparing the virus sequences and noting the different mutations, a rate of change can be estimated. HIV-1 has three different proteins that evolved at different rates. What the molecular clock model does not take into consideration is host-dependent evolution.[6]

There is enough evidence that cross transmission causes lentiviruses to evolve according to their host. SIV_{AGM} is an example of a virus evolving specifically with its host. There are four species of African Green Monkeys dispersed throughout the African continent. They are the Sabaeus monkeys in West Africa, the Tantalus monkeys in Central Africa, the Givets in East Africa, and the Vervets from East to South Africa. Each species is naturally infected with SIV_{AGM}, and each clade (evolutionary class) of SIV_{AGM} has its unique evolutionary features, rates of evolution and divergence dates, further supporting that as each species became infected with SIV_{AGM}. The evolution of that specific strain became independent of the others and more dependent on the host. It is important to keep in mind that both SIV and HIV are parasites, and in order to survive they need a host. So it is only common sense to expect them to evolve along with their respective hosts. The common ancestor of African Green Monkeys existed one million years ago, and it was probably naturally infected with the common ancestor of SIV_{AGM}.[6]

Another example of host-dependent evolution is that of SIV_{CPZ}. Chimpanzees are divided to four geographically distinct subspecies, and not surprisingly SIV_{CPZ} has four clades,[6] each of these clades is specific to its respective chimpanzee subspecies.[12]

The lack of a fossil record for viruses makes it impossible to rely on conventional methods in estimating the age of HIV. In the molecular clock model the estimation is based on rate of replication and rate of mutation calculations without taking into consideration any other factors. The major weakness of this

model is that different viral sites may evolve at different rates so this makes calculating and predicting the rate of evolution for the whole virus very difficult and faulty. In more recent studies these rate differences were taken into consideration, and the final estimation for SIV increased from 100 years to 350 years and for HIV from 50 years to 150 years. That is still inconsistent with the idea of host-dependent evolution for millions of years. Sharp and co-workers published estimations on the date of emergence for the HIV-1 M group.[6] Their initial work suggested a date around 1960,[13] but the first HIV-1 positive blood sample was collected in 1959 from a man from Zaire. The sequence of that virus strain suggested an earlier date, possibly the 1940s.

D. HIV Lifecycle

1. Overview

HIV infection begins with binding of the viral envelope glycoproteins to the CD4 receptor and one of the chemokine co-receptors, CXCR4 or CRC5 of the T-lymphocytes. This is followed by virus–cell fusion events that create a small opening in the cell membrane through which the viral materials, which include viral RNA and reverse transcriptase, are released into the cell. Once in the cell, reverse transcription of the viral genome commences, followed by integration into the cell genetic material. Viral particles are then synthesized within the cell complete with a protein coat, and they are released into the body to further infect other cells. Studies have shown that infection proceeds at a very rapid pace. In one study it was apparent that viral DNA integration occurred approximately seven hours after infection.[14]

2. Viral entry

Viral entry into the host cell can be dissected into four major events: (i) viral attachment to the cell surface, (ii) binding to the CD4 receptor, (iii) interaction of the CD4-envelope glycoprotein complex with entry co-receptors CRC5 and CCRX4, and (iv) virus–cell fusion.

The viral envelope glycoproteins gp120 and gp41 are essential for binding and fusion with the host cell. Gp120 and gp41 are processed from the N-terminal and C-terminal parts of gp160. Gp120, the larger of the two molecules, lies outside the envelope lipid bilayer and is responsible for binding with CD4 receptors and chemokine co-receptors and driving viral fusion.

The Gp120 amino-acid sequence consists of both conserved and variable regions (V1–V5). V1–V4 are exposed loops with disulfide bonds at their base. V1–V4 loops respond to antibody activity and are involved in gp120 binding to CD4 receptors as well as chemokine receptors. V1–V3 are involved in co-receptor binding as well as virus–cell fusion.[15] The V3 loop contains 35 amino acids in between Cys303 and Cys338, which are joined together by a disulfide bond. Mutations in the tip and stem of the V3 loop produced gp120 glycoproteins able to bind to CD4 receptors but unable to form syncytia. V3 neutralizing antibodies either completely blocked or greatly reduced the ability of HIV-1 infection.[16] More important are mutations on the disulfide bond residues Cys303 and Cys338. These rendered gp120 completely inactive. Mutagenesis studies indicate that deletion of the V3 loop from the viral *env* gene renders HIV completely unable to process gp160 to both gp120 and gp41, as well as hinders

syncytia formation. The exact nature of interactions between V3 and the CCR5/CXCR4 receptors is not completely understood; however, from the gp120 core crystal structure and other studies it can be assumed that electrostatic interactions between the substrate and receptor do occur.[17]

Detailed crystal structures of gp120 bound and unbound to CD4 have been published at resolutions as low as 2.5 Å.[15, 18, 19] These structures have provided more details on the complexity of the binding process, which will hopefully lead to the design of anti-HIV binding compounds that can be used in therapy. Although the exact structure of the V1/V2 and V3 loops is still not completely resolved, the core structure of deglycosylated gp120 has been determined, and the positioning of these three key loops can be deduced, allowing for better understanding of their function. The crystal structure of the gp120 core shows that it has two domains that provide the flexibility for receptor-induced conformational change. The gp120 protein backbone binds to the CD4 receptor. The antigenic side chains are not involved in this process. This allows for the alteration of the amino acid side chains without altering the backbone, and therefore limits loss of binding affinity to CD4. Such a feature gives HIV a rich antigenic diversity allowing it to escape the immune system. Another binding interaction is the “knob–socket” interaction between protruding amino acids in CD4 and holes in gp120. Such interactions may be possible targets for developing binding inhibitors.[17]

The heavy glycosylation of gp120 and gp41 proteins presents a challenge to the immune system. Sugars present themselves in the body as “self”, thereby

shielding the receptor binding domains of gp120 and not causing an antibody response. They also reduce HIV-1 binding to immunoglobulin-like B-cell receptors, which limits antibody production altogether.[14, 19, 20]

Another important feature in the gp120 binding mechanism is the positioning of the V1/V2 and V3 loops. Although there are no crystal structures available for these regions, modeling studies show them forming an umbrella that shields the CD4 binding region of gp120. Presenting the V1/V2 and V3 regions to the immune system protects HIV even further, because should an antibody succeed in neutralizing these regions, the virus can simply mutate non-essential residues and escape the immune response.[15, 17, 19, 20]

Gp41, the smaller of the two proteins, lies in the transmembrane (TM) region and mediates virus–cell fusion as well as intracellular membrane fusion (syncytia formation). Gp41 shares general structural features with other viral fusion proteins: (a) the presence of an N-terminus containing a hydrophobic glycine-rich amino acid sequence known as the fusion peptide (FP), and (b) Heptad repeats (HR) adjacent to the TM domains and the hydrophobic sequences. These are referred to as NHR for N-terminus heptad repeat and CHR for C-terminus heptad repeats.[21] The three NHRs fold into a coiled-coil structure with the three CHRs fitting into the grooves, forming a thermostable six-helix bundle. [22] The two termini are joined together by an extended loop.[23-25] The heptad repeat contains a reoccurring seven amino acid sequence (abcdefg) in which the third and fifth positions contain a hydrophobic amino acid.

The HR sequence is highly conserved, and mutagenic studies have shown that mutations in this region render HIV-1 unable to complete the membrane-fusion process, and therefore are unable to infect the cell. This shows the importance of gp41 in the viral infection/replication cycle.[22]

The fusion mechanism is a highly coordinated and regulated process that ensures that specific protein lipid interactions will occur at the right time and place. If the envelope proteins are activated too early or too late, the virus will be unable to infect.[22, 26]

Gp120 binding to CD4 receptor signals the beginning of the viral fusion reaction. Gp41 contains three immunogenic regions, two of which become exposed after CD4 binding occurs. The first region is the loop connecting the NHR's and CHR's and lie between residues 598 and 604, and the second is in the CHR helix residues 644–663. The third region contains amino acids 656–671 and lies in the transmembrane domain.[23, 27]

More dramatic conformational changes are observed after co-receptor binding occurs. Melikyan and co-workers showed that co-receptor binding is necessary in order for fusion to proceed.[28] The formation of the metastable six-helix bundle overcomes a large energy barrier and brings the two membranes closer together; however; lipid bilayer membranes have many repulsive forces between them. To overcome this energy barrier gp41 drives this process by presenting a hydrophobic region in its FP that inserts itself into the cellular membrane causing it expand.[22,23]

The fusion process has been shown to be multistep. In the first step the outer monolayer is fused. In the second step a rupture of the inner monolayer occurs creating a fusion part through which the viral materials pass into the cellular cytoplasm. The FP stabilizes this complex; in a study a sequence of amino acids taken from the FP were shown to encourage lipid mixing.[23] Gp41 is attached to the viral membrane by a transmembrane region; the TM is preceded by a tryptophan-rich region. It is not clear how these tryptophan residues contribute to the fusion process, but mutational studies have shown that this region is important for successful fusion.[22, 23, 29] Once the viral materials are in the cell, reverse transcription begins.

3. Reverse Transcription

HIV has a total of nine genes encoded onto two identical strands of genomic RNA. Following infection, one of these mRNA strands is converted to viral materials through a process called reverse transcription. Initially a reverse transcription initiation complex (RTIC) is formed. At the heart of reverse transcription is HIV reverse transcriptase (RT), a heterodimer composed of p66 and p51 subunits.[30] Both of these subunits are encoded by the viral *pol* gene, and are expressed as one gp160 subunit. A viral aspartyl protease cleaves the gp160 precursor into the functional heterodimer p51/p66. Both p66 and p51 subunits are essential in viral replication; together they form a stable dimer that is able to carry DNA transcription to completion. Crystal structures have identified two dimerization sites. The first one is a series of leucines between residues 283 and 310. The second is a series of conserved tryptophans in the connection

subdomain between residues 399 and 414. In crystal structures of RT bound to dsDNA, these tryptophan series in both dimers are in close proximity to each other. Synthetic peptides derived from this region inhibit RT dimerization and enzymatic activity.[31]

P66 resembles a right hand with a palm, fingers, thumb, and connection domains (See Figure 1). It also contains the active site and the RNase H site in its N-terminus and C-terminus, respectively. P51 is analogues to p66, but it lacks the RNase H site (C-terminus) [31-34] P51 has no catalytic activity; its main function is to provide structural support for p66. Crystal structures of bound and unbound reverse transcriptase have shed some light on the conformational changes that occur when the enzyme is bound to an inhibitor, to a double-stranded DNA (dsDNA) and to a polypurine RNA:DNA double strand.[33-39]

Understanding the RT mechanism of action in its entirety is essential in RT inhibitor design. The major conformational change between the bound and unbound reverse transcriptase is the positioning of the thumb. In the unbound RT, the thumb is in an upright position, in close proximity to the fingers subdomains. Two main points of contact have been identified: a bond between Arg78 in the fingers and the main chain of the thumb, and a nonpolar interaction between Phe61 in the fingers subdomain and Leu289. These interactions are small in size and weak in strength allowing the thumb freedom of movement to make the necessary conformational changes.[32] The RT/dsDNA and RT/RNA:DNA complexes have the same conformations, with the fingers and palm subdomains interacting heavily with the substrates present in the catalyti

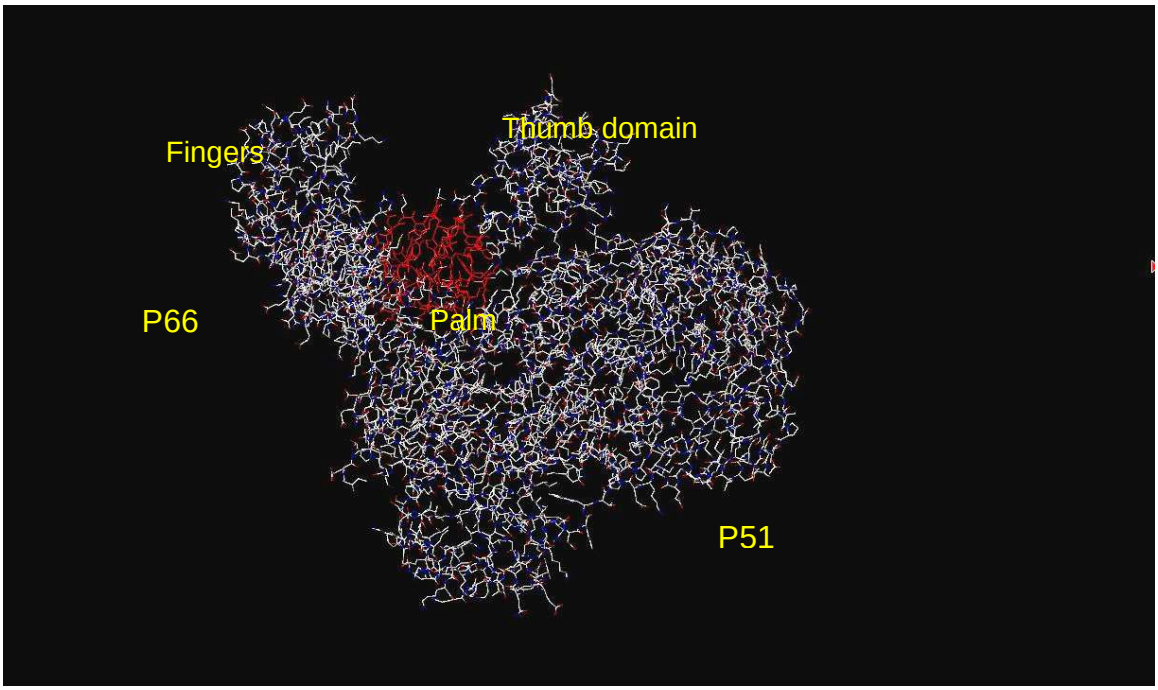

Figure 1. Reverse transcriptase bound to efavirenz in the allosteric binding pocket (red) (pdb code 1ikw).

palm subdomains interacting heavily with the substrates present in the catalytic cavity.[34, 39]

It is clear that RT is a flexible enzyme able to undergo necessary conformational changes during its catalytic activity. This feature of reverse transcriptase makes it an attractive target for drug design. (For a detailed discussion on NNRTI mechanism of action, refer to the non-nucleoside reverse transcriptase inhibitors (NNRTI) section below.)`

DNA synthesis has three major steps that are catalyzed by RT: (i) RNA-dependent DNA polymerization, where the RNA:DNA hybrid is formed, (ii) RNase H degradation of the RNA template, (iii) DNA-dependent DNA polymerization; the dsDNA is formed in this stage and is ready to be integrated into the host genome.[31, 36] Reverse transcription is initiated from the primer binding site (PBS). PBS is comprised of an 18-nucleotide viral genome sequence.[31] The reverse transcription initiation complex (RTIC) is then formed. Its structure is still not properly characterized; however, attempts to fully characterize it are underway. HIV is a parasite, so naturally it would require assistance from its host cell machinery to complete its replication cycle. For example, the RTIC is formed outside the host cell nucleus; however, in order for DNA transcription to be complete, the complex needs to be moved from the cytoplasm to the nucleus. Other cellular proteins seem to regulate HIV replication. The cellular protein barrier-to-autointegration factor (BAF) inhibits viral DNA from integration into itself. The structure of BAF is still unidentified. Cellular DNA replication processes are reprogrammed as early as 30 minutes after infection, which

suggests some sort of communication resulting from viral binding to the CD4, CCR5 and CCRX4 receptors. Once the new viral DNA strand is synthesized, integration begins.[31]

4. Integration

Integration is essential for retroviral replication. The linear-strand DNA, the product of reverse transcription, is the substrate for HIV-1 integrase. Once replication is complete, a pre-integration complex forms. Isolates of this complex contain viral DNA, reverse transcriptase, nucelopcapsid, integrase, and two cellular proteins: high-mobility-group HMG-I(Y), and BAF (barrier-to-autointegration factor). Retroviral pre-integration complexes either enter the nucleus through the nuclear pore or wait until the nuclear membrane dissolves during cellular division.[40]

Integrase binds to the viral DNA and cleaves its 3′-end groups, resulting in the removal of two nucleotides from each end, a reaction called 3'-end processing. The result is the exposure of the 3′-end hydroxyl groups where the host DNA will be connected. The second step is the insertion of the exposed viral DNA into cellular DNA. There is no site specificity for this integration step, so it could occur anywhere on the cellular DNA. Both 3′-end processing and DNA strand transfer occur by a one-step mechanism.[41, 42] In 3′-end processing water is used as a nucelophile. It is thought that DNA strand transfer occurs in a similar fashion. Although both steps are chemically similar, their binding to the integrase active site must be different, because in the DNA strand transfer, both

viral and cellular DNA must be bound to the enzyme.[40, 41, 43] The exact mechanism of these two steps is still not very clear.

Unlike reverse transcriptase, a complete crystal structure of HIV-1 integrase has yet to be obtained. However, through protease digestion and functional complementation studies, it was determined that HIV-1 integrase contains three domains: the N-terminal domain, the catalytic core domain,and the C-terminal domain. Each of these domain structures has been determined by crystallography and NMR studies.[44-46]

The N-terminus consists of 50 amino acids between residues 1 and 50. It is essential for integrase activity. The main residues involved in integration are the four conserved amino acids His_2Cys_2; this motif is characteristic of zinc-binding sites.[40, 41, 43] Mutations to any of these residues reduce the N-terminus's ability to bind to zinc and greatly affect integrase activity. Crystal structures and NMR structures have been determined; the N-terminal region has four helices, stabilized by hydrophobic interactions in the upper region, and by the zinc ion in the lower region.[41]

The C-terminus is the least conserved of all three domains. It is comprised of 80 amino acids between residues 213 and 288. It binds DNA nonspecifically, and its deletion leads to complete loss of 3'-end processing. NMR studies showed a five-strand β-barrel.[46, 47] It is not clear what the exact functions of the N- and C-termini domains are in the integration reaction. Mutations to either domain leads to low activity in the enzyme, or in some cases to complete

inhibition. A complete crystal structure may help explain the functions of these two domains.[16]

The catalytic core domain is the best characterized and studied of all three domains. It is comprised of 162 amino acids lying between the residues 50 and 212.[40, 43] It also contains the catalytic triad of acidic residues D, D–35-E. In HIV-1 integrase, this motif corresponds to Asp64, Asp116 and Glu152.[41] Mutations in this motif severely deplete or completely abolish integrase activity.[41] X-ray crystallography of the core domain revealed a five-strand β-sheet and six α-helices.[48, 49] In the crystal structure the catalytic triad residues are in close proximity to each other; they bind divalent metal ions either Mg^{2+} or Mn^{2+}. The other residues of the catalytic core region exhibit great flexibility, suggesting that DNA binding is required to bring the triad into close contact with each other to ensure proper metal binding. Metal binding is required for full integrase activity. While crystal structures have shown metals bound in the catalytic site and in the N-terminus, it is not clear if other metal binding sites are present.[43] More studies are required.

As mentioned above, each of the HIV-1 integrase domains have been well characterized; however, there are no crystal structures of the three domains together, bound or unbound to substrate DNA. Such a structure will help understand the interactions between these domains and their effect on integration.

After integration, synthesis of the viral poly-protein is accomplished using cellular machinery. Cleavage of this large poly-protein into viral proteins is catalyzed by HIV protease.

5. Cleavage of Viral Proteins Catalyzed by Protease

HIV protease is a homodimer made up of 99 residues each. Although the crystal structure on the unbound enzyme appears to be symmetrical, HIV protease is an asymmetrical enzyme. In fact similar monomer regions are not identical. The active site is located at the bottom of the dimerization site and is covered by two flexible "flaps" of β-hairpins. The β-hairpin flexibility is necessary for substrate binding and product release as well as inhibitor activity.[50] Each monomer contributes one of the catalytic aspartic acids. Each catalytic triad in both monomers contains Asp25-Thr26-Gly27. Both triads are stabilized by a hydrogen-bond network.[51] And the aspartic acid residues are close to each other in a coplanner position.[52] The hydrolysis mechanism begins with activation of a water molecule, followed with a nucleophilic attack by water on the scissile bond to form a tetrahedral intermediate. The tetrahedral intermediate then breaks down aided by proton transfer to give the desired amino and carboxylate products.[50]

E. Anti-HIV Chemotherapy

The diversity of enzymes and receptors involved in the HIV lifecycle present multiple targets for drug design. Perhaps one of the biggest challenges in designing new anti-HIV compounds arises from its tendency to mutate at high rates. HIV, particularly reverse transcriptase, is error prone with no correction

mechanism set in place. Once patients are exposed to drugs that are active against wild-type HIV, mutant strains that are resistant to therapy are selected.

As described above in detail, HIV infection begins with cell attachment and binding to CD4 receptors, followed by co-receptor binding, virus–cell membrane fusion, replication, integration and then synthesis of new viral particles. Each of these processes has a specific enzyme or receptor, and each of these targets can be considered for anti-HIV therapy.

Several anti-HIV compounds are being studied at different levels of development. I have attempted to give a short review on the different inhibitors present with a main focus on transcriptase inhibitors, in particular non-nucleoside reverse transcriptase inhibitors (NNRTIs).

1. Cellular CD4 Receptor Down-Modulators

The CD4 receptor is the main target for HIV entry into the cell. Cyclotriazadisulfonamide (CADA, see below) was shown to inhibit HIV infection by down-modulating CD4 receptor expression on cell surfaces. CADA is specific for CD4 down-modulation and does not affect other receptors such as CXCR4 and CCR5.[53] It does not directly bind to the receptors, but appears to be involved in the down-regulation of CD4 expression on cell surfaces.[54] In a recent study CADA exhibited the ability to work synergistically with other anti-HIV drugs such as nucleoside reverse transcriptase inhibitors, non-nucleoside reverse transcriptase inhibitors, nucleotide reverse transcriptase inhibitors and protease inhibitors.[55]

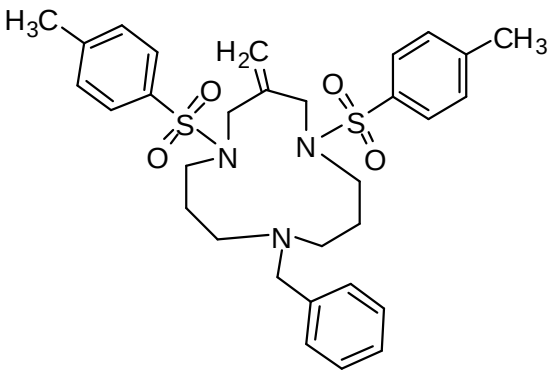

Cyclotriazodisulfonamide (CADA)

(NH_2)Leu-Gly-Lys-Phe-Ser-Gln-Thr-Cys-Tyr-Asn-Ser-Ala-Ile-Gln-Gly-Ser-Val-Leu-Thr-Ser-Thr-Cys-Glu-Arg-Thr-Asn-Gly-Gly-Tyr-Asn-Thr-Ser-Ser-Ile-Asp-Lew-Asn-Ser-Val-Ile-Glu-Asn-Val-Asp-Gly-Ser-Leu-Lys-Trp-Gln-ro-Ser-Asn-Phe-Ile-Glu-Thr-Cys-Arg-Asn-Thr-Gln-Leu-Ala-Gly-Ser-Ser-Glu-Lew-Ala-Ala-Gl-Cys-Lys-Thr-Arg-Ala-Gln-Gln-Phe-Val-Ser-Thr-Lys-Ile-Asn-Lew-Asp-Asp-His-Ile-Ala-Asn-Ile-Asp-Gly-Thr-Lew-Lys-Try-Glu(COOH)

Cyanovirin-N

2. Virus Attachment Inhibitors

Mannose-specific plant lectins from *Galanthus nivalis* (GNA) and *Hippeastrum* hybrid (HHA) have shown activity against viral envelope glycoprotein gp120. Exposure to these lectins produced HIV strains with a mutant gp120, but not gp41. These compounds (proteins) are unique in their structure, are of low toxicity, and are currently being considered as microbicides to be used topically.[56, 57] Another potential microbicide is the protein cyanovirin-N, an 11-kDa protein isolated from the cyanobacterium *Nostoc ellipsosporum*. It has a unique affinity for gp120 and inhibits both CD4-dependent and -independent binding.[58-60] BSMS378806 {(4-benzoyl-1-[4-methoxy-1*H*-pyrrol[2,3-b]pyridin-3-yl]oxoacetyl)-2-(*R*)-methylpiperazine}, another CD4 antagonist, has been identified as a new class of HIV attachment inhibitors. It has exhibited inactivity against CD4 independent viral entry, which suggests that it interferes specifically with CD4–gp120 interactions. It has shown great bioavailability and low toxicity in initial animal cell studies.[61-63]

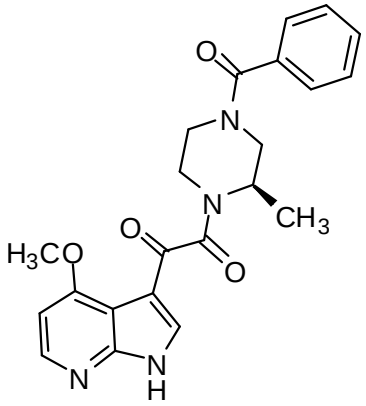

BSMS378806

3. CXCR4 and CCR5 Antagonists

After CD4 binding, gp120 interacts with either CXCR4 or CCR5 receptors. In clinical studies AMD3100, a bicyclam CXCR4 antagonist, exhibited inhibition against X4 and X4/R5 HIV strains. A dose as low as 5 μg/kg/h in individuals with X4 or X4/R5 resulted in complete loss of viral infection within ten days. Other bicyclams are being pursued as potential candidates. QSAR studies revealed that the presence of both macrocyclic cyclam rings is not necessary for anti-HIV potency. AMD3465 has only once cyclam ring and still possesses comparable potency against HIV as AMD3100.[64, 65]

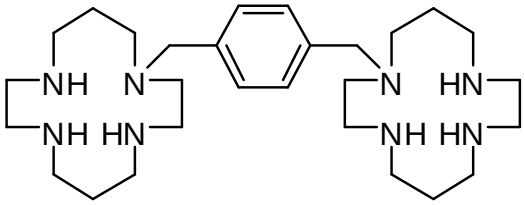

AMD-100

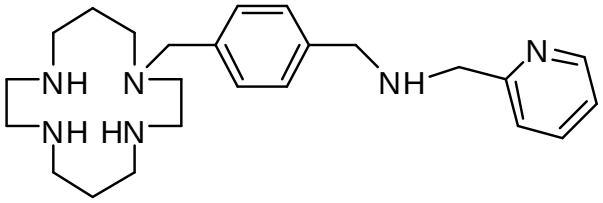

AMD-346

TAK779 is the first nonpeptidic CCR5 antagonist identified to block HIV infection at nanomolar concentrations. Unfortunately, it has very low oral bioavailability and causes severe irritation at the injection site.[66] Further research led to the discovery of the bioavailable TAK220. The structure of TAK220 is not yet revealed [65]

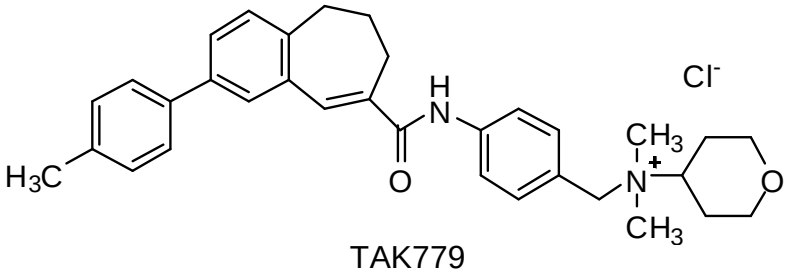

TAK779

SCH351125 was the first CCR5 antagonist advanced to clinical studies. It has the ability to reduce viral load in patients not receiving any other antiviral agents. SCH351125, SCH350581 and TAK779 bind to a putative binding pocket in the TM helices 1, 2, 3 and 7.[67-69]

Two other CCR5 inhibitors worthy of mentioning are UK427857 and MRK-1. UK427857 depletes viral load levels ten days after administration and sustains these low levels ten days after therapy was stopped. It is already in clinical trials and may become a once-a-week pill in HIV therapy. MRK-1 has high potency against R5 HIV strains, and it showed great potential as a vaginal microbicide gel for use against HIV-1 sexual transmission.[70, 71]

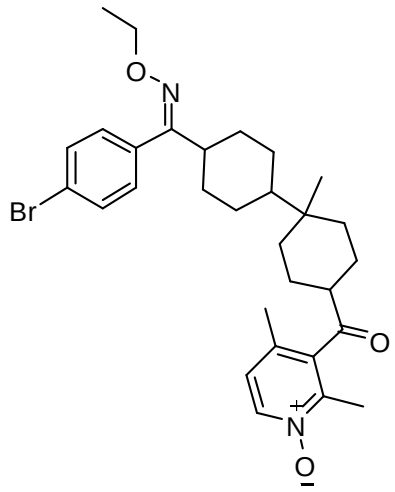

SCH351125

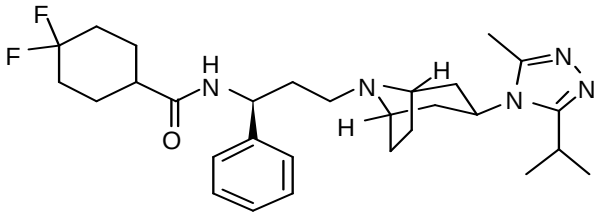

UK427857

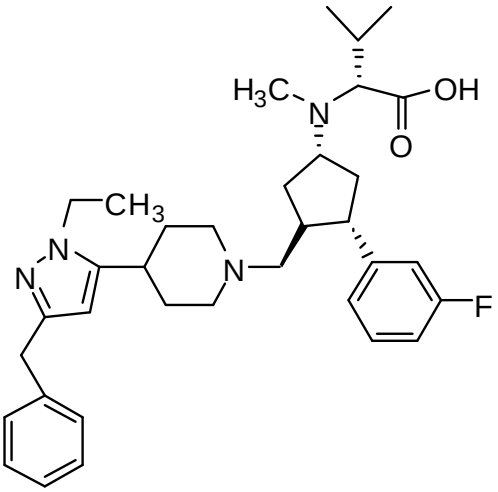

MRK-1

4. Viral Cell Fusion Inhibitors

Following co-receptor binding, gp120 dissociates from the viral envelope to expose gp41, which initiates the virus–cell membrane fusion process. Enfuvirtide, also known as T-20, DF-178, and Fuzeon, is a synthetic 36-amino acid peptide corresponding with residues 127–162 of gp41. Initial clinical trials —supported by later studies in North America, South America and Europe— showed the ability of this peptide to lower viral load by 1.5–2.0 fold during 15 days of treatment.[72] Unfortunately Enfuviritide has to be administered through an injection twice daily and causes injection-site irritation. It is also worth noting that large-scale peptide synthesis is costly.[73, 74]

5. HIV Integrase Inhibitors

There is no known cellular homologue for HIV integrase; therefore, this is potentially a good therapeutic target. The structure of the HIV integrase core domain complexed with an inhibitor was described recently, leading to the design of several diketoacids such as L-708, 906 and L-731,988, which act as inhibitors for the covalent bond formation between the 3′-end of viral DNA and cellular DNA. In a study these inhibitors were able to stop infection after seven hours. This further supports their involvement in the later stages of HIV replication.[75] Unfortunately, repeated exposure to these diketoacids resulted in mutant integrase strains.[76, 77]

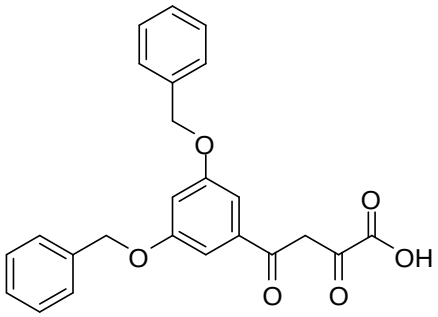

L-708,906

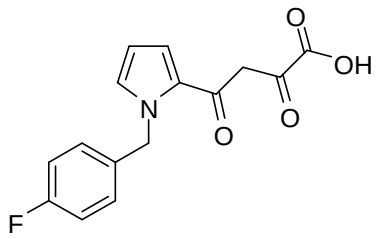

L-731,988

6. HIV Protease Inhibitors

HIV protease is responsible for the cleavage of viral precursor polyproteins to the structural proteins: p17, p24, p7, p6, p2, p1, and the functional proteins: protease (p11), RT (p51/p66) and integrase (p32). Protease inhibitors stop this process and prevent the formation of the viral particles. The protease inhibitors currently approved for therapy carry the same structural feature, a hydroxyethylene bond.[65] Astanavir, an aza-dipeptide analogue was approved for marketing by the FDA in 2003. It displayed a favorable profile to resistant PI strains.[78, 79]

The most recently approved PI by the FDA is darunavir (TMC-114), which was developed by structure-based design studies. The main objective of these studies was to design a drug that retains its activity against multidrug-resistant (MDR) viruses. GRL-02031 is another analogue of darunavir coming from the same group that developed the other two PIs. The structure of this latest compound has not been revealed. Darunavir was approved for use in MDR patients who are unresponsive to other AIDS drugs.

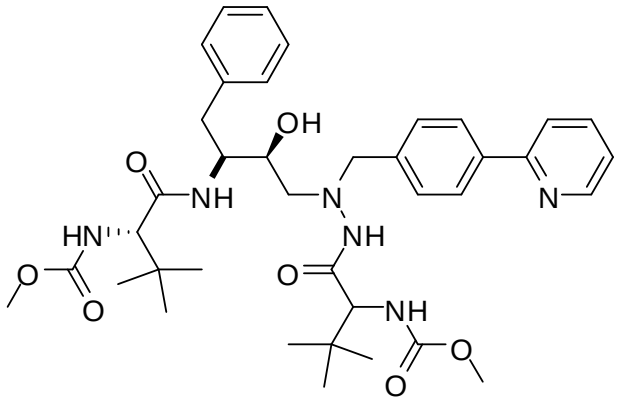

Astanavir

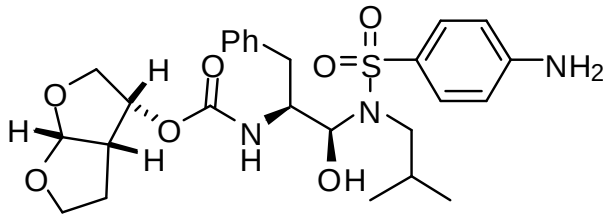

TMC-114

7. Reverse Transcriptase Inhibitors:

(a) Nucleoside/Nucleotide reverse transcriptase Inhibitors (NRTIs, NtRTIs). Upon conversion to their triphosphate form, they inhibit RT competitively by causing chain termination. They cause mutations in RT, for example some Zidovudine (AZT) resistant RTs are capable of removing the blocked primer from the active site.[80,81]

(b) Non-nucleoside reverse transcriptase inhibitors (NNRTIs): NNRTIs are structurally diverse. They bind to an allosteric pocket 10–15 Å away from the active site and cause conformational changes in the enzyme, rendering it inactive. Molecular modeling studies have been used extensively in the

design of NNRTIs; they have also played an instrumental role in understanding the mechanism of resistance.[80]

This section will discuss all three inhibitors, focusing mostly on NNRTIs.

(a) Nucleotide and Nucleoside Reverse Transcriptase Inhibitors (NtRTIs and NRTIs). NtRTIs have one phosphate group, so they only require two phosphorylation steps to become biologically active against HIV RT. They are competitive inhibitors that bind to the RT active site and terminate chain elongation. They have been shown to be very useful in patients with resistant strains of HIV. For example tenofovir, also known as Viread showed a reasonable reduction in HIV RT levels through week 96.[64] Tenofovir is a prodrug that requires deacylation prior to the phosphorylation steps.

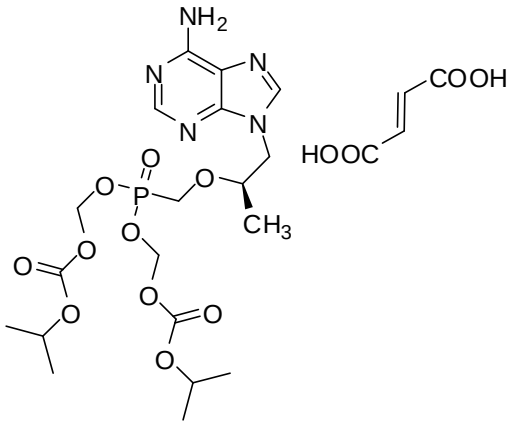

Tenofovir (Viread)

Azidothymidine (AZT) (Figure 2) was the first drug to be approved by the FDA for AIDS therapy.[4] It exhibited efficacy in lowering mortality rate and reducing the frequency of opportunistic infection during an administration period of 24 days. Further studies confirmed that prolonged therapy delayed disease

progression and lowered viral load significantly. Although AZT caused severe side effects such as bone marrow suppression, its therapeutic abilities were far more valuable than its side effects. The approval of AZT changed HIV infection from a definite death sentence to a chronic disease. Following AZT, 2′,3′-dideoxycytidine (DDC) and 2′,3′-dideoxyinosine (DDI) were reported to have anti-HIV activity. Both were effective in adults and children and were later approved by the FDA; however, their approval came with restrictions. DDC was only to be administered in combination with AZT, and DDI was only approved for patients who have developed resistance or intolerance to AZT.[82, 83] Another NRTI that was FDA approved for anti-HIV therapy is 2′,3′-didehydro-2′,3′-dideoxythymidine (D4T, stavudine, Zerit). In more recent years other NNRTIs have emerged to play a key role in combination HIV therapy. Emtricitabine, 2′,3′-dideoxy-3′-thia-5-fluorocytidine ((-)-FTC) was approved by the FDA in July 2003. It has proved to be one of the best HIV drug candidates on the market because it works synergistically with a variety of anti-retrovirals, has a long cell half life, and therefore can be administered once daily. It also has excellent bioavalability and has 4–10-fold higher in vitro efficacy compared to other NRTIs.[65] Figure 2 shows structures of different NRTIs.

(b) Non-nucleoside Reverse Transcriptase Inhibitors. HEPT (1-[(2-hydroxyethoxy)methyl]-6-(phenylsulfanyl)thymine) and TIBO (4,5,6,7-tetrahydroimidazole[4,5,1-jk][1,4]benzodiazepine-2(1H)-one and –thione) are the first two non-nucleoside reverse transcriptase inhibitors to be identified. They

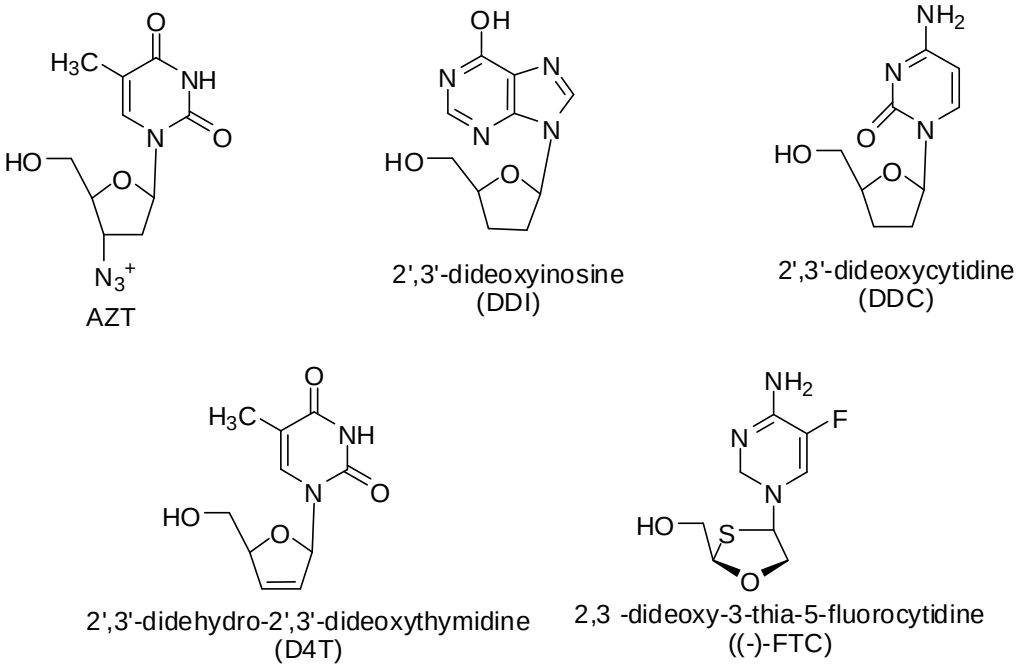

Figure 2. FDA approved nucleoside reverse transcriptase inhibitors

exhibited specific activity against HIV-1, but not HIV-2, and they were identified as reverse transcriptase inhibitors.[84]

HEPT was originally tested in 1987 for its activity against herpes simplex virus (HSV). It was found to be inactive against HSV; however, it displayed marked activity against HIV-1 RT. Following the original HEPT compound (TS-II-25), other derivatives were synthesized such as E-BPU and E-EBU-dM. The most significant HEPT derivative of all is MKC-442 (also known as I-EBU or emivirine). It was designed using structure–activity relationship studies. In early clinical studies, emivirine exhibited great bioavailability and no mitochondrial, bone marrow or reproductive toxicity. It was moved quickly to phase II studies; unfortunately, its development was discontinued.[85] Further SAR studies led to the development of more flexible HEPT derivatives such as TNK-6123. The major change in TNK-6123 is the presence of a cyclohexylsulfonyl group on C6 as opposed to a benzyl group. This was thought to give a larger range of motion for the compound so it can adapt to mutated RT pockets. This proved to be true as TNK-6123 showed 30-fold increase in activity as compared to MKC-442, and it maintained activity against the K103N and Y181C mutants.[37] Another set of HEPT derivatives are the 2-alkoxy-6-benzyl-3,4-dihydro-4-oxopyrimidines (DABOs) and 2-(cyclohexylsulfanyl)-3,4-dihydro-5-mehtyl-6-(3-methylbenzyl)-4-oxopyrimidines (S-DABOs). A few of these compounds had comparable potency against HIV-1 RT to that of MKC-442, but none superceded it. These compounds are considered to be good candidates for microbicide use. Unlike

their nucleoside reverse transcriptase counterparts, they do not just delay HIV replication. They completely suppress it for up to 40 days.[86]

In 1989 TIBO derivatives were discovered through a national screening program. TIBO's discovery led to the characterization of the allosteric pocket in which NNRTIs bind, now known as the non-nucleoside inhibitor binding pocket (NNIBP).[87] Interestingly, TIBO and HEPT were structurally different; however, they shared some common features. Both had a bridge or body, and two hydrophobic (either aromatic or aliphatic) "wings." Crystallographic studies proved that these compounds took on a butterfly-type conformation when bound in NNIBP.[88, 89] Following TIBO and HEPT, derivatives of other structurally unrelated compounds were identified as NNRTIs. Three were approved by the FDA, nevirapine (Verimune), delivaridine (Rescriptor) and efavirenz (Sustiva).[85]

NNRTIs have a unique specificity to HIV-1 RT regardless of the natural substrates present in the active site. This suggests that these inhibitors make contact within an enzyme site that is independent of the active site. They are also very specific to HIV-1 RT, and display little to no activity against HIV-2 SIV or cellular DNA polymerases α,β and γ. Chimeric enzymes of HIV-1/HIV-2 RT and HIV-1/SIV RT have been reported. The exchange of certain amino acids in HIV-2 and SIV with HIV-1 residues renders these RTs more sensitive to NNRTIs.[90-94] This suggests that amino acids that are present in HIV-1 and not in HIV-2 or SIV are important for NNRTI activity. Although this feature poses a challenge in making NNRTIs that are active against both HIV-1 and HIV-2 RTs, it also contributes to their low toxicity and high bioavailability.[5, 95-101] It is worth noting

that NNRTIs active against wt HIV-1 RT have also exhibited activity against some mutant HIV-2 RT. The main difference between HIV-1 and HIV-2 RT is the residues forming the allosteric binding pocket. In wt HIV-1 RT these are mainly hydrophobic aromatic residues, while in wt HIV-2 RT they are primarily aliphatic residues. In some mutant HIV-2 RT stratins, some residues mutate to aromatic hydrophobic amino acids, which makes it easier for wt active NNRTIs to bind; therefore, some activity is observed.[102, 103] Figure 3 shows structures of relevant NNRTIs.

F. The Non-nucleoside Reverse Transcriptase Inhibitor Binding Pocket

NNRTIs bind to an allosteric pocket located 10–15 Å away from the active site that is related structurally and functionally to the active site (Figure 4). The pocket lies in the p66 palm domain. It is mainly a hydrophobic pocket comprised of the β-sheet (β4,β7,β8), more specifically amino acids 105–110, 179–191 and β9,β10 and β11 amino acids 224–241, as well as residues 98–104 preceding β4 and residues 138,139,141 and 318. The roof of the pocket is lined by aromatic residues Tyr181, Tyr188 and Trp229. The walls are lined with Leu100, Val106 and Leu234; the floor contains the Lys101–Lys103 domain. The putative entrance of the NNIBP is thought to consist off Pro-95, Leu100, Lys101, Lys103, Val179 and Tyr181.[104] These residues are involved in an intricate hydrogen-bond network that might act like a “gatekeeper” keeping inhibitors out. Inhibitors that are successful in entering the pocket must be able to overcome the energy barrier required to break these hydrogen bonds. Steered molecular dynamic

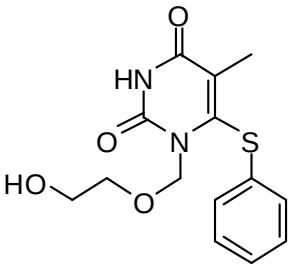

HEPT

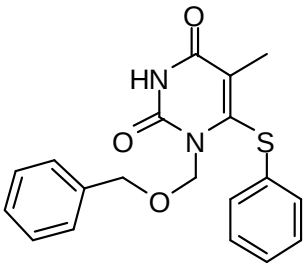

E-BPU

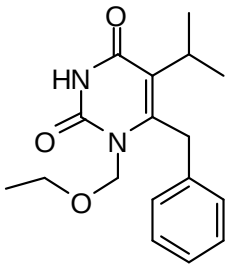

I-EBU
MCK-442
Emivirine

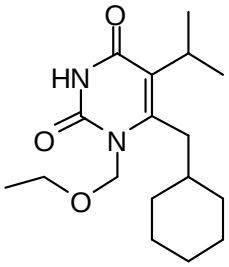

TNK-6123

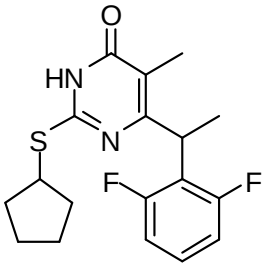

S-DABO derivative

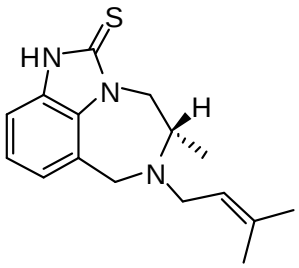

TIBO

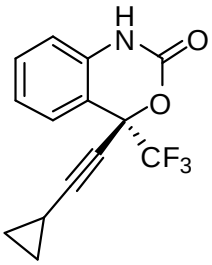

Efavirenz

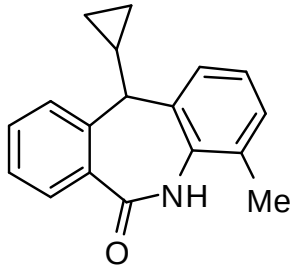

Nevirapine

Figure 3. Structures of non-nucleoside reverse transcriptase inhibitors

studies suggest that this could be accomplished by inhibitor–residue hydrogen bond formation or very strong hydrophobic interactions.[104].

Pro225 and Pro236 form the mouth of the pocket which is thought to essentially "close the door" after NNRTIs have entered.[87, 105, 106] Glu139, Thr138 of p55 play a structural role and lie left of the pocket.[33, 38, 107, 108] In general a NNRTI causes a conformational change in the β-sheet of p66 subunit locking the catalytic triad, Asp110, Asp185, and Asp186, into an inactive conformation similar to that in the noncatalytic p55 subunit, as well as locking the thumb subdomain into the inactive upright position.[105] The binding pocket does not exist in the unbound RT. In the presence of a NNRTI dramatic conformational changes occur in the pocket residues. The most noticeable change is the rotation of Tyr181 and Tyr188 side chains upwards towards the catalytic triad and the β-sheet, formed by β4,β7, and β8, shift ~2 Å.[104] This results in a decrease in catalytic activity and is considered to be the basis of NNRTI inhibition.[5, 37, 87, 105, 109]

Although structurally diverse, most NNRTIs adopt a butterfly conformation when bound to HIV-1 RT.[5] Schafer and co-workers were first to provide evidence of such conformation.[88] At the time no crystal structures of NNRTIs bound to HIV RT were available; however, through conformational studies of three inhibitor crystal structures, they found that all three inhibitors adopt a rooftop-like conformation, or "butterfly conformation." Later on, many other NNRTIs were designed to fit this conformation.[110-112] The major features needed

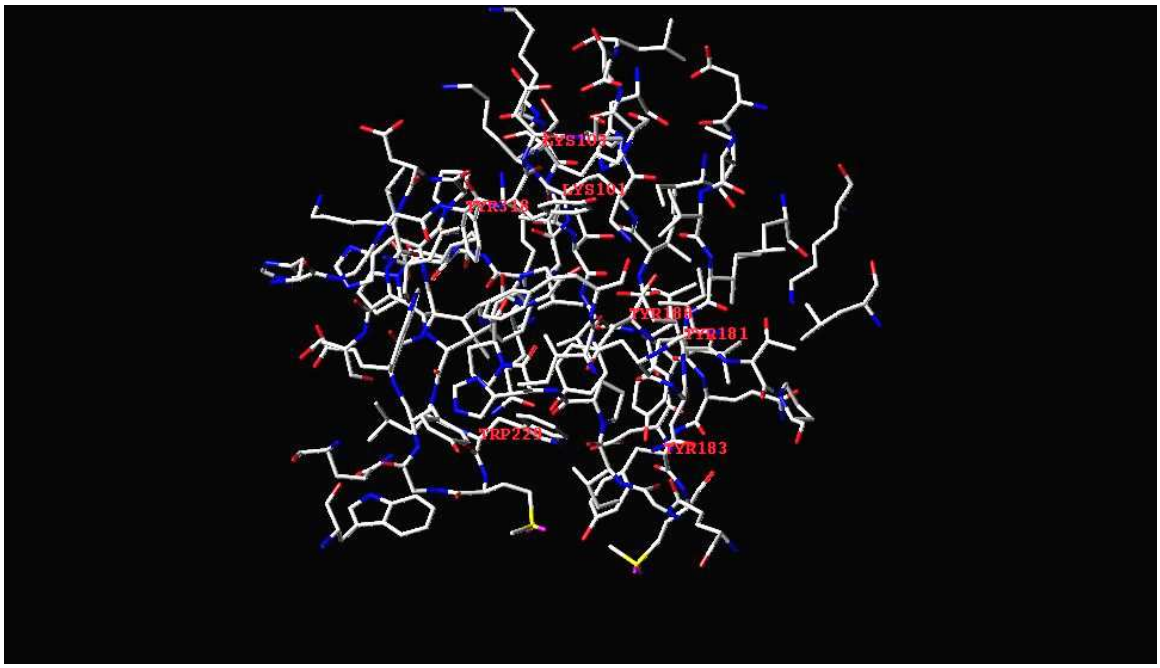

Figure 4. The non-nucleoside reverse transcriptase inhibitor binding pocket (NNIBP).

for a compound to fit the butterfly conformation are (i) two π-systems, (ii) a body or bridge that connects these two systems, usually with a thiocarbonyl, carbonyl, or sulfonyl moiety, (iii) a methyl, or alkyl, group on the meta-position of the extended π-system. The key feature that all these inhibitors share is the rigid ring structure.[88] In more flexible NNRTIs the butterfly conformation is less obvious, or in some cases nonexistent.[5]

Each NNRTI differs slightly in its interaction with the binding pocket. The π–π interactions with Tyr181, Tyr188, Trp229, and Tyr318 are the most important interactions, followed by electrostatic interactions with Lys101,103 and Glu138. With the exception of nevirapine, all NNRTIs form hydrogen bonds with at least one of these residues. The van der Waals interactions with Leu100, Val106, Val179, Tyr181, Cys190, Trp229, Leu234, and Tyr318 are also important in stabilizing NNRTIs in the pocket.[5]

Hydrogen bonding has especially proved to be important for efavirenz in maintaining its activity against the clinically relevant Y181C strain.[113] Generally, a hydrogen bond requires a distance less than 3.2 Å and an angle of 120º ± 30º. The presence of a hydrogen bond adds ~2.5 kcal/mol to the binding energy, further stabilizing the NNRTI/pocket complex.[114]

G. NNRTI-Induced Mutations

The first NNRTI-induced mutations discovered were the K103N (Lys103→Asn103) and Y181C (Tyr181→Cys181) strains. These two mutations rendered RT resistant to all NNRTIs. More specific mutations to individual inhibitors have been observed as well, for example HEPT, derivatives induce

K103N, V108I and Y181C mutations.[115] Other mutations that are observed are G190E, L100I, V106A, L74V, V75I, L100I, E138K, and P236L.[84] Although mutations make NNRTIs less attractive as therapeutic options, some of these compounds such as MKC-442 and efavirenz maintain good activity against mutant RT strains.[84] Efavirenz maintains its activity levels in mutant strains V108I, E179D, Y181C as in wt HIV-1 RT.[116] Severe resistance to NNRTIs in patients is only observed with double mutant strains; however, it is unclear how quickly these double mutations arise in vivo in patients under NNRTI therapy. Some of the most common double mutations are L100I/K103N, K101D/K103N, and K103N/Y181C.[84] Mutant RT's resistance to NNRTIs varies from one inhibitor to another. In other words, some mutations may cause little effect on one inhibitor but render others completely inactive. Table 1 shows resistance mutations that appear in patients taking NNRTIs as part of there HIV therapy.[5] Each of these mutations elicit a different reaction from the three FDA-approved NNRTIs. [5] Interestingly, RT's resistance profile to NNRTIs differs completely from resistance to NRTIs. All NNRTI mutations occur in the NNIBP pocket, while NRTIs mutations occur all over the RT enzyme, and strains resistant to NNRTIs maintain their activity against NRTIs and vice versa.[5] This further stresses the importance of combination therapy.

H. Sultams: A novel class of NNRITs

Gussion and co-workers based their molecular modeling study on a low-resolution (2.9 Å) crystal structure to generate an all-atom molecular model of th

Table 1. Resistance mutations in patients treated with nevirapine(NEV), deliviradine (DLV), and efavirenz (EFV).[5]

Amino Acid Mutations	NNRTI that may select for the mutation
98-Ala→Glu	NEV
100Leu→Ile	NEV, DLV,EFV
101-Lys→Glu	EFV
103-Lys→Asn/Thr	NEV,DLV,EFV
106-Val→Ala	NEV,DLV
108-Val→Ile	NEV,DLV
135-Ile→Met/Thr/Leu	EFV
179-Val→Asp/Glu	EFV
181-Tyr→Cys/Ile	NEV,DLV,EFV
188-Tyr→Cys/His/Leu	Nev,DLV,EFV
190-Gly→Glu/Ala/Ser	NEV,DLV,EFV
225-Pro→His	EFV
233-Glu→Val	DLV
236-Pro→Leu	DLV
238-Lys→Thr	DLV

NNIBP. A pocket was generated from the reverse transcriptase crystal Cα coordinates.[117]

This was followed by docking experiments of nevirapine and a few other analogues in order to identify elements of a pharmacaphore. Following the identification of key functional groups in the pharmacaphore, a search on the NCI database of over 200,000 compounds produced 300 hits. The search was then modified to give 33 compounds including nevirapine and NSC119833 (Figure 5).

Further NCI database searches and 3D QSAR (quantitative structure–activity relationship) studies paired with biological testing of the hit compounds led to the identification of NSC-108406 (Figure 5) with an $IC_{50} \pm 0.3$ μM. Watanabe and co-workers were the first to report a synthetic route to sultam family of which of NSC-108406 is a member.[118] Further work in our labs developed several synthetic routes to over 65 analogues of these sultams.(Work unpublished).

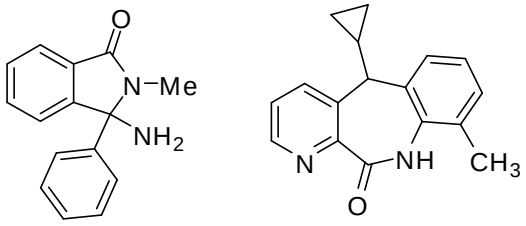

NSC119833 Nevirapine NSC-108406

Figure 5. Structures of NSC119,833, nevirapine and NSC-108,406.

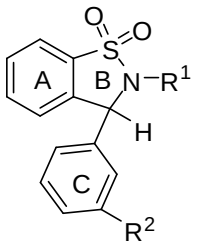

Figure 6. General structure of sultams developed by the Baker group

Sultams are derivatives of isothiazoles with an aromatic ring fused at C4 and C5. The sultams developed in our lab have the general formula shown in Figure 6 above. The numbering begins with the sulfur atom. Both rings A and C are aromatic rings, while ring B is a heterocyclic ring. The nitrogen is either secondary or *tert*iary depending on the nature of R^1. R^2 in the *meta*-position on ring C varies in functionality. In some derivatives ring A was substituted at C6, C7 or both. The general synthetic route to these sultams is outlined in Scheme 1

Scheme 1

.

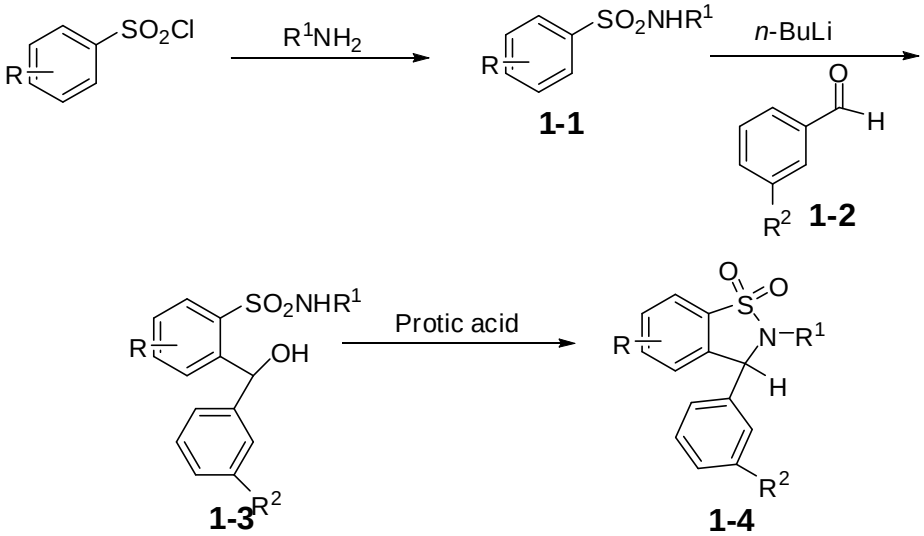

The synthesis commences with the coupling of a substituted benzenesulfonylchloride to a primary alkyl amine. Lithiation at the *ortho*-position (termed *ipso* lithiation) is established using an alkyllithium reagent such as *n*-butyllithium. The lithiated species is then coupled to an aryl aldehyde (**I-2**), and then cyclization is accomplished by using a protic acid to afford a racemic mixture sultam **I-4**. The racemate was then separated with chiral HPLC, and the enantiomers were submitted the NCI for anti-HIV studies.[119]

Synthesis of sultams with halogen substitution required a modification to the original route. The use of alkyllithium reagents for coupling is not suitable due to the presence of a halogen on ring A. Lithium–halogen exchange can occur, which may lead to other side reactions and unwanted products. Halogen-subsitituted *o*-aminobenzophenone (**2-1**) undergoes diazotization using HONO. SO_2 is then added in the presence of ionic copper to form the sulfonyl functionality. Condensation of (**2-2**) leads to the cyclization of the isothiazole ring (**2-3**). Hydrogenation of the imine functionality, followed by alkylation gives the desired sultam (**2-5**) in a racemic mixture (Scheme 2).

To synthesize sultams with substitutions on ring C, yet another synthetic route had to be devised (Scheme 3). 2,4-Dimethoxyphenyl-(4-methoxyphenyl) methylamine is condensed with benzenesulfonylchloride. The product is lithiated and coupled to an aryl aldehyde or ketone. The monoalkylated and dialkylated compounds are isolated, and both are cyclized using a strong protic acid to give the desired sultam.[119]

Scheme 2

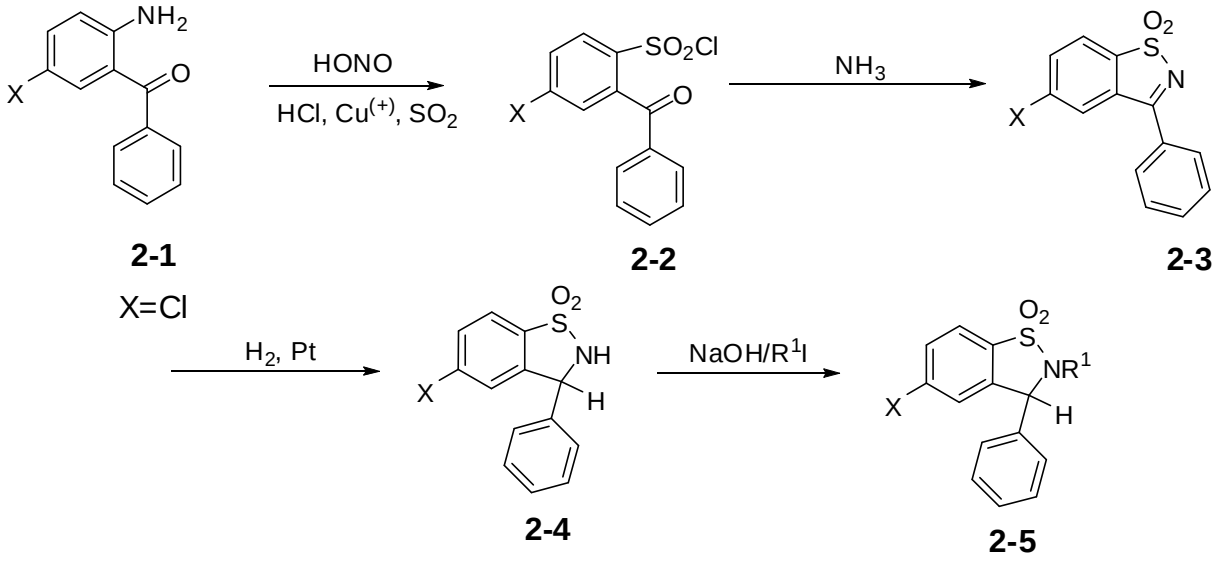
NH2
X
O
HONO
HCl, Cu(+), SO2
SO2Cl
X
O
NH3
O2
S
N
X
2-1
X=Cl
2-2
2-3
H2, Pt
O2
S
NH
X
H
NaOH/R1I
O2
S
NR1
X
H
2-4
2-5

Scheme 3

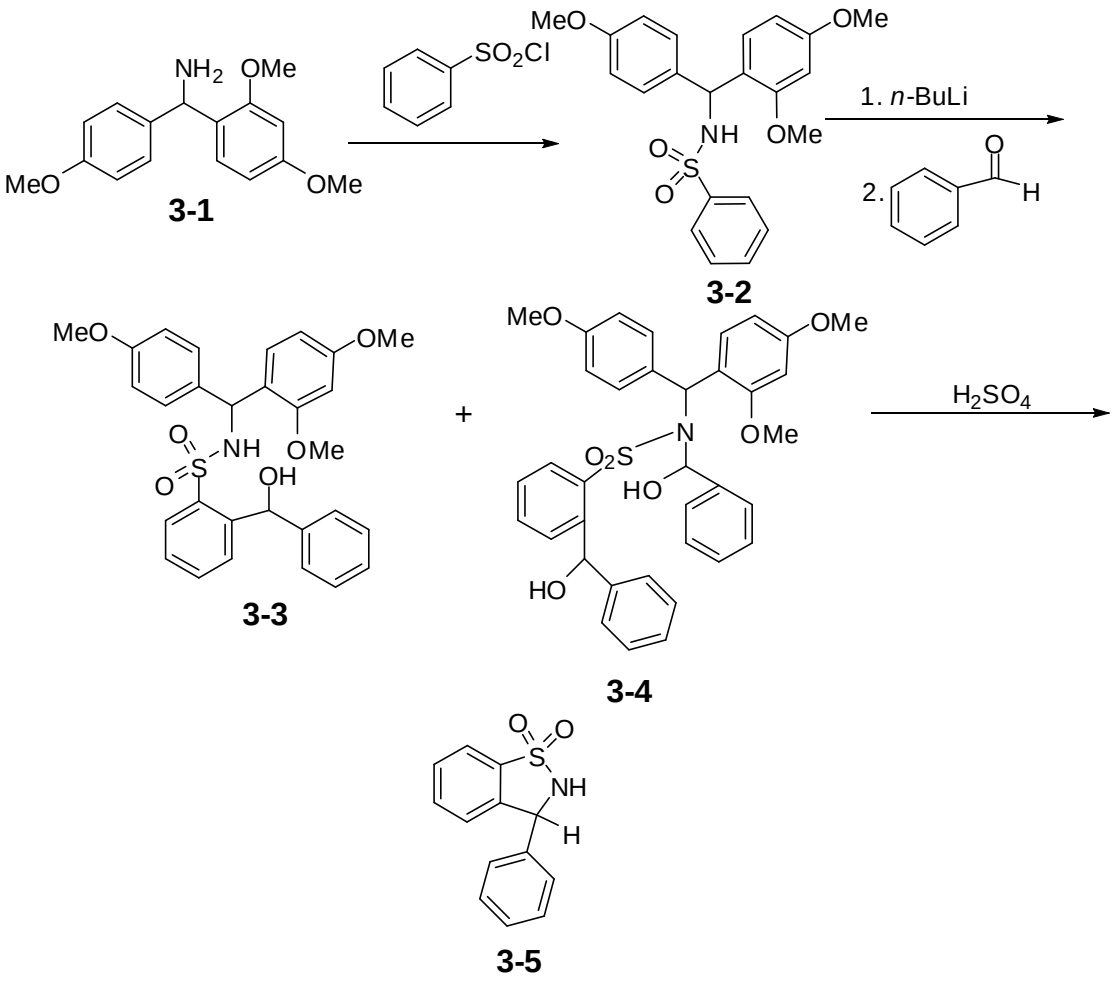
NH2
OMe
MeO
OMe
3-1
SO2Cl
MeO
OMe
NH
OMe
O
S
O
1. n-BuLi
2.
O
H
3-2
MeO
OMe
O
NH
OMe
S
O
OH
3-3
+
MeO
OMe
N
OMe
O2S
HO
HO
3-4
H2SO4
O
O
S
NH
H
3-5

Another class of sultams is those with a CF_3 group at C3. The synthetic route leading to such compounds begins with the coupling of *tert*-butylamine with benzenesulfonyl chloride (**4-2**). Alkylation of the resulting sulfonamide (**4-3**) is afforded by treatment with sodium hydride and iodomethane. The resulting product is then lithiated and coupled to an aryl ketone. Sulfuric acid catalyzed cyclization produces the desired

Separation of these racemates was accomplished either by chiral HPLC using a Chiralcel OD column or by derivitization of these compounds into their diastereomers, then separation through chromatography and recrystallization.

Scheme 4

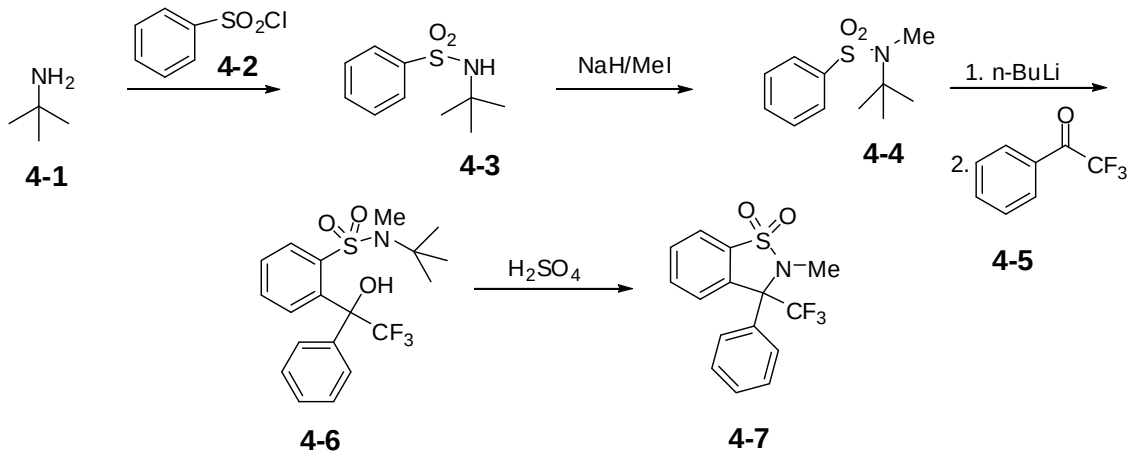

Scheme 5

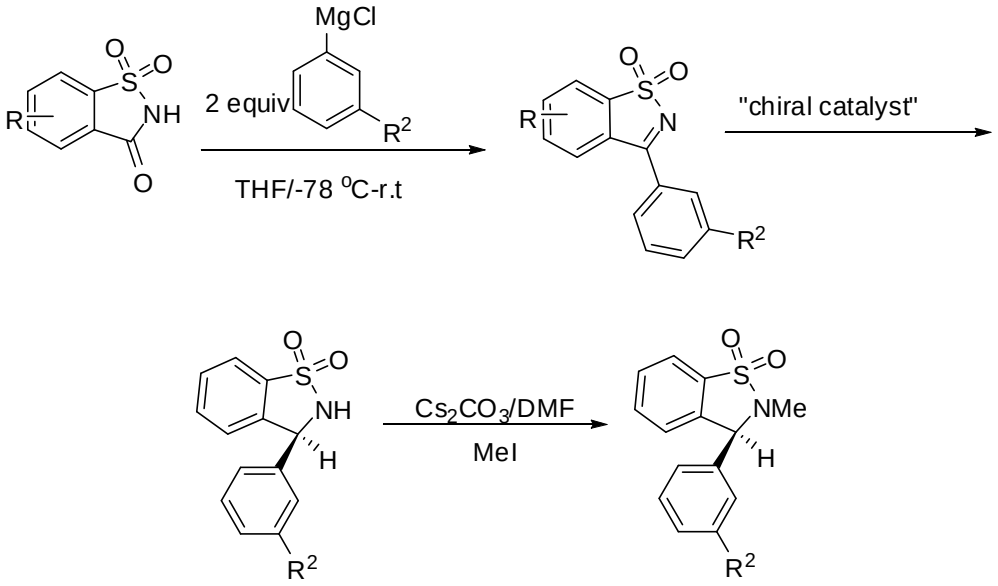

Biological studies of all of these compounds showed decreased activity when the A ring was substituted. The preferred substitution on ring C was the *meta*-position. In order to synthesize additional sultams with substituents on the *meta*-position of ring C, another synthetic route was devised. In this route saccharin was used to install rings A and B. It was coupled with an aryl Grignard reagent to give 3-aryl-1,2-benzisothiazole 1,1-dioxide. The C=N imine bond was then reduced enantioselectively to give enantiomerically pure products. Methylation using Cs_2CO_3 and iodomethane gave the desired sultams (Scheme 5).

A report in *C & E News* suggested that rhodium can be used to give racemic mixtures in various amine reductions.[155] Using pentamethylcyclopentadienyl as a ligand in place of the η^6-arene ligands that were traditionally used in such complexes,[121] especially in the Noyori ruthenium catalyst for C=O and C=N hydrogenations. Our laboratories designed and

prepared a chiral Rh-Cp* complex. Pentamethylcylopentadienylrhodium chloride dimer {[Cp*$RhCl_2$]$_2$} was coupled to (1*R*,2*R*)-*N*-*p*-toluenesulfonyl)-1,2-diphenylethylenediamine {(1*R*,2*R*)-TSDPEN} to afford the *R,R*-catalyst and (*1S,2S*)-TSDPEN was used to prepare the *S,S*-catalyst. Although the catalyst is considered to possess three chiral centers, the metal and the two centers on the TSDPEN ligand, it will be refered to as *S,S* when the *S,S*-ligand is used and *R,R* when the *R,R*-ligand is employed. The structure of the *R,R*-catalyst was confirmed with X-ray crystallography, and its activity was tested on a variety of compounds. Although the resulting enantioslectivity is modest, simple recrystallization methods of these enantio-enriched mixtures afforded the pure enantiomers. Polar solvents were preferred; however, dichloromethane was just as efficient and the enantioselctivity was not affected. The most suitable proton source was found to be formic acid/triethylamine azeotrope. Reactions failed when 2-propanol/triethylamine was used. The substrate-to-catalyst ratio (S/C) is 200:1, while the Noyori catalyst requires a ratio of 100:1. Reactions times were short, and yields were very good. The enantioselectivity of this catalyst proved to be interesting. Generally, the *S,S*-catalyst produced the *R* product and vice versa; however, this observation is greatly affected by the nature of the substrate. The bulkier groups such as the sultams with an aromatic C ring followed this phenomenon, and the smaller compounds such as sultams with alkyl groups in place of ring C gave the opposite results.[122] It is worth noting that this catalyst exhibited very good stability, and was not hygroscopic or sensitive to

air as many similar complexes are. It also remained active at low temperatures, and higher temperatures did not seem to affect its enantioselectivity or activity.

With the short synthetic route using saccharin, and the enantioselective catalyst at hand, we have designed and prepared new sultams with potential anti-HIV activity.

II. Statement of the Problem

AIDS is currently the largest worldwide epidemic known in this century. In an effort to join the many medicinal chemists in their battle against AIDS, we plan to use computer-aided docking experiments to design new sultams that will be active against wild-type reverse transcriptase (wt RT), as well as mutant RT, in particular the Y181C RT strain. Using RT crystal structure coordinates, the target sultams will be docked into the allosteric pocket of RT, and flexible docking (FlexiDock) experiments performed, using genetic algorithms to find the lowest energy conformation. The results will be analyzed for distances between the ligand and key residues and hydrogen bonding sites. While the calculated energies produced by FlexiDock in the SYBYL program are not real, they will serve as relative references to compare different fits. A synthetic route will then be designed leading to the synthesis of these compounds. From the modeling studies a set of compounds based on our 2,3-dihydro-3-(*m*-methylphenyl)-1,2-benzisothiazole 1,1-dioxide and Merck's efavirenz will be examined. The best candidates structures will then be synthesized for evaluation.

In the course of this work, we will collaborate with Professor John Turner and his student Megan Bragg on some NMR studies of the rhodium catalyst to identify the catalytic cycle. While Turner and co-workers will study the catalytic cycle through variable-temperature NMR studies, as well as some 2D experiments, we will attempt to further support their findings through molecular modeling studies. The same principles of docking a substrate into an enzyme will be used. Various sultams will be docked into the catalyst. The complex will

then be minimized and analysis of bond lengths and angles used to predict interactions.

III. Results and Discussion

A. Modeling

1. The Tripos Force Field

The four major components in the energy expression of the Tripos force field are the following:[123-125]

(a) Stretching energy expression: the energy of a bond stretched or compressed from its original bond length.

$$E_{str} = \sum E_{str}\,(1/2)k_i^{d}\,(d_i - d_i^{0})^2$$

d_i = the length of the ith bond (Å)

d_i^{0} = equilibrium length of the ith bond (Å)

k_i^{d} = Bond stretching of force constant (kcal/(mol)(Å)^2)

(b) Angle-bending energy term: the energy from bending bond angles out of their natural values.

$$E_{bend} = \sum E_{bend}\,(1/2)\;k_i^{\theta}(\theta_i - \theta_i^{0})^2$$

θ_I = angle between two adjacent bonds

θ_i^{0} = the equilibrium value of the θ

k_i^{θ} = angle force constant (kcal/(mol)(º)^2)

(c) Out-of-plane bending energy term: energy of bending planar atoms out of their plane.

$$E_{oop} = \sum E_{oop}\,(1/2)k_i^{oop}\,d_i^{2}$$

d_i = distance between the center atom and the plane of its substituents.

K_i^{oop} = the force constant for out of plane bending (kcal/(mol)(^{o})^2

(d) Torsional energy term: energy due to twisting around bonds.

$$E_{tors} = (1/2)\, V_i^{\omega}[1+S_i\cos(|n_i|\cdot\omega_i)]$$

V_i^{ω}= Torsional barrier (kcal/mol)

S_i = +1 minimum energy when staggered, –1 minimum energy when eclipsed

n_i = Periodicity

ω_l = torsion angle

(e) van der Waals energy term: energy resulting from van der Waals interactions.

$$E_{vdw} = \sum_{i=1} \sum_{i>j} E_{ij}\left[(1.0/a_{ij}^{12})-(2.0/a_{ij}^{6})\right]$$

E_{ij} = van der Waals energy constant (kcal/mol)= $(E_iE_j)^{1/2}$

$a_{ij} = r_{ij}/(R_i + R_j)$

r_{ij} = distance between atoms i and j (Å)

R_i = van der waals radius for the atom I (Å)

The Tripos energy expression also contains optional terms such as energy from electrostatic interactions and energies from distant, angle and torsional constraints as well as a multifit energy term associated with multifits. These expressions are only used when information about them is specified. In the FlexiDock modeling studies described here and in the simple minimizations done on the sultams, no constraints were defined prior to the calculations; therefore,

these energy terms were not used in these calculations. However, distance and angle constraints were used in the rhodium catalyst molecular modeling studies so some of these terms were automatically incorporated into the calculations. It is important to keep in mind that any energy produced by a force field is not real, meaning it holds no physical value for individual conformations. Energy values are used as points of reference to compare different conformations for a given molecule as well as difference among a set of similar molecules.

The Tripos force field was used in its default parameters for all inhibitor/protein docking experiments. For the rhodium catalyst calculations parameters for the rhodium metal center were added from the SYBYL metal database provided to all users.

2. Charges

All small-molecule charges were calculated using the Gasteiger-Hückel method, which is a combination of two calculations. The π charge is assumed to be delocalized on all π atoms and calculated first using the Hückel method,[126] and then the σ charge is calculated using methodology outlined by Gasteiger and Marsili.[127, 128]

All protein charges were calculated using the Pullman and Berthod method, which is a combination of two methods, the Del Re method for σ charge calculation and the Hückel method for the π charge calculation.[129, 130]

3. FlexiDock

FlexiDock is a docking program that utilizes crystal structure coordinates of known protein/inhibitor complexes. The protein atoms are fixed coordinates in

space, while the ligand is mobile, i.e., rotation and translation of the ligand in space can be applied. The protein residue side chains can be designated as flexible. To achieve faster calculation times, only single non-ring bonds and amide bonds were allowed to flex (rotate). FlexiDock uses the Tripos force field (ff) to calculate energies of the different conformations generated by the genetic algorithm. The default parameters between the two force fields are essentially the same; however, a few differences are present and they are summarized in Table 2 below.

FlexiDock uses a steady-state genetic algorithm to generate, propagate and reproduce these genes. Genetic algorithms are global optimizers that employ terminology and methodology from Mendelevian hereditary practices and Darwinian evolutionary theories in which the most fit members of a population are allowed to propagate into future generations.

Table 2. Default Settings in FlexiDock and Tripos Force Field (from SYBYL FlexiDock Manual).

Default Condition	FlexiDock	Tripos Force Field
Hydrogen van der Waals radius	1.0 Å	1.5 Å
Hydrogen van der Waals Є	0.03	0.042
van der Waals distance cut off	16.5 Å	8.0 Å

The algorithm begins with the formation of the initial population of chromosomes. A chromosome is a set of possible torsional, translational, and rotational positions a flexible bond might have. The number of genes on each chromosome depends on the number of rotatable bonds specified. The chromosomes are then evaluated for energy using the the Tripos ff. The best fit members of a population are then allowed to mutate or cross over. The new generation is then evaluated again for energy values and so on and so forth.[131] The purpose of FlexiDock calculations is to explore the diverse solution space available for a specific problem. FlexiDock monitors this diversity by monitoring the percent of gene convergence. When 95% of the genes have converged, the calculation terminates, and the best twenty solutions are placed in a molecular database. The number of generations used in a FlexiDock run depends on the number of flexible bonds designated by the user. A more flexible ligand/protein complex requires a larger number of generations. It is agreed that a minimum of 500 to 1000 generations per gene are required to produce reasonable results.[131] A gene is the total number of flexible bonds in the ligand and the protein plus six. The default setting for FlexiDock is 3000 generations. This value assumes there are no flexible bonds in the ligand or protein; therefore:

$$(0 + 6)\ (500) = 3000$$

In the FlexiDock experiments reported here the average number of bonds being flexed in both protein and ligand were around 50 bonds. This means a minimum of 28,000–56,000 generations are needed to produce some results. This of course is a minimum value and a higher number of generations is

acceptable. To allow a larger solution set to be discovered the maximum number generations was 130,000. Each complex was minimized at least three times at varying seed numbers. This allows FlexiDock to explore a wider range in the solution space. Each run gave 20 solutions, and all 60 solutions for each of these runs were evaluated quantitatively and qualitatively. A hydrogen-bond site was not specified in these studies. Distances and angles between potential hydrogen donors and acceptors were evaluated.[114] Based on these results, hydrogen bonding was predicted between the ligand and certain residues in the pocket.

4. Preparing the Protein

Two major FlexiDock studies were prepared using wt RT and Y181C RT bound to efavirenz (pdb code 1ikw, 1jkh).[132, 133] The crystal structures were obtained from the protein databases. Efavirenz was extracted and deleted from the crystal structure. Hydrogens were added at random orientations, and Pullman charges were calculated for each protein. A minimization was performed where the protein is treated as an aggregate or rigid structure and the hydrogens are considered flexible. This was necessary to optimize the position of the added hydrogens. Minimizations on the protein crystal structures were attempted; however, these studies did not yield any major differences in the orientation of the protein backbone.

5. Defining the pocket

The non-nucleoside inhibitor binding pocket (NNIBP) was defined based on available biochemical and molecular modeling data.[31, 88, 108, 109, 134-136] Hydrophobic interactions require a distance between the ligand and the residue

of 4 Å.[114] Weaker binding interactions do occur at distances larger than 5 Å; however, any residue that is more than 10 Å away is not considered for binding. Such residues may be important for binding pocket formation or structural stabilization but not direct ligand–residue interactions. The pocket was defined as a sphere with a radius of 10 Å and the inhibitor at its center. Manual inspection of the residues included in this sphere showed that all the key residues that form the NNIBP are present (see The non-nucleoside reverse transcriptase binding pocket section in the Introduction).

6. Preparing the sultams

All sultams were sketched using the Sketch Molecule menu in SYBYL. Hydrogens were then added and Gasteiger–Hückel charges were calculated. A quick minimization was then employed to minimize the adjust bond lengths and angles that may have been distorted during the sketching process.

7. Docking the sultams

In docking experiments it is very helpful to have a starting position that the inhibitor can be placed in. Efavirenz coordinates in the crystal structure were used to position the sultam inhibitor. The sultam was superimposed on top of efavirenz while it was still in the pocket and a three-atom fit was performed. Efavirenz was then deleted from the sequence, and the sultam merged into the enzyme. This technique provides a better pre-positioning of the inhibitor and eliminates the cumbersome process of manually docking inhibitors into the pocket. RMS values for the sultam/efavirens fit are reported in Table 3.

Table 3. RMS values for sultam/efavirenz fit

Sultam	RMS
3-(Cyclopropylethynyl)-2,3-dihydro-2-methyl-1,2-benzisothiazole 1,1-dioxide	0.36
3-(Cyclobutyethynyl)-2,3-dihydro-2-methyl-1,2-benzisothiazole 1,1-dioxide	0.32
3-(*tert*-Butylethynyl)-2,3-dihydro-2-methyl-1,2-benzisothiazole 1,1-dioxide	0.29
3,3-Bis(cyclopropylethynyl)-2,3-dihydro-2-methyl-1,2-benzisothiazole 1,1-dioxide	0.32
3,3-Bis(cyclbutylethynyl)-2,3-dihydro-2-methyl-1,2-benzisothiazole 1,1-dioxide	0.32
3,3-(di-*tert*-Butylethynyl)-2,3-dihydro 2-methy 1,1-dioxide	0.32
3-(Cyclopropylethyl)-2,3-dihydro-2-methyl-1,2-benzisothiazole 1,1-dioxide	0.39
3-(Cyclobutylethyl)-2,3-dihydro-2-methyl-1,2-benzisohtiazole 1,1-dioxide	0.31

8. Preparing the FlexiDock File

The FlexiDock file is prepared by following a checklist provided by the FlexiDock menu:

(a) Define pocket: The pocket is defined as the NNIBP previously specified plus 1 Å around it.

(b) Extract ligand: Ligand is extracted and deleted from the protein sequence. This is done to allow each of these structures to be prepared separately.

(c) Remove water molecules: FlexiDock removes all water molecules that belong to the set {WATER}. These water molecules were generated when the pdb files were read in from the protein database.

(d) Check atom types: This provides an option to modify any atom types that may have been improperly downloaded from the pdb file. This was particularly common in previous SYBYL versions; however, the current version SYBYL7.2 has less of a problem.

(e) Add hydrogens: Since hydrogens were previously added on both the protein and ligand, no more hydrogens were added at this stage.

(f) Add charges: the charges for the protein and the sultam have been individually calculated so the charges do not need to be reloaded again

(g) Rotatable bonds: For the 3-(alkylethynyl)-2,3-dihydro-2-methyl-1,2-benzisotiazole 1,1-dioxide (alkylethynyl sultam series), the N-methyl bond was allowed to rotate. Flexible Residues: Lys101, Lys103, Tyr181or Cys181 (for Y181C mutant strain), Tyr183, Tyr188 (Cys188 for Y188C), Trp229, Tyr318 were all chosen to have flexible side chains. (See below for a discussion on the reasoning behind choosing these ligands).

(h) Specify hydrogen-bond sites: No hydrogen-bonding sites were pre-specified in these studies. The ligands were allowed to flex in the pocket without any H–bond constraints. Then using distances and angles between the ligands and hydrogen-bonding residues, we predicted the presence of a hydrogen bond.

(i) Pre-position ligand in the pocket: Since the sultam was fitted to the efavirenz coordinates in the RT pocket, it was not necessary to alter the ligand's position any further.

(j) Name file: Create a name for the FlexiDock File

(k) Write output file: this creates the FlexiDock file with the name specified in the previous step

(l) FlexiDock it: this begins the flexidock calculation.

Once the FlexiDock run is started, a random seed number is generated. All random seed numbers were noted. As mentioned earlier the number of generations used was 130,000 generations in each of the runs. Once FlexiDock was done, a set of twenty solutions are placed in a molecular database along with their energies.

9. FlexiDock Studies

The residues chosen for flexing are mentioned above. Each of these residues plays a key role in inhibitor binding. Lys101 forms hydrogen bonds with wt RT. Lys103 is part of the lysine triad Lys101–Lys103 (wing 1) and its orientation positions Lys101 for hydrogen bonding with the bound inhibitor. It is also involved in pocket formation. In the Lys103→Asp103 (K103N) mutant strain efavirenz looses a good percentage of its activity because Lys101's orientation is distorted and no hydrogen bond is formed.[137, 138] Tyr181, Tyr188 and Trp229 form the hydrophobic region of the pocket also known as the wing 2 region.[5, 85, 104] A number of π–π hydrophobic interactions form the basis of NNRTI binding to RT. Most inhibitors rely on the three main aromatic ring-stacking interactions; parallel (strong), staggered (medium) and T-shaped interactions (weak).

Tyr181→Cys181 is the most frequently occurring mutation observed in HIV patients receiving NNRTIs as part of their regimen. Trp229 is the only

conserved amino acid across all HIV-1 reverse transcriptase strains in wt RT as well as Y181C RT. Tyr318 is part of the wing 1 region, which is mostly comprised of non-aromatic residues such as the lysine triad. Analysis of the observed distances between efavirenz and Tyr318 in wt RT and Y181C RT suggests that this residue increases in importance as wing 1 loses some of its hydrophobic character in Y181C.

In order to keep calculation times within reason, the aforementioned residues were chosen to be the focus of the docking experiments. The NNRTI binding pocket formation and binding process is a flexible and complex process. As these residues open up to form the binding pocket, they cause both local and global movement in the enzyme leading to inhibition of activity. The FlexiDock studies reported here are localized studies and do not take into consideration the global effects on the overall protein conformation. The sultams shown in Figure 7 are considered to be structurally related to efavirenz. Analyses of the docking results were done in comparison to efavirenz and its position in the NNIBP pocket. Table 4 reports the distances and hydrogen-bond angles for efavirenz in (a) wt and in (b) Y181C RT.

In binding studies a hydrophobic interaction is considered strong if the distance between the ligand and residue is less than 4 Å. A distance between 4 and 5 Å is thought to cause a moderate binding interactions, and anything larger than 5 Å is classified as a weak binding interaction.[114] The FlexiDock cut off for van der Waals interaction is 16.5 Å; however, any distance greater than 10 Å will be considered negligible.

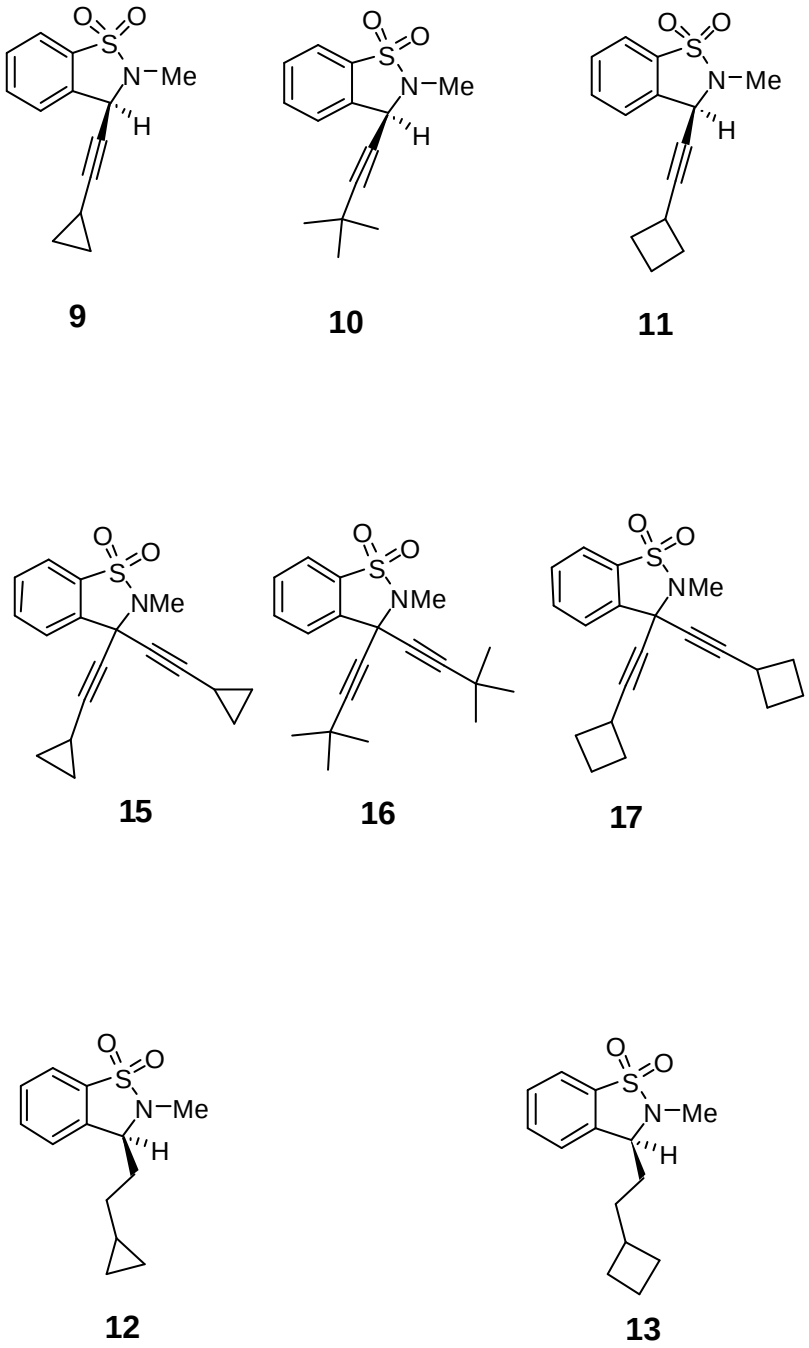

Figure 7. Structures of the alkylethynyl sultam series.

Table 4. (a) Distances and H-bond angle in the efavirenz/wt RT complex. (b) Distances and H-bond angle in the efavirenz/Y181C RT complex

a.

Efavirenz	Residue in wt RT	Distance (Å)	Angle of H-bond if present (º)
C=O	Lys101	2.06	98.55º
Cyclopropyl	Tyr181	2.544	
	Tyr183	7.23	
	Tyr188	5.96	
	Trp229	4.49	
Aromatic ring	Tyr318	5.84	

b.

Efavirenz	Residue in Y181C RT	Distance (Å)	Angle of H-bond if present (º)
C=O	Lys101	2.31	97.76
Cyclopropyl	Cys181	—	
	Tyr183	7.26	
	Tyr188	3.99	
	Trp229	4.04	
Aromatic ring	Tyr318	5.00	

Efavirenz forms a hydrogen bond in both the wt and Y181C RT with distances between the amide carbonyl in efavirenz and Lys101 at 2.06 Å and 2.31 Å for wt and Y181C, respectively, with angles of around 98º for both. Both angle and distance values are within what is needed for hydrogen bonding to occur in biological systems.[114] Efavirenz is known to cause selection for Y181C mutation. This is greatly supported by the significantly small distance, 2.54 Å, between the cyclopropyl group and Tyr181 in wt RT. In wt RT the cyclopropyl ring is almost 6 Å away from the Tyr188, but this distance is decreased by 2 Å in Y181C.

This occurs to compensate for the loss of the major hydrophobic interaction at Tyr181→Cys181. It is also worth noting that the cyclopropyl group becomes almost equidistant from both Tyr188 and Trp229 at 4 Å. The aromatic ring in efavirenz is 6 Å away from Tyr318, and it is positioned in a T-shaped orientation towards the ring. It could be hypothesized that the weakest type of π–π interaction, the T-shaped interaction, is occurring here. In Y181C the aromatic ring is closer to Tyr318 by 0.8 Å; however, its orientation does not change. Figure 8 shows the positions of efavirenz in both wt RT and Y181C Rt.

Tables 5–7 display the distances and hydrogen-bond angles (when hydrogen bonding is present) calculated by FlexiDock for 2-(alkylethynyl)-2,3-dihydro-2-methyl-1,2-benzisothiazole 1,1-dioxide (the alkyethynyl sultam series, compounds **9**–**11)**. The Flexidock calculations predict a hydrogen bond between the sulfonyl group of cyclopropylethynyl sultam (**9**) and Lys101. The distance observed after calculations is 2.10 Å and an angle of 115º.

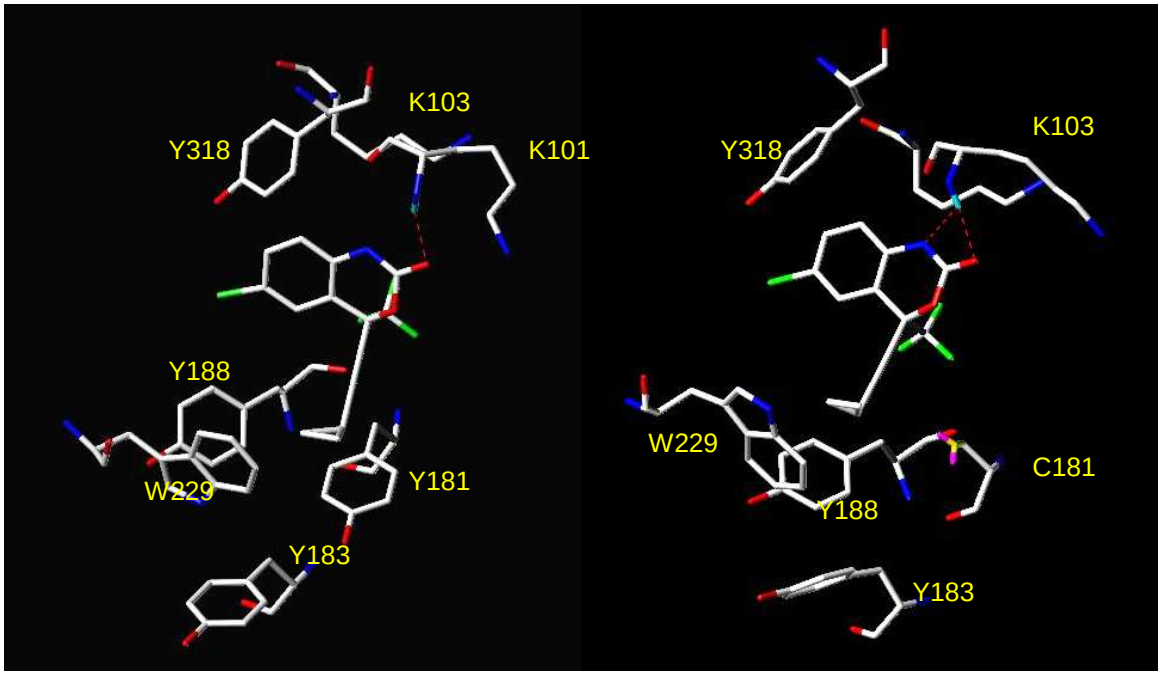

Figure 8. Efavirenz in wt RT (left) and Y181C (right).

Table 5. (a) Flexidock distances for cyclopropylethynyl sultam (9); (a) wt RT; (b) Y181C RT

5a.

Cyclopropylethynyl sultam	Residue in wt RT	Distance (Å)	Angle of H-bond if present (º)
SO_2	Lys101	2.10	115
Cyclopropyl	Tyr181	4.20	
	Tyr183	7.85	
	Tyr188	5.6	
	Trp229	4.54	
Aromatic ring	Tyr318	6.11	

5b.

Cyclopropylethynyl sultam	Residue in Y181C	Distance (Å)	Angle of H-bond if present (º)
SO_2	Lys101	2.19	119.06
Cyclopropyl	Cys181	—	
	Tyr183	7.86	
	Tyr188	4.32	
	Trp229	5.24	
Aromatic ring	Tyr318	4.86	

Table 6. FlexiDock results for *tert*-butylethynyl sultam (**10)** in (a) wt RT, (b) Y181C.

6a.

tert-Butylethynyl sultam	Residue in wt RT	Distance (Å)	Angle of H-bond if present (º)
SO_2	Lys101	3.00	—
tert-Butyl	Tyr181	5.09	
	Tyr183	7.88	
	Tyr188	4.3	
	Trp229	4.55	
Aromatic ring	Tyr318	4.91	

6b.

tert-Butylethynylsultam	Residue in Y181C	Distance (Å)	Angle of H-bond if present (º)
SO_2	Lys101	2.13	127
tert-Butyl	Cys181	–	
	Tyr183	7.19	
	Tyr188	4.19	
	Trp229	4.75	
Aromatic ring	Tyr318	4.74	

Table 7. FlexiDock results for cyclobutylethynyl sultam (**11**) in (a) wt RT and (b) Y181C RT.

7a.

Cyclobutylethynyl sultam	Residue in wt RT	Distance (Å)	Angle of H-bond if present (º)
SO_2	Lys101	4.27	—
Cyclobutyl	Tyr181	4.61	
	Tyr183	7.54	
	Tyr188	4.60	
	Trp229	4.01	
Aromatic ring	Tyr318	5.95	

7b.

Cyclobutylethynyl sultam	Residue in Y181C	Distance (Å)	Angle of H-bond if present (º)
SO_2	Lys101	2.31	124
Cyclobutyl	Cys81	—	
	Tyr183	7.70	
	Tyr188	4.41	
	Trp229	4.87	
Aromatic ring	Tyr318	4.85	

For the *tert*-butylethynyl sultam (**10**), no hydrogen bond is predicted. The distance observed is 3 Å,. According to Mager and co-workers distances greater than 2 Å greatly weaken hydrogen bonding.[114] It is difficult to definitively conclude whether the *tert*-butylethynyl sultam (**10)** forms a hydrogen bond with Lys101. The cyclobutylethynyl sultam (**11)** is 4.27 Å away from Lys101. A large distance such as this one suggests that no hydrogen bond is formed. In wt RT all three alkyl groups (cyclopropyl (**9**), *tert*-butyl (**10**), and cyclobutyl (**11**)) are between 4 Å and 5 Å away from Tyr181 which is at least 2 Å greater than the distance observed for efavirenz in the pocket. The distances from Tyr188 vary from one sultam to the other. The cyclopropylethynyl sultam (**9**) has the largest distance of all three inhibitors at 5.6 Å, while *tert*-butylethynyl sultam (**10**) and cyclobutylethynyl sultam (**11**) have similar distances ranging from 4.3–4.6 Å , suggesting hydrophobic interactions with this particular residue for both inhibitors. All three inhibitors show a smaller distance between their alkyl groups and Tyr188 than that observed in the efavirenz/wt RT crystal structure. All three inhibitors are more than 5 Å away from Tyr183, which is a result similar to that observed in the efavirenz/wt RT complex. For the conserved Trp229 cyclopropylethynyl- (**9)** and *tert*-butylethynyl (**10)** sultams are positioned at 4.5 Å from this residue. Efavirenz is also around 4.5 Å.

Perhaps the most important observation for all three inhibitors in wt RT is that none of them favor a hydrophobic residue as is observed in the efavirenz pocket. It would be interesting to see whether or not these molecules induce aspecific mutation in wt RT much like efavirenz. A visual inspection of aromatic

ring A finds all three inhibitors in a staggered orientation with Tyr318 and the distance calculated for all three is around 6 Å. This could be a staggered π–π weak interaction, but it is very hard to determine that. Figure 9 depicts all three alktylethynyl sultam in wt RT superimposed over efavirenz. Figure 10 shows each docked in the pocket separately. The white ligand in both figures is efavirenz. Cyclopropylethynyl is red, *ter*-butylethynyl is blue and cyclbutylethynyl is green. Hydrogen bonds are depicted with red or yellow dashed lines.

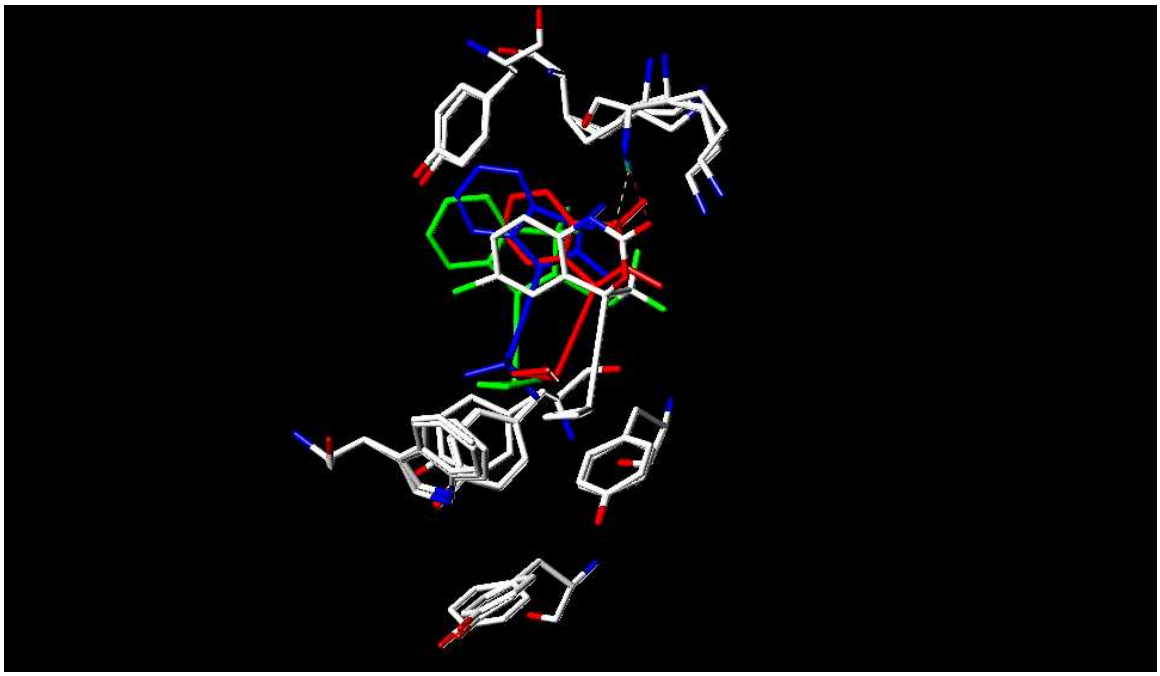

Figure 9. All alkyethynyl sultams docked into wt RT and superimposed on the Efavirenz wt RT pocket. Red (cyclopropylethynyl), blue (*tert*-butylethynyl), green (cyclobutylethynyl), white (efavirenz). The yellow dotted line H-bond between Lys101 and cyclopropylethynyl sultam and red dotted line represents a hydrogen bond between Lys101 and efavirenz..

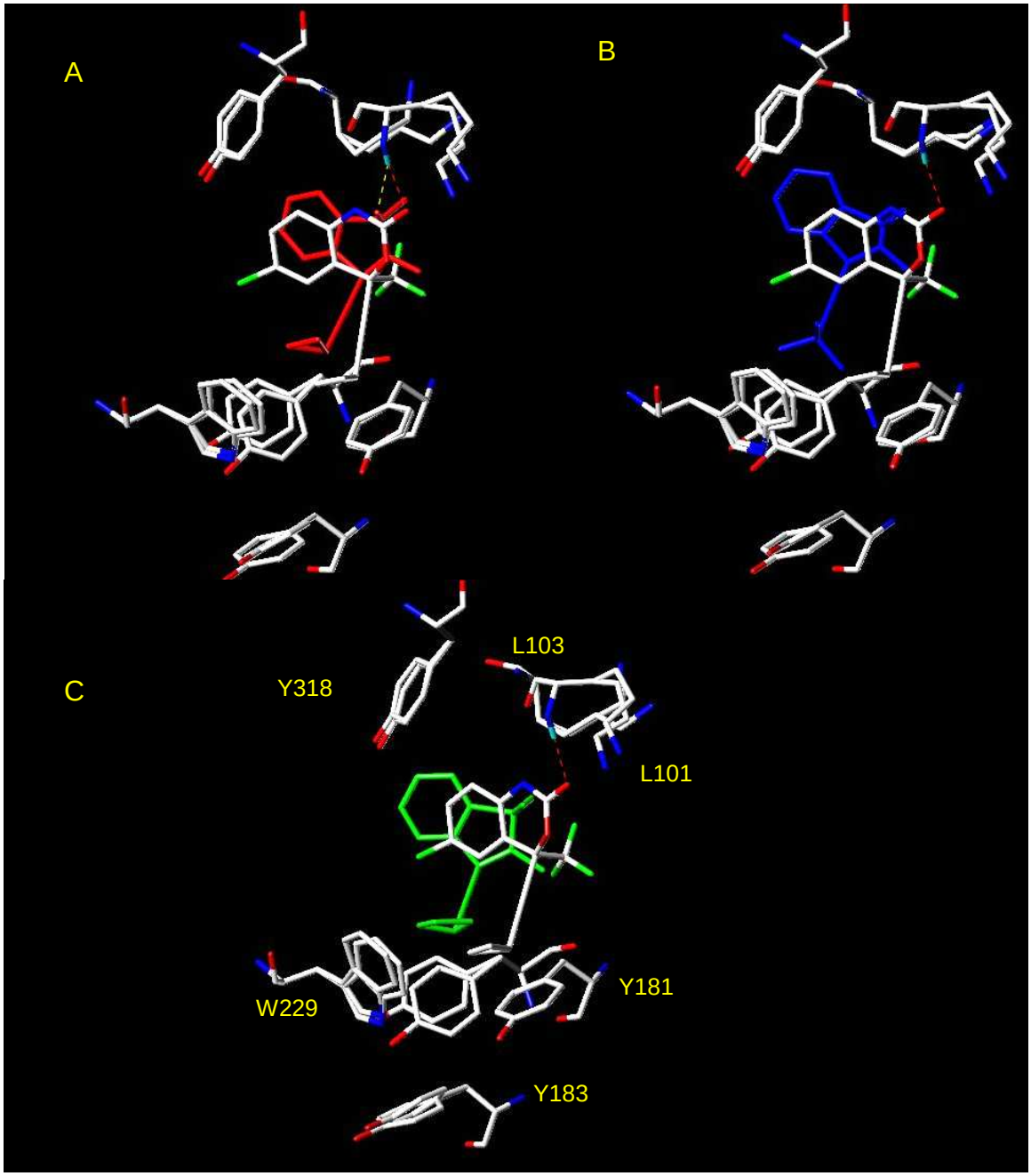

Figure 10. The alkylethynyl sultam series shown with efavirenz in wt RT and Y181C RT.

A noticeable change is that all three sultams lie closer to Lys101, and a hydrogen bond is predicted to form for all three of them. The most dramatic decrease in distance between the SO_2 group and the Lys101 NH hydrogen is observed in the cyclobutylehthynyl sultam where a decrease of 1.86 Å is reported. The calculated distances between SO_2 and NH Lys101 range between 2.13 Å and 2.31 Å, and the observed H-bond length in efavirenz Y181C crystal structure is 2.31 Å. Two sultams have shorter hydrogen-bond lengths than those observed in the crystal structure of the efavirenz/Y181C RT complex. The angles for these bonds range between 119º and 127º. All angles are within the range observed for hydrogen bonding in biological systems (Figure 11).[114] Visually these sultams appear to bind more similarly to efavirenz in this mutant pocket than in the wt pocket. Refer to Figures 11 and 12 for images of the docked sultams in Y181C superimposed on the efavirenz pocket.

Due to some synthetic challenges, of the three molecules discussed above, we were only able to synthesize 3-(*tert*-butylethynyl)-2,3-dihydro-2-methyl-1,2-benzisothiazole 1,1-dioxide (**10**) as a racemic mixture. However, five other compounds that were produced as side products or unexpected products were isolated. The 3-(cycloalkyl)-2,3-dihydro-2-methyl 1,2 benzisothiazole 1,1-dioxides (cycloalkylethyl sultams, compounds **12** and **13**) and the 3,3-(dialkyl)-2,3-dihydro-2-methyl-12-benzisothiazole 1,1-dioxide (dialkylated sultams, compounds **15**, **16** and **17**). Although these two groups of compounds were not part of the original work, they made interesting candidates for docking experiments.

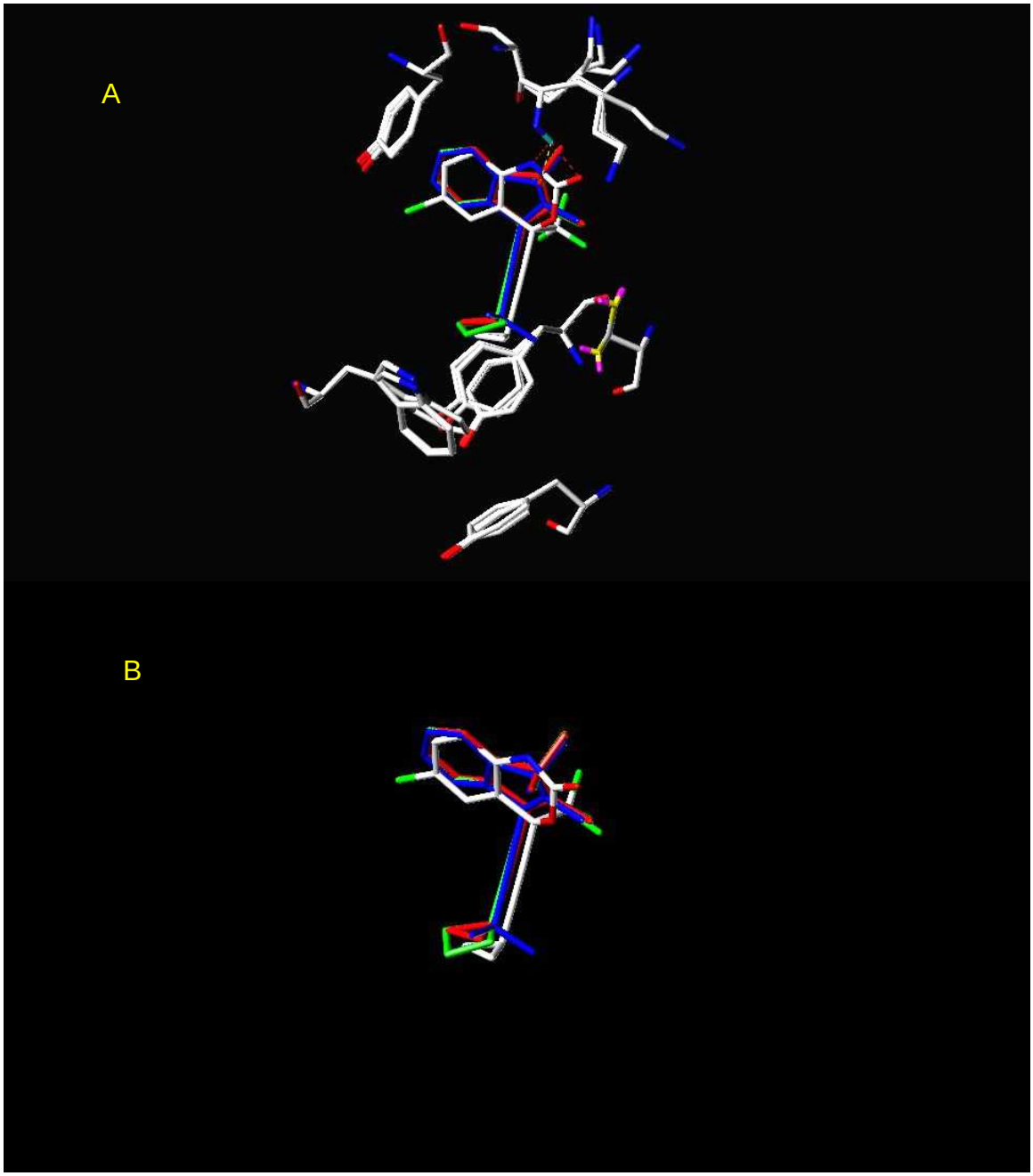

Figure 11. (A) 3-(cycloalkyethynyl) sultam in Y181C RT/efavirenz pocket. (B) 3-(cycloalkylethynyl) sultam in pocket. Residues not shown

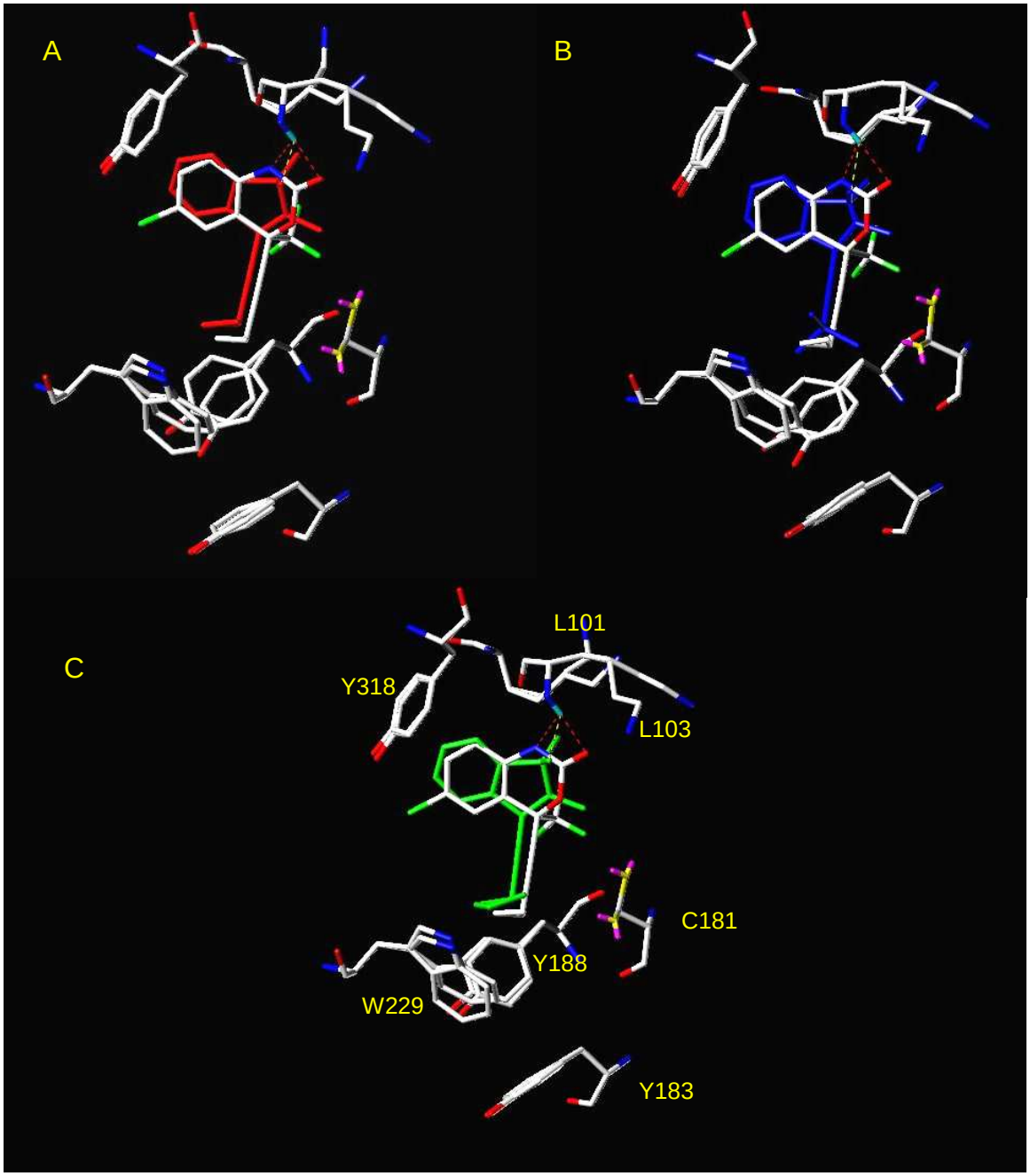

Figure 12. (A) cyclopropylethynyl sultam in Y181C RT, (B) *tert*-butylethynyl sultam in Y181C RT, (C) cyclobutylethynyl sultam in Y181C RT.

Both 3-(cycloalkylethyl)-2,3-dihydro-2-methyl-1,2-benzisothiazole 1,1-dioxides (**12** and **13**) were docked into wt RT and Y181C following the same protocol outlined earlier with at least three separte experiments at different random seed numbers and 130,000 generations. Each study gave twenty possible solutions. The lowest energy conformation was then evaluated for distances, hydrogen-bond lengths and hydrogen-bond angles. In the wt RT both cycloalkylethyl sultams produced flipped conformations (Figure 13). Both the cyclopropyl and cyclopbutyl groups are in the wing 1 region. Figure 14 shows these two sultams superimposed with the efavirenz pocket without any amino acid residues. It is also important to note the orientation of the ethyl group which appears to be extremely strained. To quantitatively get a grasp on the energy of these conformations, the lowest energies of both studies were compared to the lowest energies from the Y181C docking studies. For **12**, the lowest energy in the wt RT pocket shown above is –260 kcal/mol while the lowest energy for the Y181C pocket is –219 kcal/mol (41 kcal/mol decrease in energy). In the Y181C the binding conformation of this sultam is similar to that observed in the efavirenz pocket. It is important to stress that these energies have no real physical value but serve as a point of reference in comparing the different binding conformations. It is necessary here to rely on the energy values rather than the distances and angles because these two conformations are completely different, and their groups do not lie in the same regions of the pocket

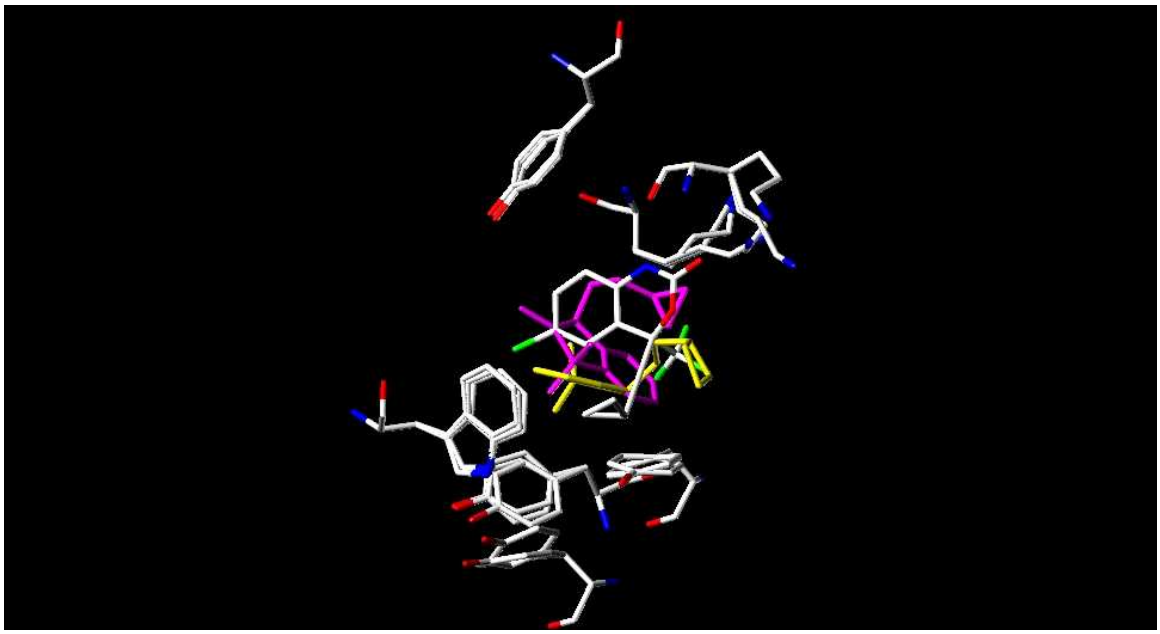

Figure 13. 3-(Cycloalkyethynyl) sultam in wt RT

as efavirenz. For the cyclobutylethyl sultam **13,** the lowest energy conformation observed in wt RT is –244 kcal/mol, while it is –212 kcal/mol for Y181C (32 kcal/mol energy change). Again the binding conformation of the cyclobutylethyl sultam **13** in Y181C mimicks that of efavirenz in Y181C and wt RT. Tables 8 and 9 report distanced and angles observed for both sultams. Figure 14 depicts them in the Y181C RT cavity superimposed onto the efavirenz/Y181C RT crystal structure.

Both inhibitors are predicted to form hydrogen bonds with Lys101. The calculated distance between the sulfonyl group and NH of Lys101 is 1.77 Å and 1.74 Å for cyclopropylethyl sultam (**12**) and cyclobutylethyl sutlam (**13**), respectively, (2.3 Å for efavirenz) with angles of 130.69º and 131.69º (Tables 8 and 9). Both inhibitors have distances that are no more than 5 Å away from Tyr188,Tyr183, and Trp229. The cyclopropyl and cylobutyl rings are closest to Tyr188 with a distance of approximately 4.10 Å for both. The binding conformations of both inhibitors are very similar to that of efavirenz in the pocket (Figure 14). Of all the inhibitors docked so far, these compounds make the most interesting candidates for biological evaluation. The energies of these two inhibitors in this particular pocket are significanlty lower than the calculated energies of the other sultams discussed above. The alkylethynyl sultam series lowest binding energies range between –260.01 kcal/mol and –269.65 kcal/mol, while the lowest binding energies for the cycloalkylethyl sultam series are less than –220 kcal/mol. Table 10 lists the lowest binding energies in both wt RT and Y181C.

Table 8. Distances and hydrogen-bond angles between cyclopropylethyl sultam and key resideus in Y181C RT.

Cyclopropylethyl sultam	Residues in Y181C	Distance (Å)	Angle of H-bond if present (º)
SO_2	Lys101	1.77	130.69
Cyclopropyl	Cys81	—	
	Tyr183	7.74	
	Tyr188	4.10	
	Trp229	4.66	
Aromatic ring	Tyr318	4.80	

Table 9. Distances and hydrogen-bond angles between cyclobutylethyl sutlam and key residues in Y181C RT.

Cyclobutyllethyl sultam	Residues in Y181C	Distance (Å)	Angle of H-bond if present (º)
SO_2	Lys101	1.74	131.69
Cyclobutyl	Cys81	—	
	Tyr183	7.49	
	Tyr188	4.09	
	Trp229	4.51	
Aromatic ring	Tyr318	4.75	

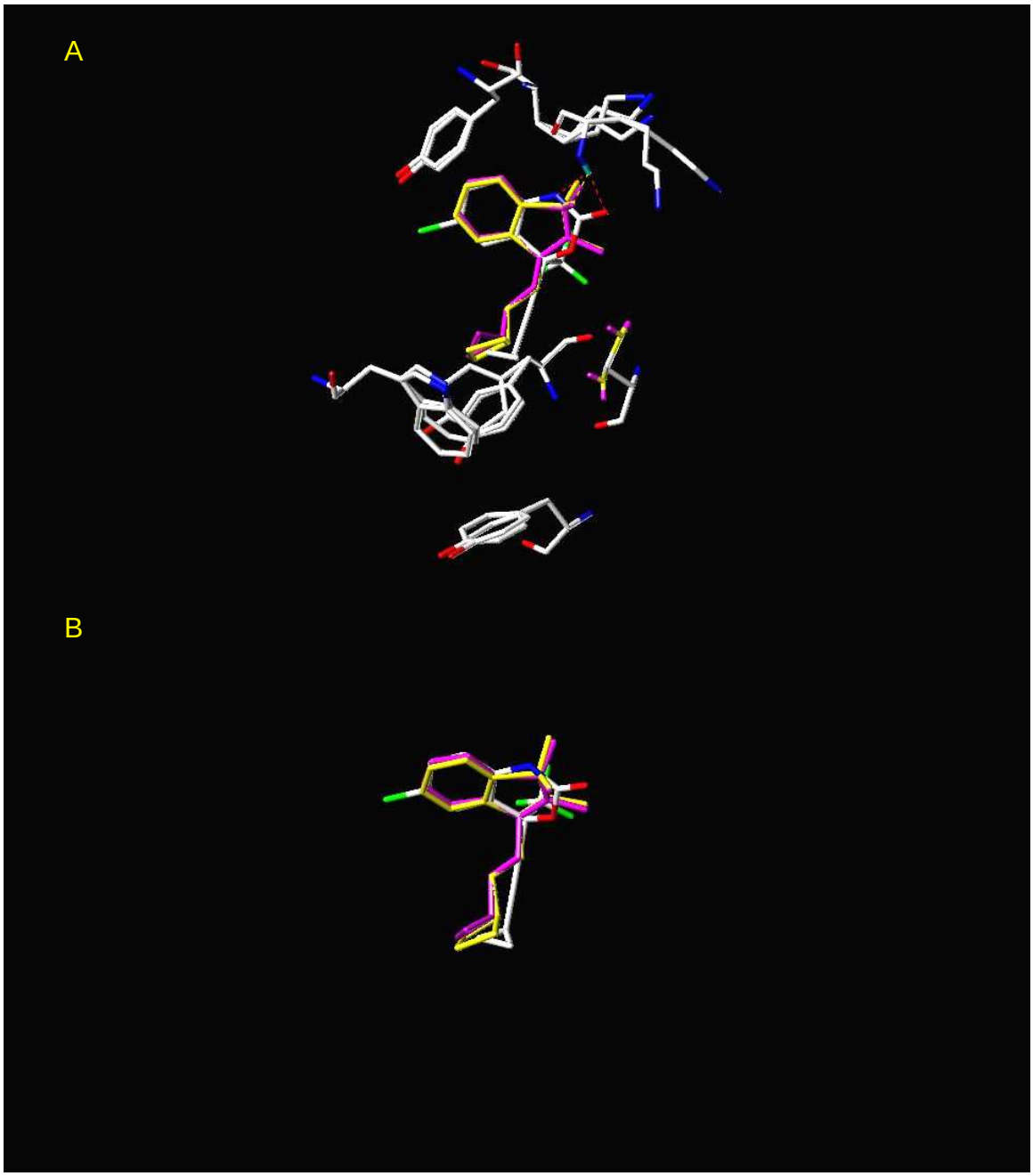

Figure 14. (A) Cyclopropylethyl sultam (magenta) and cyclobutylethyl sultam (yellow) in Y181C RT with efavirenz (white). (B) All three inhibitors in the pocket with no residues shown.

Table 10. . Calculted energies in both wt RT and Y181C RT

Inhibitor	wt RT Calculated Energy (kcal/mol)	Y181 C RT Calculated Energy (kcal/mol
Cyclopropylethynyl sultam (**9**)	–282.73	–269.65
Cyclobutylethynyl sutlam (**11**)	–284.04	–269.29
tert-Butylethynyl sultam (**10**)	–276.10	–260.01
Cyclpropylethyl sultam (**12**)	–260.00	–219.00
Cyclobutylethyl sultam (**13**)	–240.00	–212.00

The isolation of 3,3-bis(allylethynyl)-2,3-dihydro-2-methyl-1,2-benzisothiazole 1,1-dioxides (bisalkylated sultams compounds **15**–**17**) as side products from our reactions (see synthetic discussion section) prompted docking experiments into wt RT and Y181C. The three compounds proved to be too large for the wt RT. The docking experiments were tried several times, and the lowest binding conformation was either placed outside of the pocket or in conformations that made no contacts with the key residues being inspected. As mentioned earlier, although NNRTIs are strucurally diverse, they all make key contacts with specific pocket residues. These contacts were not observed in these studies.

Compounds **15**–**17** were docked into Y181C RT using the efavirenz/Y181C RT crystal coordinates. The binding conformations of all three compounds did not adopt a similar orientation to that off efavirenz. However, bis(cyclopropylethynyl) sultam (**17**) and bis(*tert*-butylethynyl) sultam (**16)** exhibited interesting binding interactions with certain pocket residues. Tables 11 and 12 report the calculated distances. The sulfonyl group for bis(cylopropylethynyl) sultam (**17**) is no longer oritented toward Lys101, but instead points directly at the SH moeity of Cys181. The distance measured is 3.96 Å. The bis-*tert*-butylethynyl (**18**) sultam has its SO_2 group also oriented in a similar fashion with a shorter distance of 2.37 Å. SYBYL does not predict a hydrogen bond between the ligand SO_2 and Cys181; however, these docking experiments were performed at least three times, and sixty possible solutions were inspected. The SO_2 position was always reoriented towards Cys181. This

Table 11. Distances between dicyclopropylethynyl sultam and key residues in Y181C RT

Ligand	Residue	Distance (Å)
SO_2	Cys181	3.96
Cyclopropyl (A)	Tyr183	5.72
	Tyr188	5.77
	Trp229	4.3
Cyclopropyl (B)	Tyr318	3.75

Table 12. Distances between the dyclopropylethynyl sultam and key residues in Y181C.

Ligand	Residue	Distance (Å)
SO_2	Cys181	2.37
tert-butyl (A)	Tyr183	7.32
	Tyr188	5.006
	Trp229	4.42
tert--butyl (B)	Tyr318	3.26

indicates that some sort of electrostatic interaction is ocurring, most probably a hydrogen bond. The second most noticeable interaction is the position of one of the cyclopropyl groups and *tert*-butyl groups. Both are oriented directly toward the aromatic ring of Tyr318 and the calculated distances are 3.75 Å and 3.26 for cyclopropyl (**15**) and *tert*-butyl (**16)**, respectively. Tyr183 remains at least 5 Å away from each ligand. Trp229 seems to also make contact with one cyclopropyl group and one *tert*-butyl group at a distance less than 4.5 Å. Whether these distances lead to binding and activity cannot be concluded from these results. Since these compounds do not adopt a similar orientation to efavirenz in this pocket, it is difficult to compare the observed crystal structure distances and the calculated distances of our compounds. And it is also difficult to predict acitivity. However, upon comparison of these structures with the nevirapine/Y181C RT crystal structure, it was discovered that these bisalkylated sultams have similar binding conformations to that of nevirapine (Figure 15). Nevirapine has very low activity against mutant RT strains, particularly those with mutations in the hydrophobic region such as Y181C and Y188C.[85]

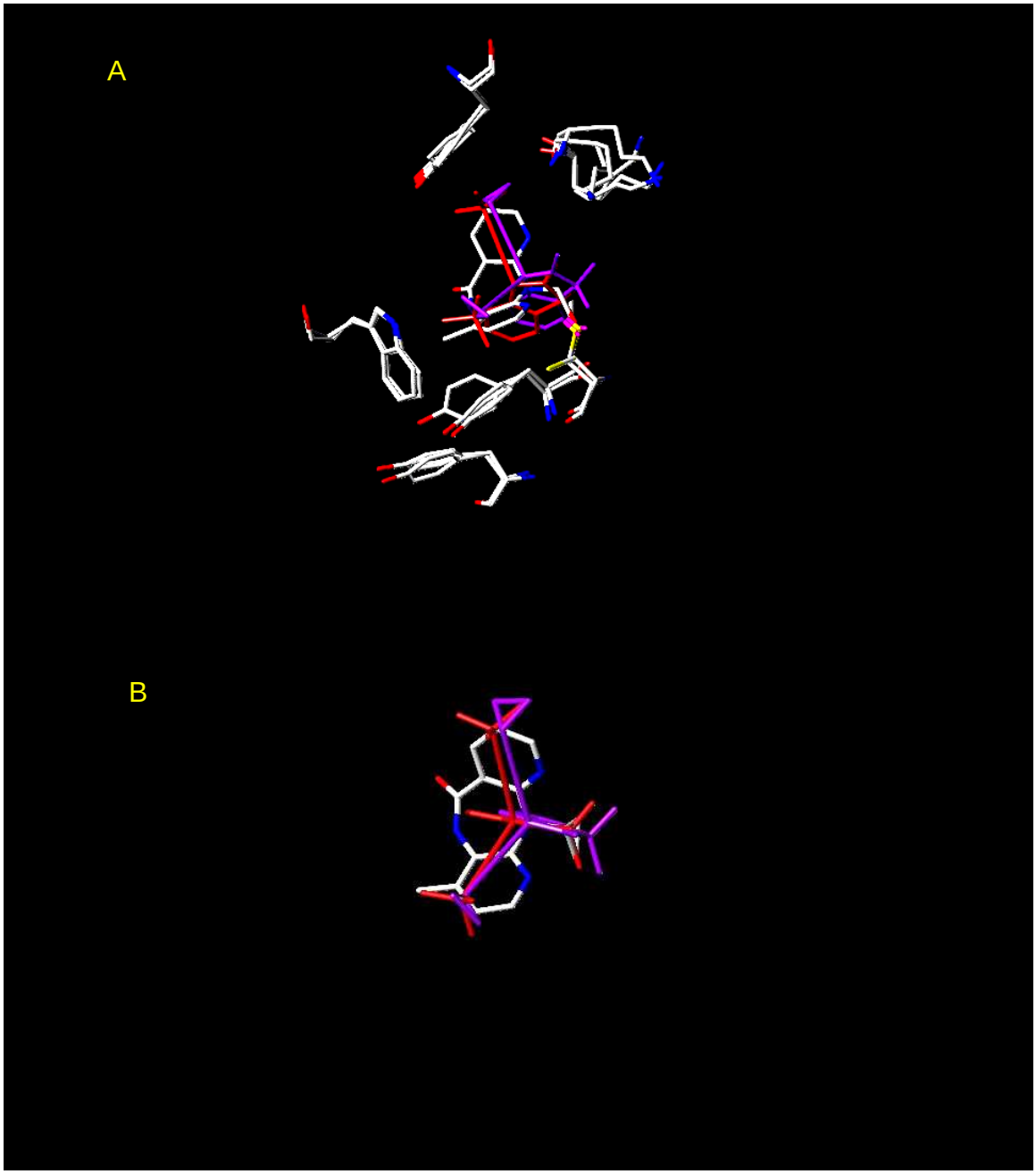

Figure 15. Dialkylated sultam 15 and 16 in Y181C/nevirapine pocket. (A) Dicyclopropyl (violet), di-*tert*-butyl (red) nevirapine (white) with all residues. (B) All three inhibitors without residues.

B. Synthesis

1. 3-(Alkylethynyl)-1,2-benzisothiazole 1,1-dioxide

The original synthetic route leading to the ethynyl series followed a similar plan developed by Baker et al. to synthesize 3-(*R*)-aryl-2,3-dihydro-2-methyl-1,2-benzisothiazole 1,1-dioxides (Scheme 5).[119] Two equivalents of aryl magnesium chloride or bromide Grignard reagents were coupled with one equivalent of saccharin to give the respective 3-(aryl)-1,2-benzisothizole 1,1-dioxides in good yield.[119] Following the same logic, a synthetic route was outlined using alkynylithium reagents with saccharin to give the desired 3-(alkylethynyl)-1,2-benzisothizole 1,1-dioxides using methodology developed by Abromovitch et al. (Scheme 3).[139]

Scheme 6

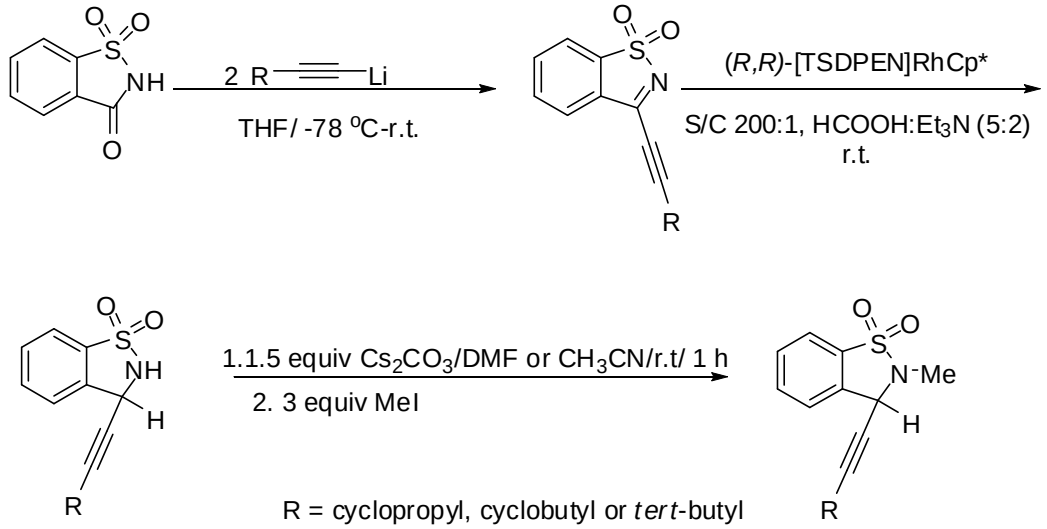

The alkylehtynyllithium species is first generated by metal exchange with *n*-butyllithium under anhydrous conditions, a nitrogen atmosphere and low

temperature –78 ºC–(–40 ºC). The saccharin is then added dropwise via a syringe. The reaction is warmed to room temperature overnight. It is then cooled to 0 ºC and quenched with saturated NH_4Cl (aq). It quickly became apparent that the desired 1,2-benzisothizole 1,1-dioxides were not being formed by this reaction.

Examination of ^{1}H NMR, ^{13}CNMR and HRMS data suggests a 3,3-bisalkylated product (Scheme 7). The ^{1}H NMR spectrum of compound **12** has an aromatic signal at 7.74–7.75 ppm that integrates to four protons. A multiplet at 1.29–1.20 ppm belongs to the CH in the cyclopropyl group, but integrates to two protons. The multiplets between 0.81 and 0.68 ppm are signals for the cyclopropyl CH_2 groups, and those integrate to six protons. Furthermore, compound **12** has a signal at 5.0 ppm which disappears upon addition of D_2O, confirming that this is an exchangeable proton, most probably the NH proton. Had this been the desired sulfonimine, an exchangeable proton should not be present nor should there be a 2:1 ratio between the alkyl and aromatic region. Moreover, the ^{13}C NMR spectrum lacks the imine signal typically observed around 160 ppm, but it has a peak at 52 ppm. DEPT experiments indicate that this signal belongs to a quaternary carbon.

To further support the theory that this indeed was the 3,3-bisalkylated product, all three compounds were submitted to high-resolution mass spectrometry atmospheric pressure photoionization (HRMS-APPI). The observed *m/z* came within either the third or fourth decimal place of the calculated mass for all three samples. HRMS-APPI is a gentle ionization method

that does not rely on acid/base reactions to create the molecular ion. Instead, the sample is passed through a nebulizer where it is bombarded by a UV/vis light source. A molecular ion radical is then formed by absorption of a photon and subsequent loss of an electron.

Scheme 7

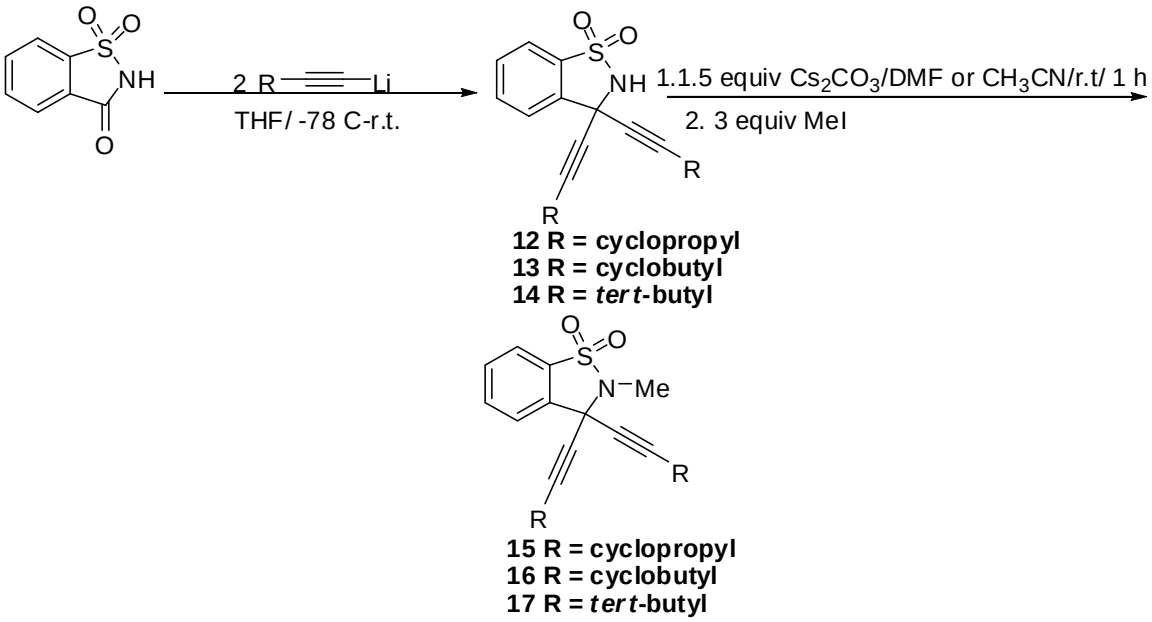

These results were surprising, especially in that this methodology has been used in the synthesis of similar 1,2-benzisothiazole 1,1-dioxides, albeit in low yields.[139, 140] Scheme 8 depicts a proposed mechanism for the bisalkylation reaction. The first step is an acid–base reaction where the acidic N–H proton is abstracted to form intermediate **8-A**. Intermediate **8-A** then abstracts from a proton source. Considering that the reaction is performed under anhydrous conditions and an aprotic solvent, it is difficult to explain the origin of this proton. Upon further consideration, it is possible that the reformed alkyne in step 1

provides the proton source. This forms intermediate **8-B**. Attack by another equivalent of the alkylethynyllithium species affords intermediate **8-C**. The electron pair on the nitrogen then fold back to form imine (**8-D**) causing an $[OH]^-$ to leave. Another equivalent of the lithium reagent then attacks the imine bond, and upon workup the bis-(alkylethynyl) product is formed. Scheme 8 depicts a stepwise mechanism based on the synthetic results observed. Whether intermediate **8-A** does really exist or if the first two steps occur in a concerted fashion leading to intermediate **8-B** remains unclear. What is obvious from the products isolated is an $[OH]^-$ must leave in some form.

Other mechanistic pathways have been considered where the alkylethynyllithium species attacks the carbonyl first. However saccharin is acidic with a pK_a of ~2.0, and acetylenic protons have pK_a of ~25. This suggests that the first step has to be an acid–base reaction. Another possible mechanism is shown in Scheme 9. Here the alkylethynyllithium abstracts a hydrogen from saccharine and forms the lithiated saccharine species **9-A**. Another equivalent of alkylethynyllithium then attacks the carbonyl to give intermediate **9-B**. The protonation of the nitrogen is accomplished by using saccharine which is already present in solution as the proton soruce. The oxygen electrons then collapse to reform the carbonyl group and **9-E** is formed. Acidic workup gives the bisalkylated sultam.

The saccharin is added dropwise to the alkylethynyllithium solution, so at any given moment in time there is an excess amount of lithium reagent relative to saccharin. We attempted to avoid this dialkylation by adding the lithium species

to the saccharin, but that only gave the same results with even lower yield due to the decomposition of the lithium species. Maintaining a low temperature throughout the reaction and quenching at –78 ºC did not change the results. The use of alkylethynylmagnesium bromide reagents was unsuccessful at varying temperatures, and saccharin was the only compound isolated from the reaction mixture.

Scheme 8

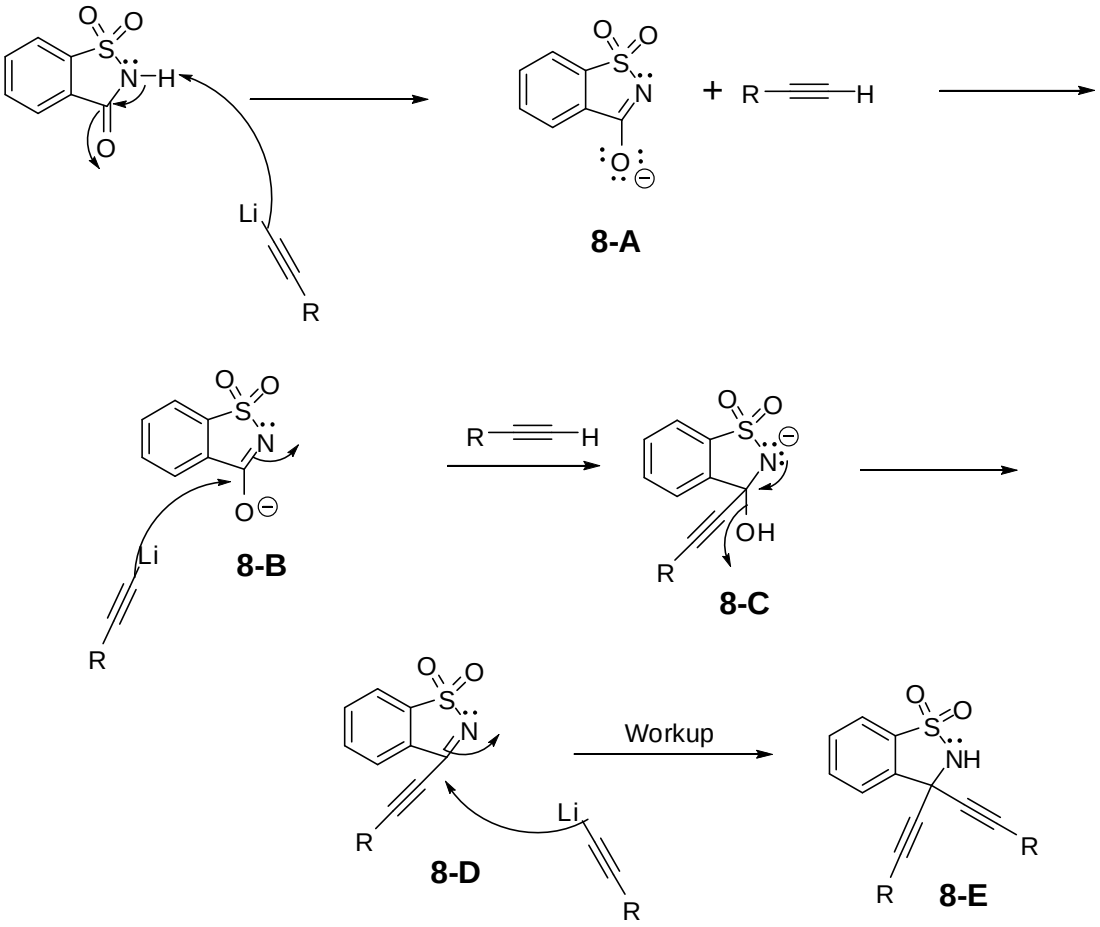

Scheme 9

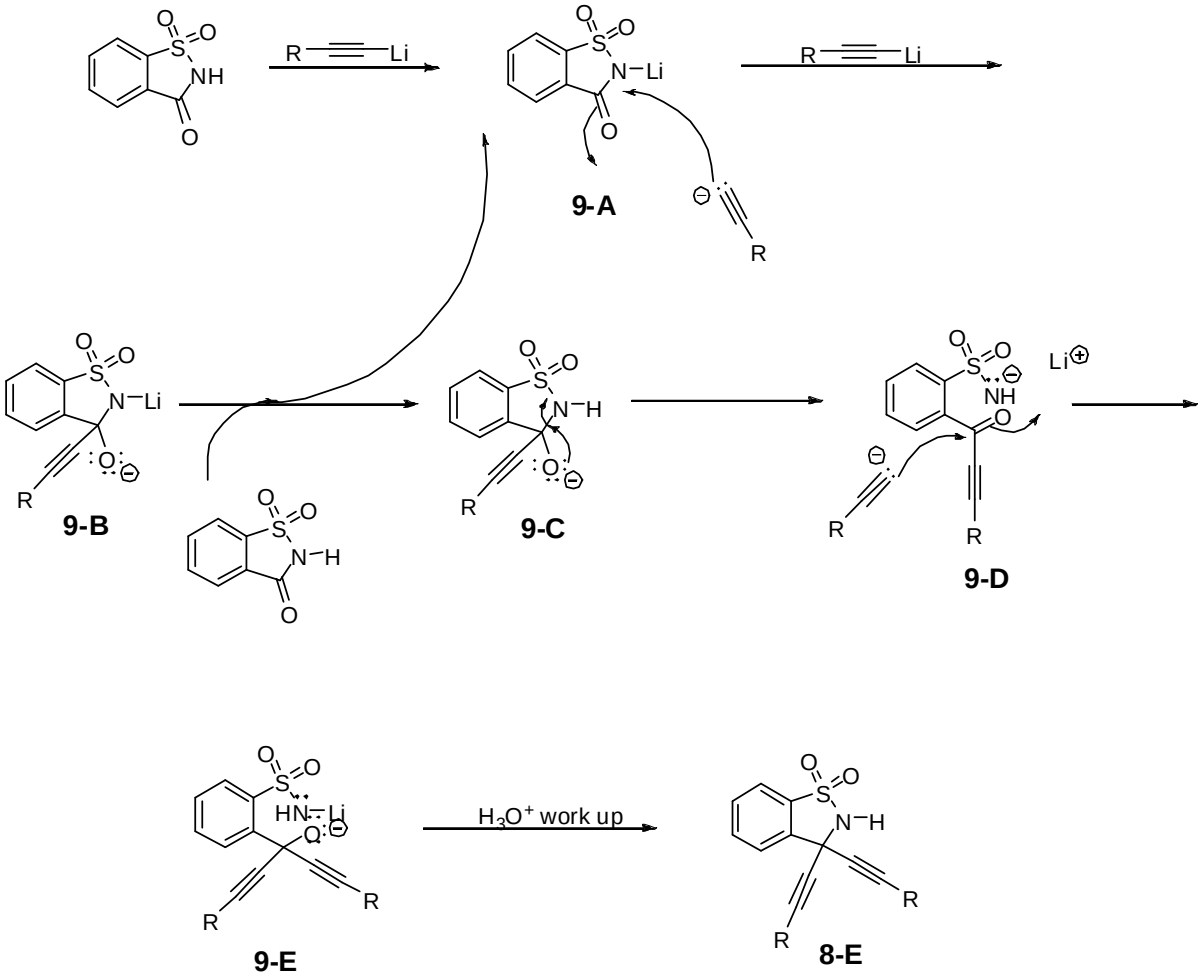

It was clear at this point that a new approach is needed to accomplish the task at hand. The new synthetic route shown below (Scheme 10) utilized methodology developed by Davis and co-workers.[140] 3-Ethoxy-1,2-benzisothiazole 1,1-dioxide is prepared from 3-chloro-1,2-benzisothiazole 1,1-dioxide. It is then coupled to the alkylethynyllithium species. Davis and co-workers reported that the success of this method varied depending on the lithium reagent used. The yields were generally better than the ones reported for the

saccharin couplings, but in some cases either very low yields or no product formation was reported.[140] This method was attempted several times, but even with reflux the reactions did not lead to products.

Scheme 10

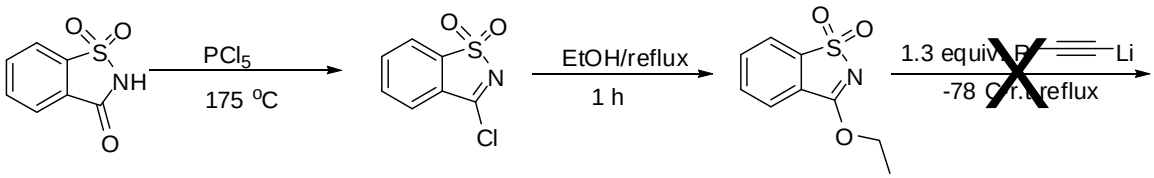

Considering that the chlorine would be a better leaving group than the ethoxide, a synthetic plan utilizing 3-chloro-1,2-benzisothiazole 1,1-dioxide directly was put together. Scheme 11 represents the full synthetic route to the target molecules. Preparation of **1** is accomplished by the molten reaction of phosphorus pentachloride (PCl_5) at 180 ºC, then cooling to 100 ºC and applying vacuum to remove $POCl_3$ that formed during the reaction. Recrystallization from hot toluene provided **1** in 78% yield. ^{1}H NMR and ^{13}C NMR spectra were obtained and matched the expected signals. No NMR data for this compound is available in the literature. The observed mp is 139–143 ºC, and the value reported in the literarture is 140–144 ºC.[141]

This methodology was developed for the synthesis of 2,3-dihydro-3,3-dimethyl-1,2-benzisothiazole 1,1-dioxides,[142] but has not been reported as a route for the preparation of 3-alkyl-1,2-benzisothiazoles. The coupling reaction between 3-chloro-1,2-benzisothiazole (**1**) and the alkylethynyllithium reagent proved to be problematic. Initially one equivalent of 3-chloro-1,2-benzisothiazole

1,1-dioxide was dissolved in dry THF and added very slowly to the lithium reagent solution at 0 ºC.

Shceme 11

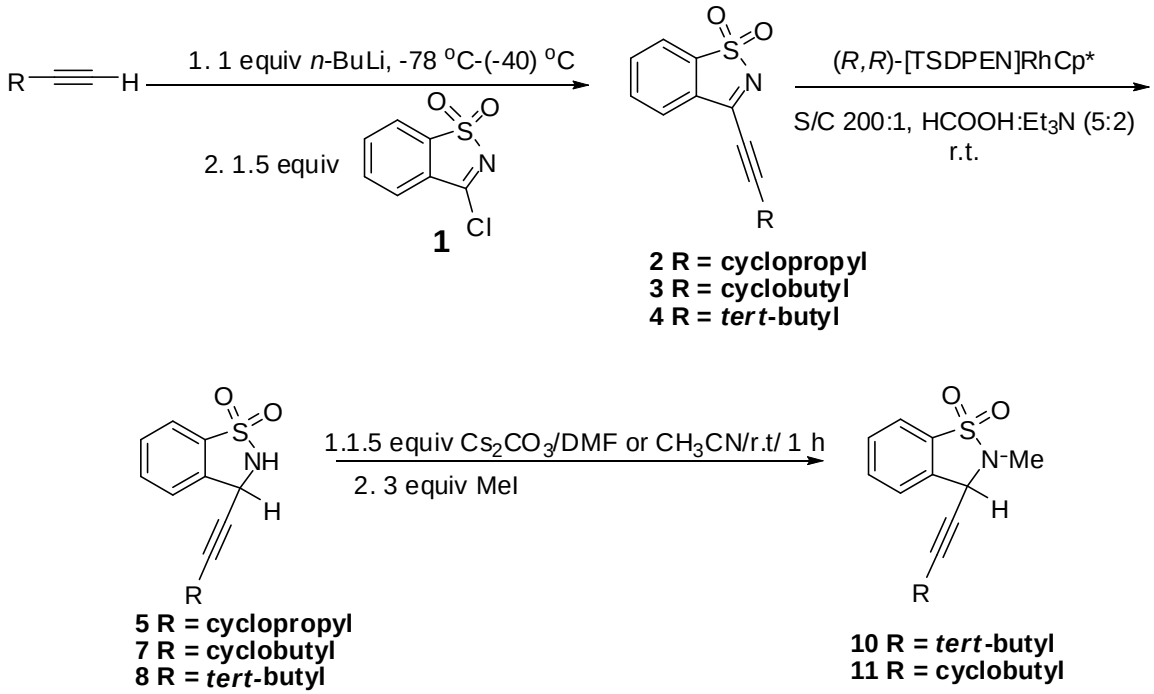

Then the reaction was quenched with saturated NH_4Cl (aq) at 0 ºC. The major products isolated were 3,3-bisalkyl-2,3-dihydro-1,2-benzisothiazole 1,1-dioxides (compounds **12**, **13**, **14**). All structures were confirmed by ^{1}H NMR and ^{13}C NMR spectroscopy and HRMS-APPI analysis, and the results matched those of the products obtained from the saccharin route. Once again the reaction was attempted at variable temperatures. One equivalent of 3-chloro-1,2-benzisothiazole 1,1-dioxide was added at –78 ºC, and the reaction was quenched at –40 ºC, but no change was observed. The lithium reagent was

alkylating the chloro pseudosaccharine twice in a mechanism such as that shown in Scheme 12.

Scheme 12

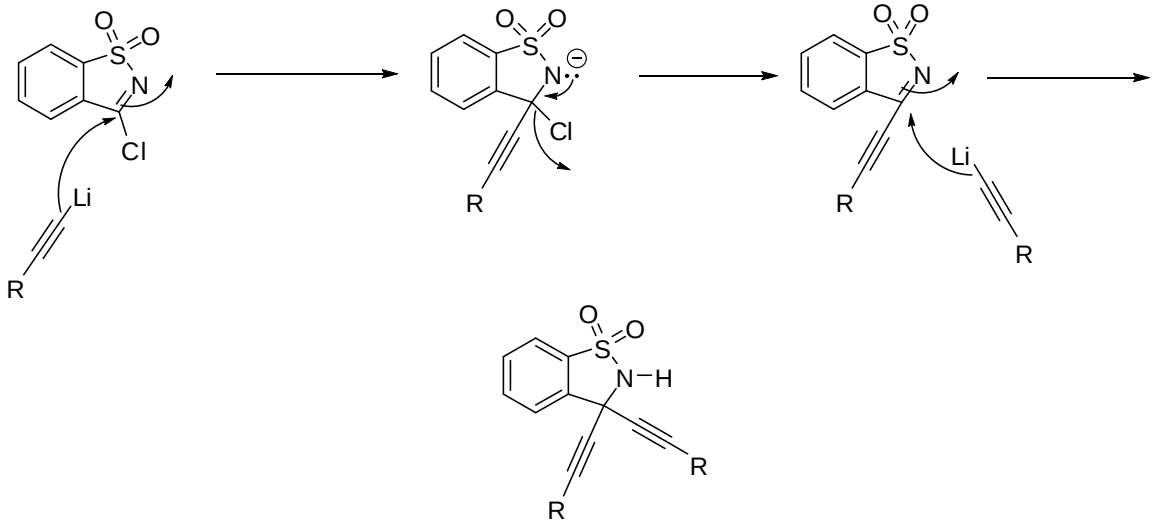

The number of 3-chloro-1,2-benzisothiazole 1,1-dioxide equivalents was varied. Three reactions were run at the same time using 1.1, 1.3 and 1.5 equivalents (**1**) to one equivalent of alkylethynyllithium reagent. The reaction temperatures were maintained at –78 ºC during and after the addition, and the addition rate was dropwise at a medium speed. The bisalkylated product was once again the major product; however, the 2-(alkylethynyl)-1,2-benzisothiazole 1,1-dioxide was also observed. The reaction was monitored by TLC during the addition, and a new higher migrating spot began to form towards the end of the addition period. ^{1}H and ^{13}C NMR spectroscopy indicated that this newly observed product is the desired 3-(alkylethynyl)-1,2-benzisothiazole 1,1-dioxide. The next goal was to eliminate the formation of the bisalkylated product altogether.

3-Chloro-1,2-benzisothiazole 1,1-dioxide was dissolved in THF, and it was poured directly onto the alkylethynyllithium reaction mixture. The flask was refitted with a septum and a nitrogen line, and it was monitored by TLC for one hour. It was then quenched with saturated NH_4Cl at –78 ºC. The dialkylated product formation was greatly diminished when 1.1 and 1.3 equivalents were used as observed by TLC. It formed in small amounts when 1.5 equivalents of **1** were used for the cylopropylethynyl (**2**) and *tert*-butylethynyl (**4**) analogues, but it was never completely eliminated from the reaction mixture. However, the dialkylated product formed for the cylobutylethyne analogue regardless of the number of equivalents used. Although using this technique greatly improved the yields for these reactions, the overall % yields remained moderate for all three compounds (**2**, **3** and **4**). Davis and co-workers reported moderate to good yields depending on the alkyllithium species used.[140]

2. 2,3-Dihydro-3-(alkylethynyl)-1,2-benzisothiazoles 1,1-dioxides

The next step was the reduction of the imine bond using the rhodium catalyst (Figure 16) developed by Mao and Baker[122, 143] who reported great success with this catalyst in the enantioselective synthesis of 3-(aryl)-2,3-dihydro-1,2- benzisothiazole 1,1-dioxides. According to Mao and Baker the *R,R*-catalyst gave the *S* stereochemistry and vice versa. However, they observed that this

trend decreased and was completely reversed as the size of the C-3 group decreased.

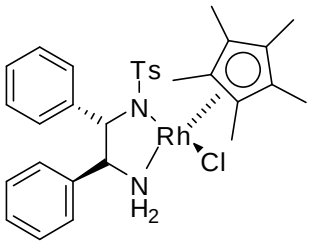

Figure 16. Structure of ((*R,R*)-*N*-(*p*-tolunesulfonyl)-1,-2-diphenylethylenediamine)-rhodium-(pentamethycycopentadienyl)-Cl ((*R,R*)-[TSDPEN]RhCp*Cl).

Initially methodology developed by Mao and Baker was used. While the reaction conditions seemed to work, reaction times were 6 h. Reduction of compound **4** into **8** proceeded smoothly with good yields (60%). Reductions of 3-(aryl)-1,2-benzisothiazole 1,1-dioxide proceeded with much higher yields. During the purification process, it became apparent that the benzisothiazoles contained small amounts of the bisalkylethynyl products which may explain the lower yield in the desired product since our starting material was not 100% pure. Complete separation of these compounds was successful. Reduction of **2** and **3** into **5** and **7**, respectively, (Scheme 13) was not successful. The ^{1}H NMR spectra of the new compounds have unexpected signals in its aliphatic region. The two new signals integrate to 2H each suggesting —CH_2 groups. The ^{13}C NMR spectrum lacked the alkyne signals observed in the other 1,2-benzisothiazole-3-(*tert*-butylethynyl)-2,3-dihydro 1,1-dioxide (**8**) and had two new

signals in the aliphatic region as well. The observed *m/z* for compound **5** $[M+H]^+$ is 238.0907 (234.0510) and for compound **7** 250.969 (247.067) an increase of four units or four hydrogens. All of these results help prove that the compounds obtained from this reduction are the 3-(cyclopropylethyl)- and 3-(cyclobutylethyl)-1,2-benzisothiazole 1,1-dioxides. To avoid the reduction of the alkyne moiety, variable reaction conditions were attempted. The reaction was first monitored by low resolution EIMS. Small aliquots of the reaction at 20 min, 30 min and 60 min were taken, and no trace of the desired compound was found. The isolated products after 30 minutes and up were that of the over-reduced compounds **6** or **23** (Scheme 13).

Scheme 13

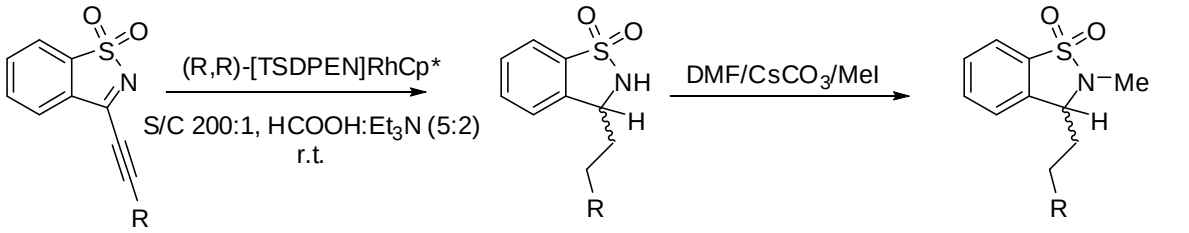

2 R = cyclopropyl
3 R= cyclobutyl

6 R = cyclopropyl
23 R = cyclobutyl

12 R = cyclopropyl
24 R = cyclobutyl

The active form of the catalyst is the Rh-hydride species. The pre-catalyst shown in Figure 16 is converted to the active catalyst by hydride transfer from the formate ion present in the azeotropic mixture onto the metal center with loss of a chlorine ion. The catalyst was dissolved in a small amount of dry dichloromethane, and one equivalent of azeotropic mixture was added. Carbon

dioxide gas bubbles were observed, as CO_2 is released as the formate ion loses a hydride to the metal center to form the active complex. The mixture was stirred for 10 min, and then a solution of compound **2 or 3** in dry dichloromethane and one equivilant of formate to substrate were added. A color change from red to a dark brown color was observed within 15 min. The reaction was quenched and purified, and only starting material was recovered. This procedure was repeated several times with varying reaction times (30, 60, 120 min). The only product isolated, if any, was compound **6** or **23**. As mentioned above, the reaction was complete at approximately 2.5 h. Compounds **6** and **23** exhibited no optical activity. The reason for the reduction to the alkyl compound is not known at this time.

3. 3-(Alkylethynyl)-2,3-dihydro-2-methyl-1,2-benzisothiazole 1,1-dioxide

Methylation of compounds **6**, **23** and **8** into compounds **12**, **24**, and **10**, respectively, was carried out using Cs_2CO_3 as base and iodomethane as the methylating reagent in either *N,N*-dimethylformamide (DMF) or acetonitrile. The reactions proceeded to completion at room temperature. The synthetic route followed by Mao and Baker employed DMF as a solvent system due to the solubility of Cs_2CO_3 in DMF. Cs_2CO_3 was found to be equally soluble in acetonitrile, and the reactions proceeded to completion. The use of acetonitrile is more convenient because DMF is difficult to remove from the reaction mixture.

The progress of the reaction was monitored by TLC, and surprisingly two spots were observed. Both spots ran closely to each other much like two

diastereomers of the same compound. Both spots were collected together, and their ^{1}H NMR and ^{13}C NMR spectra were obtained. The ^{1}H NMR spectrum of **10** contained two H3 and two N-CH_3 signals. HRMS-APPI for 2,3-dihydro-2-methyl-3-(*tert*-butylethynyl)-1,2-benzisothiazole 1,1-dioxide (**10**) observed only one *m/z* at 262.0933 (262.0902). HRMS-APPI for 2,3-dihydro-2-methyl-3-(cyclopropylethyl)-1,2-benzisothiazole 1,1-dioxide (**12**) and for 2,3-dihydro-2-methyl-3-(cyclopropylethyl)-1,2-benzisothiazole 1,1-dioxide failed. No other significant peaks were observed. Apparently 3-alkyl-2-alkyl-1,2-benzisothiazoles do not easily ionize. Variable light source intensities did not cause these compounds to ionize. However, ^{1}H NMR and ^{13}C NMR spectra clearly indicate the expected structures. Further analysis would be needed for these compounds.

4. A complete analysis of 10

Both components of compound **10** were successfully isolated. The fast-migrating spot is designated **10a**, and the slower migrating spot is referred to as **10b**. Recrystallization of these two spots was only successful for **10a**. When compound **10b** was resdissolved for recrystallization, a TLC sample was taken, and two spots reappeared. When the crystals of **10a** were redisolved for 2D NOESY experiments, a 1D ^{1}H NMR spectrm was obtained. From this spectrum it was determined that the signal at 5.59 ppm is H3 for **10a**, and the signal at 3.12 ppm belongs to the *N*-methyl protons in **10a**. As the sample remained in solution, the other two signals reappeared, and TLC indicated the formation of

10b again. 2D NOESY experiments were run on the mixture. A cross peak between the singlet at 5.99 ppm and the singlet at 3.12 is observed, but no cross peak is observed between the singlets at 6.13 ppm (H3 in **10b**) and 3.21 ppm (CH_3 in **10b)**. These results confirm that the orientation of the methyl group on the nitrogen varies between **10a** and **10b** and that H3 in **10a** is clearly within 5 Å or less from the methyl group on the nitrogen, while H3 in **10b** is more than 5 Å away. From these results one can hypothesize that **10a** and **10b** are conformers of the same molecule. HRMS-APPI analysis only show the *m/z* expected for **10**. Other sultams have been reported to exhibit such a phenomena where two conformers are in equilibrium in solution.[144] To further support our hypothesis, variable-temperature ^{1}H NMR experiments were carried out (Table 13). Our attention was focused on the N-CH_3 singlets at 2.38 ppm and 2.24 ppm. The two methyl group signals clearly show movement toward coalescence as the temperature rises. At 300 K the Δ ppm between the two signals is at 0.14 ppm. A gradual decrease in the difference between the two peaks and a slight broadening of the peaks was observed as the temperature increased. The highest temperature reported here is 405 K. Unfortunately, at 410 K, the probe temperature would not stabilize. To avoid the risk of overheating the probe, the experiments was halted. The exact coalescence point was not observed. The results observed exhibit enough of a patern to conclude that the methyl signals were indeed coalescing.

Table 13. VT ^{1}H NMR experimental results

Temperature (K)	N-CH_3 (**10a**)	N-CH_3 (**10b**)	Δ (ppm)
300	2.38	2.24	0.14
315	2.45	2.33	0.12
350	2.62	2.54	0.08
365	2.70	2.63	0.07
380	2.77	2.71	0.06
390	2.81	2.77	0.04
395	2.82	2.78	0.04
400	2.82	2.79	0.03
405	2.86	2.83	0.03

5. 3,3-Bis-(alkylethynyl)-2,3-dihydro-2-methyl-1,2-benzisothiazole 1,1-dioxide

Although the 3,3-bis-akylated compounds were not synthetic targets for this project, they were methylated as well. They were also docked into reverse transcriptase and evaluated for potential anti-HIV activity. The methylation reactions for compounds **12**,**13** and **14** afforded compounds **15**,**16** and **17**, respectively, in very good yields (Scheme 4). NMR spectroscopy and HRMS-APPI confirmed these structures.

C. Modeling of 3-(m-cyclopropylpheynyl)-2,3-dihydro-2-methyl-1,2-benzisothiazole 1,1, dioxide (m-cyclopropylpheny sultam 18) and 2,3-dihydro-3-(isopropylfuranyl)-3-methyl-1,2-benzisothiaozole 1,1-dioxide (isopropylfuranyl sultam 19)

Another series of compounds were docked into wt RT and Y181C (Figure 17). The structures were inspired by the original sultam NSC-108406. Both of these sultams have first generation NNRTI structural features. Both have two aromatic rings that form the π and the extended π systems. Both have a substituted ring C on position-3 or the *meta*-position. The unique feature of **19** is that the extended π system in ring C is a heterocyclic ring. This compound was designed with Y181C RT in mind. Since loss of activity in mutant RTs is attributed to loss of pocket hydrophobicity, and therefore loss of major binding interactions, it was hypothesized that a heterocyclic ring may be able to form a hydrogen bond with CYS181.

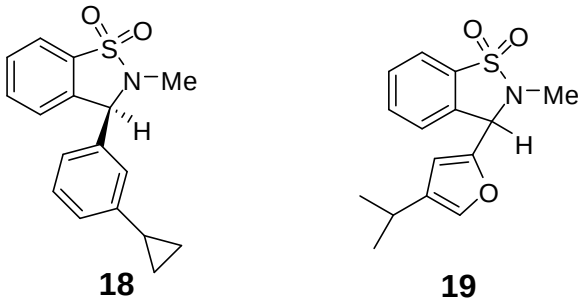

18 **19**

Figure 17. Sultams inspired by NSC-108406.

The methyl group in NSC-108406 was substituted with a cyclopropyl group in the *meta*-position. This was inspired by efavirenz and its high activity against wt RT and its sustained activity against mutant RT strains. Compound **18** was docked into the wt RT and Y181C. Tables 14 presents FlexiDock results for **18** in wt RT. In the wt RT pocket the distances observed are quite interesting. Each ring in the ligand makes close contacts with specific residues, and each residue is within 4–5 Å of one of these rings. This ensures that all key residues are bound to a part of the ligand. Whether this means this inhibitor will be more tightly bound to the pocket remains to be seen through biological activity studies. The cyclopropyl ring makes two close contacts with Tyr181 (3.94 Å) and Trp229 (4.37). Ring C, on the other hand, makes a close contact with Tyr188 (4.37 Å). All three residues are essential for NNRTI binding to wt RT. Unfortunately SYBYL does not predict a hydrogen bond with Lys101 (3 Å). Although this compound is not considered to be structurally related to efavirenz, its orientation was still compared to efavirenz in the pocket. Visual inspection of docked models do not show much similarity between the binding conformations of the two compounds, but based on the measured distances of **18** and the observed distances of efavirenz/wt RT crystal structure, both cyclopropyl groups make very close contact with Tyr181 (Figure 18). And both are 4.5 Å or less away from Trp229.

Table 14. Presents the results for *m*-cyclopropylphenyl sultam (1) in wt RT.

Ligand	Residue	Distance
SO_2	Lys101	3.39
Cyclopropyl	Tyr181	3.94
	Tyr183	7.59
	Tyr188	5.93
	Trp229	4.35
Ring C	Tyr181	5.98
	Tyr183	8.84
	Tyr188	4.37
	Trp229	5.55
Ring A	Tyr318	5.108

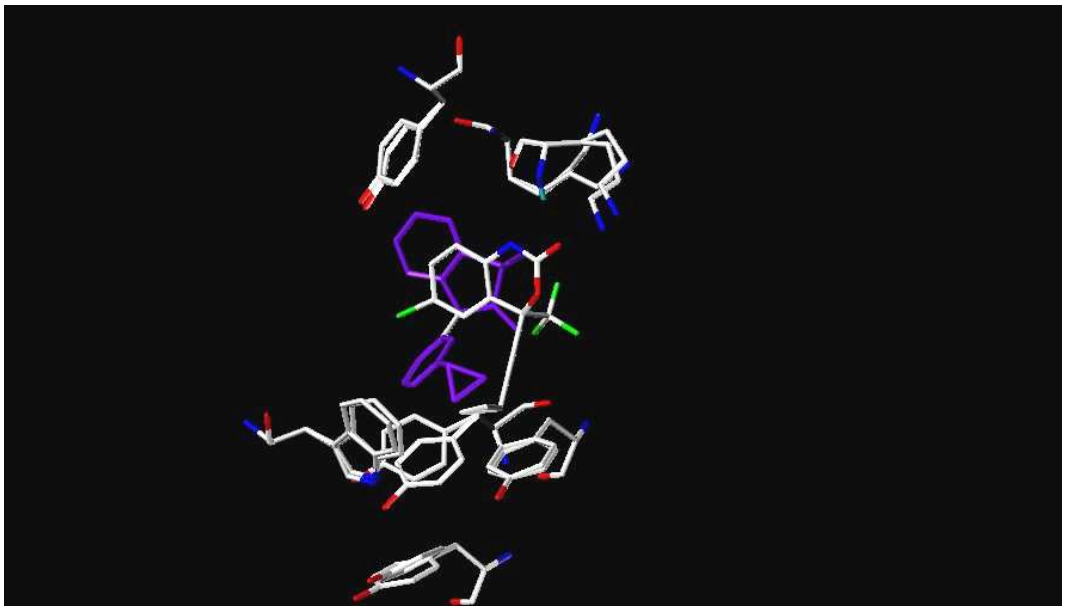

Figure 18. 3-(*m*-Cyclopropylphenyl) sultam in wt/efavirenz RT complex

Docking into Y181C provided the results reported in Table 15. Unfortunately no *hydrogen bond* was predicted for **18** with Lys101 (3.34 Å). Much like the alkylethynyl series, the cyclopropyl group makes a stronger contact with Tyr188 (3.78 Å) than in the wt pocket (5.18 Å). This is due to the loss of the large aromatic interaction with Tyr181 as it mutates to Cys181. Noticeably the distance between the cyclopropyl ring and Trp229 drops under 4 Å in the Y181C pocket. The cyclopropyl ring also makes a significant change in its orientation towards Tyr183 (Figure 19). Until now all the contacts observed between the alkyl/cycloalkyl inhibitor groups located in wing 2 of the pocket have been over 5 Å. This was expected as Tyr183 is involved in pocket formation rather than direct binding. However the cyclopropyl group in **18** moves closer to Tyr183 (4.73 Å) a drop in distance of almost 3 Å compared to the wt RT pocket (7.59 Å). This observation is completely opposite to the trend reported in efavirenz and all the docked sultams. Upon loss of the aromatic Tyr181 to Cys181, these inhibitors seem to move towards wing 1. This was characterized by the decrease in distance with Tyr318 and Lys101, as well as the hydrogen bond predictions observed in some. Compound **18**, however, reorients itself in the hydrophobic region so that it makes more hydrophobic contacts with other aromatic residues such as Tyr183. The cyclopropyl group is popular in drug design due to its unique electronic feature. Cyclopropyl groups have a slight sp^2 character allowing them to behave as π-systems; therefore, their interactions with aromatic rings can be considered π–π interactions.

Table 15. *m*-Cyclpropylphenyl sultam (18) ligand–residue in Y181C RT pocket.

Ligand	Residue	Distance
SO_2	Lys101	3.34
Cyclopropyl	Cys181	—
	Tyr183	4.73
	Tyr188	3.78
	Trp229	3.98
Ring C	Cys181	—
	Tyr183	7.88
	Tyr188	4.21
	Trp229	5.20
Ring A	Tyr318	5.89

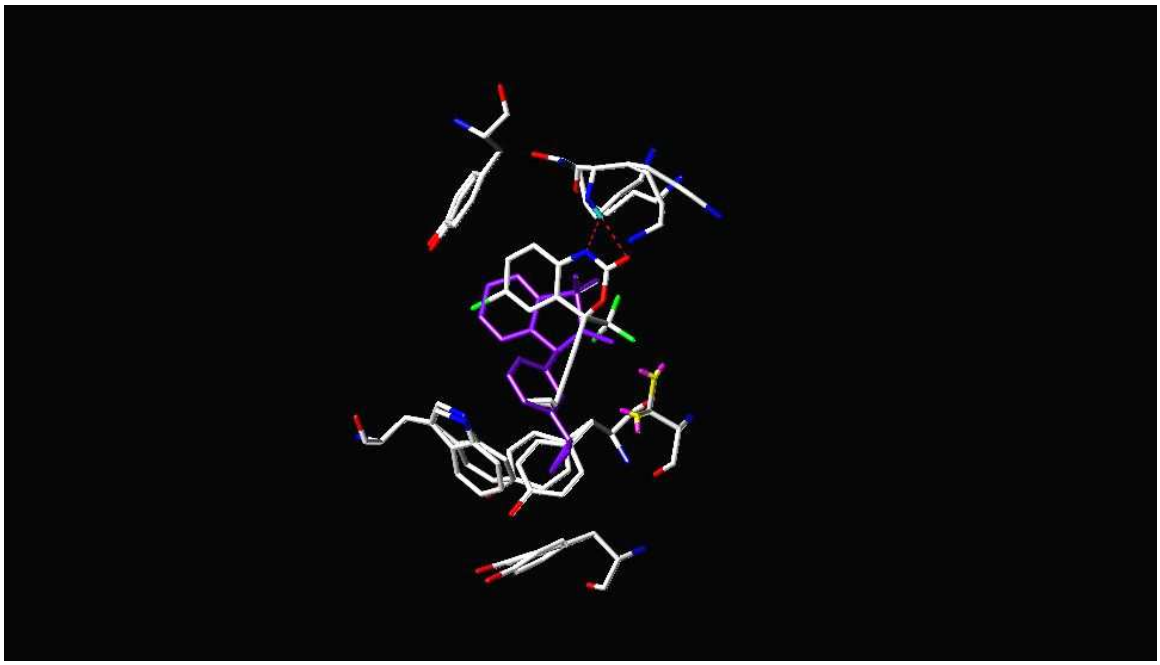

Figure 19. *m*-(Cyclopropylphenyl) sultam (**18**) in Y181C RT superimposed with efavirenz.

3-(Isopropylfuranyl) sultam (**19**) was also docked in wt RT and Y181C RT. Compound **19** adopts a similar orientation in the wt pocket as **18**. The isopropyl group makes contact with Trp229 at a distance of less than 4 Å. No hydrogen bond is predicted, and the distance calculated between the sulfonyl group and Lys101 is 3.25 Å. In general this compound does not have any unique features in its binding conformation that sets it apart from the other inhibitors. Table 16 and Figure 20 show the results of the docking experiments.

In the Y181C RT pocket the most important change noted is the orientation of the furan ring oxygen. After several FlexiDock experiments, the oxygen in the furan ring was always oriented towards the SH in Cys181(Table 17 and Figure 21).

Table 16. FlexiDock results for isopropylfuranyl sultam in wt RT.

Ligand	Residue	Distance
SO_2	Lys101	3.25
Isopropyl	Tyr181	5.74
	Tyr183	7.72
	Tyr188	4.63
	Trp229	3.76
Ring C	Tyr181	6.07
	Tyr183	9.78
	Tyr188	4.79
	Trp229	6.79
Ring A	Tyr318	5.19

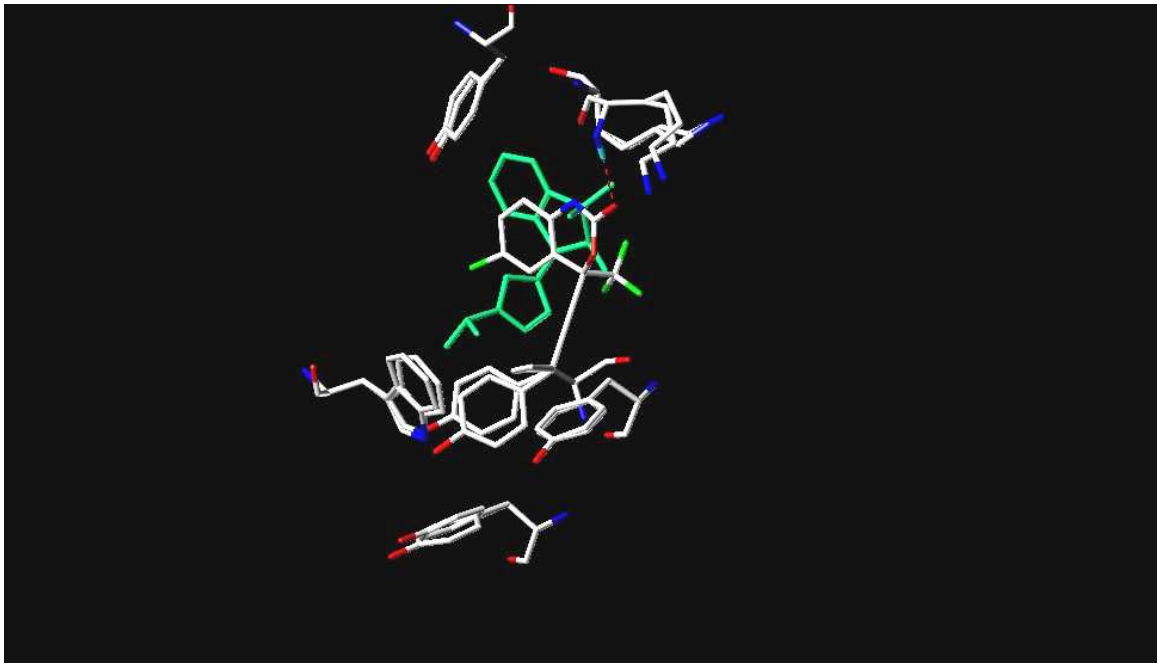

Figure 20. 3-(I*so*-propylfuran) sultam (green) in wt/efavirenz RT(white).

.

Table 17. 3-(Isopropylfuranyl) sultam (**19**) ligand–residue distances in Y181C RT.

Ligand	Residue	Distance
SO_2	Lys101	3.16
Isopropyl	Cys181	——
	Tyr183	7.02
	Tyr188	5.18
	Trp229	3.89
Isopropyl Oxygen	Cys181	3.33
Ring C	Tyr183	8.89
	Tyr188	4.55
	Trp229	6.72
Ring A	Tyr318	5.03

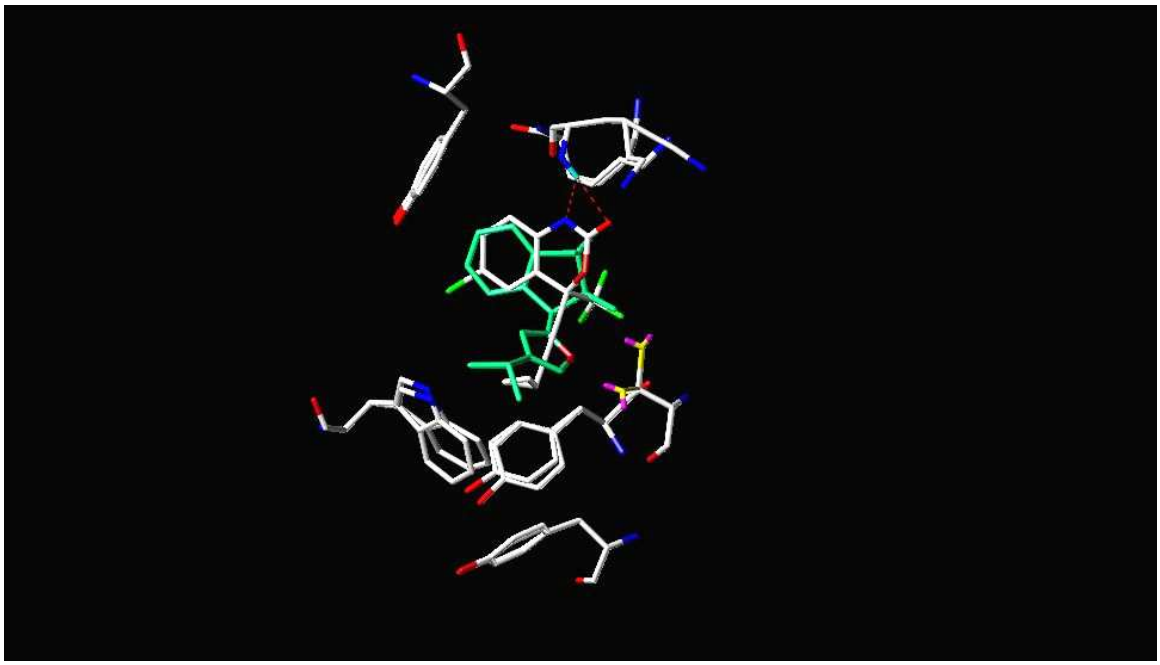

Figure 21. 3-Isopropylfuranyl sultam (19) in Y181C/efavirenz RT.

This is almost a 180º rotation from its position in the wt RT pocket. The distance observed between the oxygen and the Cys181 SH is 3.33 Å. No hydrogen bond is predicted; however, the repeated observation of this result in varying experiments suggest some sort of interaction occurring.

D. Modeling of a Rhodium Catalyst

Mother Nature seems to have mastered the most simple and complex of reactions in the most elegant pathways. Oxidoreductases such as alcohol dehydrogenases catalyze transfer hydrogenations to convert carbonyl compounds into alcohols using NADH or NADPH as cofactors.[145] These reactions are usually extremely stereoselective. However, organic chemists have yet to master the ease in which nature can produce enatiomerically pure compounds. Organic synthesis requires economical and practical reagents that can be utilized at different reaction scales. Catalytic-transfer hydrogenation has received much attention in recent years. The search for nonhazardous enantioselective metal catalysts for transfer hydrogenation dates back to 1976 when Imai and co-workers reported hydrogen transfer from organic compounds to ketone and aldehydes catalyzed by dihydrotetrakis(triphenylphosphine)-ruthenium(II) ($RuH_2(PPh_3)_4$).[146] The process remained primitive and not very well understood until recently. Efforts from Pfalts,[147]Genet,[148] Lemair[149] and Evans[150] produced respectable results, but these reactions were limited by their low enantioselctivity and catalytic activity, as well as low substrate-to-catalyst ratios (S/C). In recent years ruthenium complexes have been improved to overcome

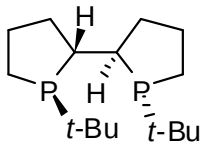

(*S,S,R,R*)-TangPhos

Figure 22. Structure of TangPhos ligand.

the low reactivities and enantioselectivities observed in these reactions.[122, 145, 151]

The most recent work in the area of hydrogen-transfer catalysis comes from Yang and co-workers. They use palladium-diphosphane complexes for the hydrogenation of *N*-tosylimines. They found that palladium-TangPhos (Figure 22) catalyzed hydrogenations most efficiently compared to other complexes used. Reactions proceeded with 99% *ee* and excellent yields.[152]

The saccharin-based synthetic route developed by Baker and co-workers (Scheme 3) for the synthesis of a variety of sultams required an enantioselective reduction of C=N double bonds. Mao and Baker found that the commercially available RhCp* complex reduces imines into racemic amines under mild conditions. They then developed a chiral Rh catalyst for the asymmetric transfer hydrogenation of imines into chiral amines.[122]
Pentamethycylopentadienylrhodium chloride was compbined with (*1R,2R*)-N-(*p*-tolunesulfonyl)-1,2-diphenylehthylenediamine [(*1R,2R),*-TSDPEN] in dicholormethane and triethylamine to give the desired complex **20**. ^{1}H NMR and ^{13}C NMR spectroscopy, along with single crystal X-ray crystallography were used to fully characterize the structure of **20** (Figure 23).

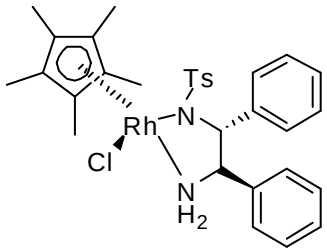

Figure 23. Structure of *R,R*-**20**

The best reaction conditions utilized an azeotropic mixture of formic acid/triethylamine (5:2) with a 200:1 substrate-to-catalyst (S/C) ratio. For the sultam series the presence of an aryl group on position 3 was found to affect the stereoselectivity. *R,R*-**20** gave the *S* enantiomer when C3 had an aromatic group; however, these results were complete opposites when C3 was substituted with a methyl or small alkyl group.[122]

In order to understand the stereoselectivity of this catalyst, a full characterization of the catalytic cycle is needed. Bragg and co-workers in collaboration with Baker and co-workers were able to propose a catalytic cycle through 1D, 2D and variable low-temperature NMR experiments.[153] Scheme 14 shows the catalytic cycle as proposed by Bragg et al.[153] The catalytic cycle begins with the formation of the activated hydride species. The imine sultam (3-(aryl)-1,2-benizothiazole 1,1-dioxide) then approaches the catalyst. Hydrogen transfer occurs, and the reduced sultam is bound to the catalyst. The newly reduced sultam is then released, and it is thought that the solvent stabilizes the ionic rhodium complex formed until another formate ion binds to the metal center to form the hydride species and the cycle continues.

Scheme 14

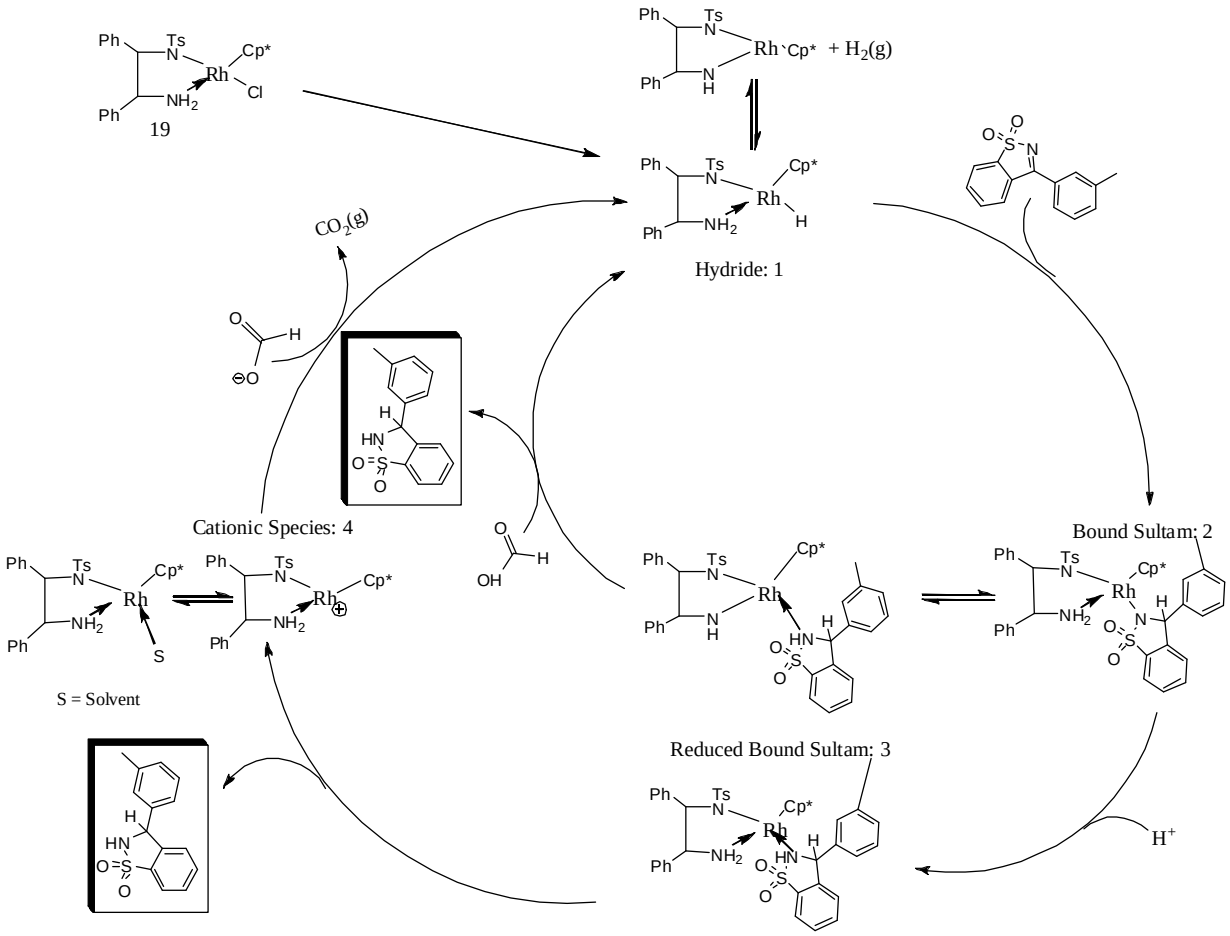
19
Hydride: 1
Bound Sultam: 2
Reduced Bound Sultam: 3
Cationic Species: 4
S = Solvent
$CO_2(g)$
$H_2(g)$
H^+

Modeling studies were employed in an attempt to further understand the catalytic cylcle and explain the stereoselectivity observed. Employing the same principles used in inhibitor/enzyme docking experiments, molecular dynamic studies were performed on the docked imine sultam.

In order to explain the stereoslectivity of the catalyst, a series of imine sultams were docked in two different approaches. The “original” and the “reverse” approach. The original approach is the conformation leading to the enantiomer reported to be the major one produced experimentally. The reverse approach is the conformation leading to the other enantiomer, which was either not observed or observed in low yield.[122]

The studies reported here present initial results. A survey of the literature indicated that the use of Tripos ff and the SYBYL package in such modeling studies is completely novel. The Tripos ff comes with a set of metal parameters typically used in biological systems such as Mg, Ca, Mn and Co. To be able to use the Tripos ff in this project, the rhodium catalyst parameters needed to be added to the force field parameter files. The lack of literature on modeling studies for similar rhodium catalysts led to a different approach.

The basic rhodium parameters were obtained from the Tripos metal parameters files that accompany the SYBYL package (Table 18). These parameters only supplied the essential information for the force field to recognize the atom and include it in calculations. Second, a search of the Cambridge Crystal Structure Database (CCDC) was performed to find different bond angles

Table 18. Rhodium metal parameters from the SYBYL databse.

Parameter Name	Parameter Value
Mnemonic atom type	“Rh”
Heteroatom Symbol	“Rh”
Valence	6
Geometry	OH (octahedral)
Equivalent atom type	Cr.OH (chromium octahedral)
Atomic number	45
Color code	Yellow
Can der Waals radius	1.69
Formal charge	0
Electronegativity	2.28
H–bond Donor	NO
H–bond Acceptor	NO
Lone Pair	0
Temp factor	9.00
Atomic weight	102.9.05
Sybyl 3.x atome type ID	926
Sybyl 3.x mnemonic atom type	“Rh”

and bond lengths for similar complexes. The mean of each value was taken and used as a constraint in energy calculations. This helped guide the Tripos ff and stopped illogical and extremely high energy structures from being produced. Table 19 lists the mean bond angles and bond lengths from the CCDC search.

A preliminary study on several crystal structures of similar Rh complexes was carried out. All complexes were subjected to the Tripos ff minimizations, and the bond angle and bond lengths were monitored. Structures with unreasonable bond angles or bond lengths, or bent aromatic ring were not used in further calculations. Typically these structures have higher energies than the other conformations. The results observed were very encouraging. RMS values were never larger than 0.056, and bond angles and lengths did not change too much from the values observed in the crystal structures. The focus then turned onto the synthetically relevant (*R,R*)-[TSDPEN]Rh-Cp*-Cl ((*R,R*)-**20**).

The *R,R*-**20** crystal structure was downloaded from the Cambride Crystallographic Data Centre (CCDC, code WOLCOP). Bond constraints were only applied for the Rh–Cp* lengths. Bond-angle values for NH–Rh–NTs, NH–Rh–Cp*, NTs–Rh–Cp*, Cl–Rh–NH, Cl–Rh–NTs were constrained to the mean values in Table 19 . A minimization was performed using the Tripos force field and Gasteiger–Hückel charges. In the first calculation no rigid structures were defined. This led to a strained Rh–Cp* bond and a higher energy than the initial crystal energy. To avoid this problem, the Rh–Cp* bonds were defined as “active aggregates”.

Table 19. CCSD bond length and bond angle search results.

Bond Lengths	
Bond	Mean Bond Length (Å)
Rh–Cl	2.43
Rh–N	2.11
Rh–Cp*	1.78
Bond Angles	
Angle	Mean Value (º)
N–Rh–Cl	87.77
N–Rh–N	78.07
N-Rh–Cp*	130.84
Cl-Rh-Cp*	125.34

Members of an active aggregate are minimized together as one unit. This was necessary, because the Tripos force field did not have a bond definition for the Cp*–Rh bonds. It is worth noting that constraining bond lengths between these two entities was not enough, as the aggregate was needed in order for reasonable structures to be produced. It is important to remember that aggregates are not "rigid", i.e., they do not move. Figure 24 depicts the crystal structure of *R,R*-**20** and its minimized structure superimposed on top of each other with an RMS value of 0.055. Table 20 reports the crystal structure and minimized structure bond lengths and bond angles. The initial energy is observed to be 504.463 kcal/mol, and the final energy is 338.266 kcal/mol. Although these energy values have no physical meaning, they are used as points of reference. Observing an energy drop is good, as this means the calculations are producing positive results.

Next we substituted the chlorine atom in the crystal structure with a hydrogen and ran the same minimization on the *R,R*-**20***H* (the hydride species is the active form of catalyst). The initial energy of the complex was 676.41 kcal/mol, and the final energy was 343.54 kcal/mol. Figure 25 presents the minimized *R,R*-**20***H* superimposed on the *R,R*-**20** crystal structures (RMS = 0.036) Table 21 compares bond lengths and angles between the crystal structure and the hydride species. Table 21 reports the crystal and minimized hydride bond lengths and angles. The results observed are comparable to those observed in the minimized *R,R*-**20** structure.

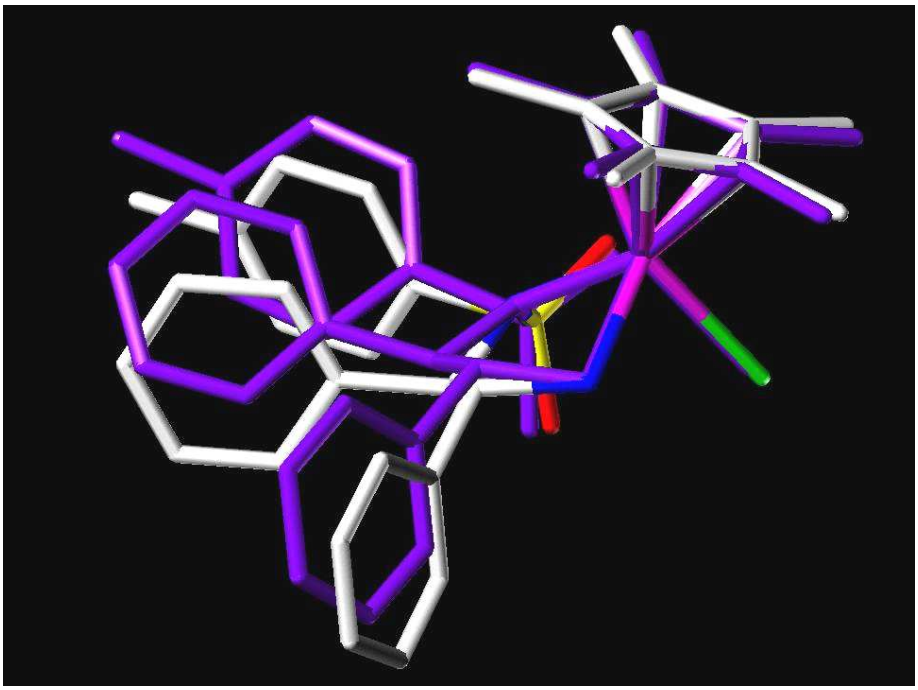

Figure 24. *R,R*-20 crystal (white) superimposed on *R,R*-20 minimzied (violet).

Table 20. Crystal vs. minimized bond lengths and angles for *R,R*-**20**

R,R-Cl			
Bond Lengths	Crystal	Calculated	Δ
Rh-NTs	2.186	2.096	0.09
Rh-NH	2.102	2.064	0.038
Rh-Cl	2.412	2.188	0.224
Rh-Cp*	1.832	1.832	0
NTs-C1	1.473	1.448	0.025
NH-C2	1.481	1.475	0.006
Angles			
NTs-Rh-NH	77.27	77.34	-0.07
Nts-Rh-Cl	94.01	94.01	0
NH-Rh-Cl	84.09	84.14	-0.05
Nts-Rh-Cp*	130.26	130.39	-0.13
NH-Rh-Cp*	129.85	129.97	-0.12
Nts-C1-C2	108.14	104.96	3.18
Nh-C2-C1	106.87	110.1	-3.23
Rh-Nts-C1	113.42	115.71	-2.29
Rh-Nh-C2	108.68	102.53	6.15

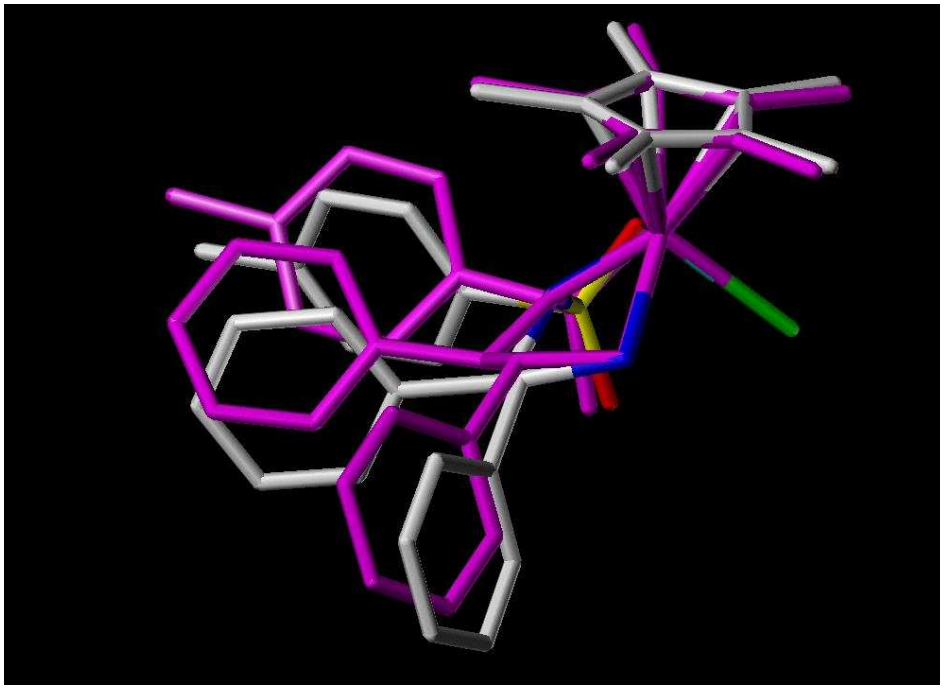

Figure 25. *R,R*-**20***H* (violet) superimposed on *R,R*-20 after minimization.

Table 21. Hydride vs. crystal bond lengths and angles.

Bond Lengths	Crystal	Calculated	Δ
Rh-Nts	2.186	2.106	0.08
Rh-NH	2.102	2.079	0.023
Rh-H	(Rh-Cl)2.412	1.025	1.387
Rh-Cp*	1.832	1.832	0
Nts-C1	1.473	1.448	0.025
NH-C2	1.481	1.476	0.005
Angles			
Nts-Rh-NH	77.27	77.33	-0.06
Nts-Rh-Cl	94.01	94	0.01
NH-Rh-Cl	84.09	84.14	-0.05
Nts-Rh-Cp*	130.26	130.37	-0.11
NH-Rh-Cp*	129.85	129.95	-0.1
Nts-C1-C2	108.14	105.15	2.99
Nh-C2-C1	106.87	110.4	-3.53
H-Rh-Cp*	125.31	125.09	0.22

Please note the the crystal contains a Rh–Cl while the minimized hydride catalyst contains Rh–H bond. It would be expected to observe a significant difference between these two bonds. Our results indicate that the Rh–H bond length is 1.025 Å. The Rh–Cl bond length is almost double that. These results are considered acceptable and reasonable.

The new parameter files for the Tripos force field were loaded. The minimized *R,R*-**20***H* and 3-(*m*-methylphenyl)-1,2-benzisothiazole 1,1-dioxide (**21**) were retrived (Figure 26).

Compound **21** (refered to as imine sultam) was docked into the catalyst cavity using the Dock program in SYBYL. The Dock program is a manual docking program. The "enzyme"/catalyst and inhibitor are each identified. The catalyst was then fixed in space, and the inhibitor's position was adjusted into the cavity. An interactive dialogue box keeps track of steric and electrostatic energies as the inhibitor's position is adjusted. The imine substrate position was adjusted to give the lowest energy possible.

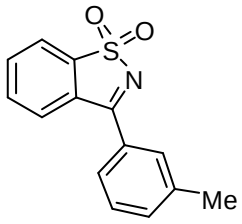

21

Figure 26. Structure of 3-(*m*-methylphenyl) 1,2-benzisothiazole 1,1-dioxide (**21)**.

Two docking experiments were carried out. In the first docking experiment, the imine sultam is positioned so that its sulfonyl group is towards the catalyst NH_2 moiety (Figure 26 A). In the second experiment the sulfonyl group is docked toward the *N*–Ts moiety; this conformation will be refered to as "reverse" (Figure 26 B). Yamakawai and co-workers published two studies that dealt with chiral η^6–arene–ruthenium(II) complexes.[154, 155] In molecular orbital calculations they attempted to identify the mechanisms of action by which asymmetric transfer hydrogenation of carbonyl compounds catalyzed by these complexes proceed.[154] They also performed density functional theory-based (DFT) studies to shed some light on the origin of enantioselectivity in these reactions.[155] Based on their DFT studies they predicted that in aryl ketones CH/π interactions between the arene ring and aryl ketone are the basis of enantioselectivity. According to their findings the *R,R*-catalyst gives the *R* alcohol and vice versa. The rhodium catalyst in question affords the exact opposite selectivity in imine reductions, especially when a bulky aromatic ring exists on ring C. (Refer to figure 6.)

In the original approach in the docking experiment, it is assumed that CH/π interactions do occur. The "reverse" docking conformation assumes that no π interactions govern enantioselectivity. The substrate/catalyst complex is then converted to a FlexiDock input file. This is only done to create a file with both catalyst and substrate in the same molecular area. This is essential in order to be able to minimize the complex as one unit. A molecular dynamics experiment is then performed using the same specifications for aggregates and distance

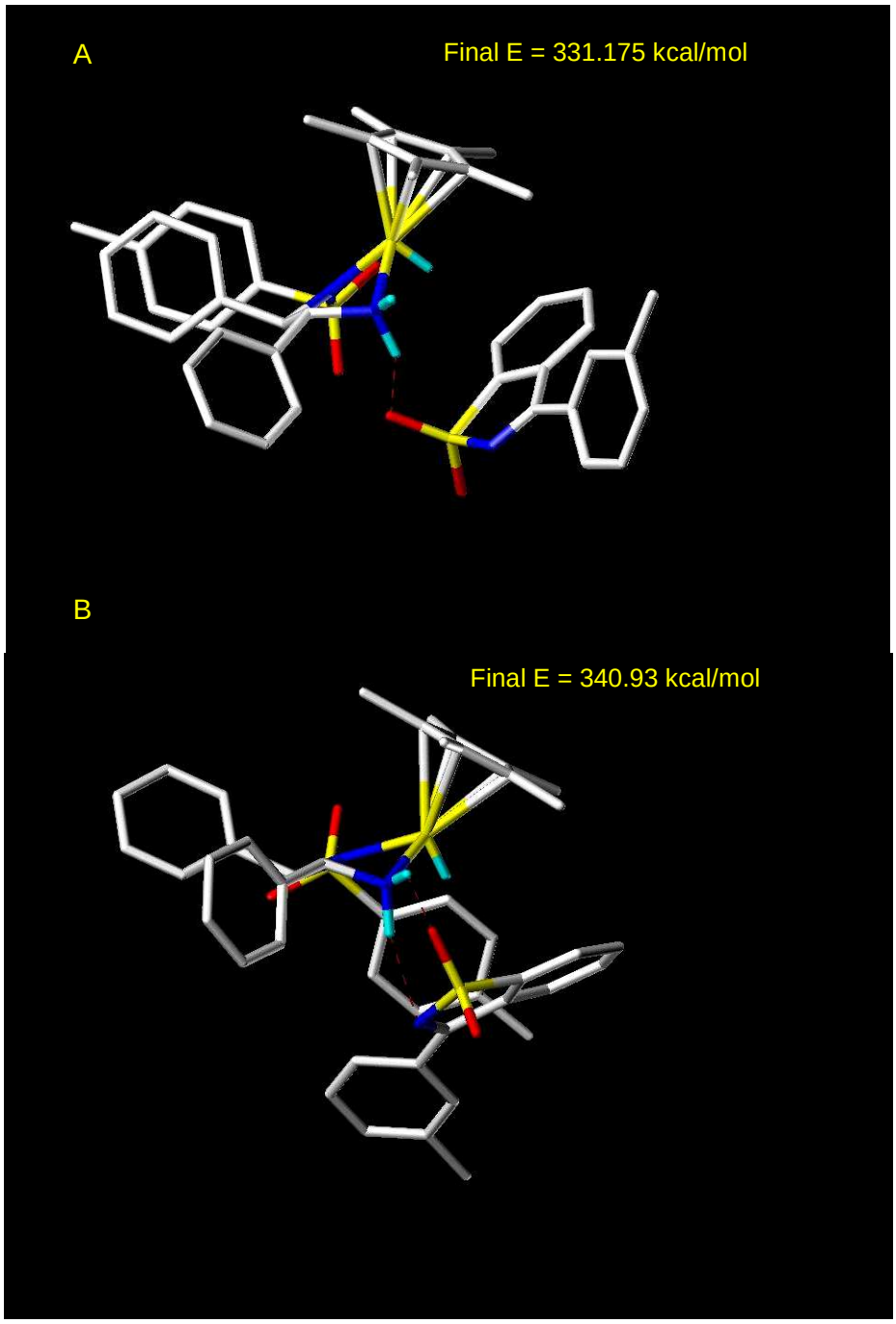

Figure 27. (A) imine substrate docked into ***R,R*-20***H*. (B) imine substrate docked in “reverse” mode

constrains as before. The energies between the two possible substrate approaches are reported and compared. Figure 27 displays both docked conformations with the final energies for each. The final energy of the docked imine sultam is lower than that of the “reverse” conformation, with a difference of ~10 kcal/mol observed between these two complexes. The first complex leads to the *S* stereochemistry on the sultam while the second leads to the *R*.

Experimentally, the *S* enantiomer is the major product isolated from this reaction. The energy difference observed could explain why the original approach is preferred. The *R* or “reverse” approach is relatively higher in energy and therefore is expected to be a minor contributing structure along the conversion pathway.

Next *n*-butylimine (**22**) and methyl imine (**23**) (Figure 28) were docked into the catalyst cavity in both the “original” approach and the “reverse approach. The energy of the first approach which leads to the *R* enantiomer is 126 kcal/mol, and the energy of the “reverse” approach is 117 kcal/mol, which is a difference of 9 kcal/mol. For a small molecule system a change of ~10 kcal is considered significant. Based on these observations the *R* enantiomer should produce the major product. Indeed this is observed experimentally (Figure 29 and Figure 30 show both approaches).[122]

Compound **23**’s results also matched its experimental observation. The “reverse” approach produced the lowest complex energy. This approach leads to the formation of the *R* enantiomer a result that agrees with the experimental results reported by Mao and Baker.[122]

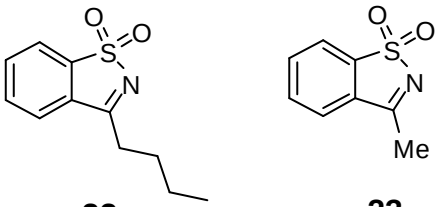

22 **23**

Figure 28. *n*-Butyl imine (**22**) and methyl imine (**23**).

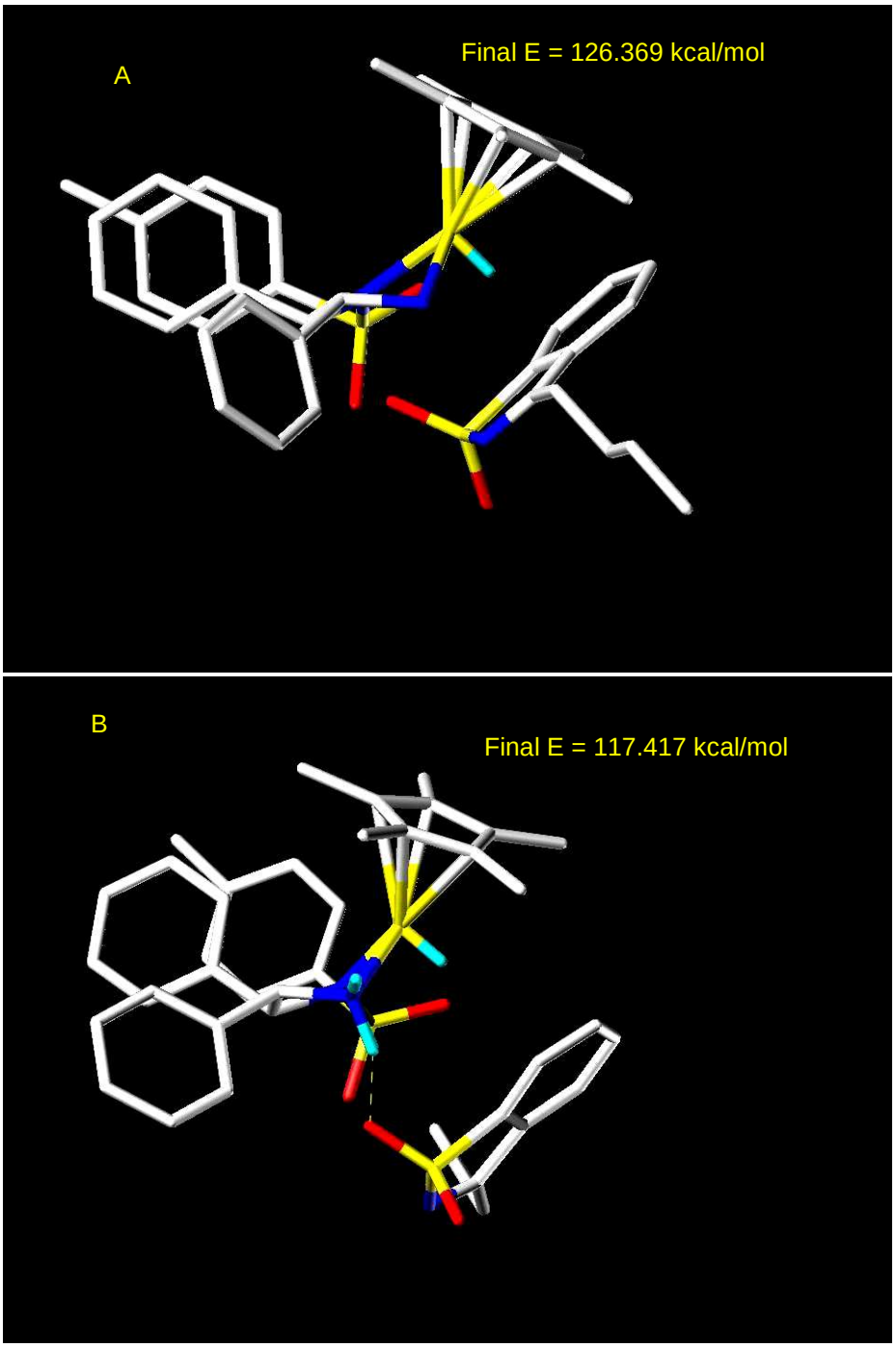

Figure 29. *n*-Butyl imine sultam in *R,R*-**20***H* cavity. (A) original approach, (B) reverse approach

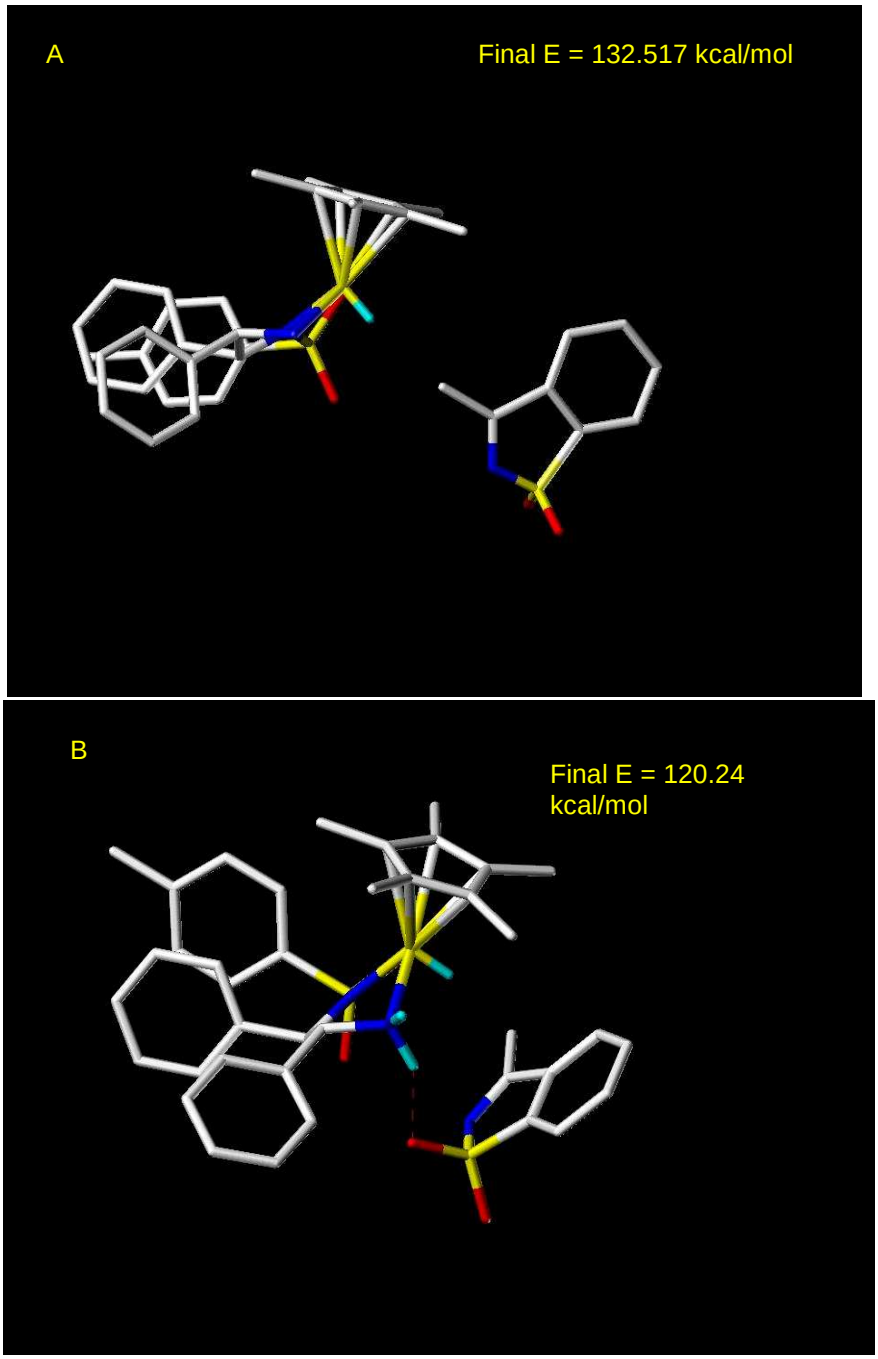

Figure 30. Methyl imine sultam in *R,R*-**20***H* (A) original approach; (B) reverse approach.

3-(Cyclopropylethynyl)-1,2-benzisothiazole 1,1-dioxide was also docked into the catalyst cavity. Figure 31 shows both original and “reverse” approach. The calculated energy for the original approach is 441.23 kcal/mol and for the reverse approach 434.62 kcal/mol. Based on the pattern observed in the previous docking experiments, the R stereochemistry should be preferred. However, synthetic studies yielded products with no optical activity, which indicates that the catalyst did not enantioselectively reduce the imine bond. Moreover, for the cyclopropyl and cyclobutyl analogues, the alkyne was also reduced to the alkane. The *tert*-butyl analogue was found to be optically inactive; however, its triple bond remained intact. This is probably due to steric hindrance as the *tert*-butyl group is bulkier than the small ring structures.

The modeling studies presented above are considered only initial modeling studies. We used these compounds to establish the best parameters for such experiments. It was very disappointing to find that not only did the catalyst not reduce the alkylethynyl sultam series stereoselectively, but it also reduced the alkyne bond into an alkyl bond for two out of three of the target compounds. It is clear from the experimental results that the approach of substrate to catalyst is greatly governed by steric effects. In the future further mechanistic studies are needed. A study of different substrates with a wide variety of substituents at C-3 is also required in order to determine when the catalyst exactly switches from stereoselectively producing *S* to producing racemic mixture, to stereoselectively producing *R*.

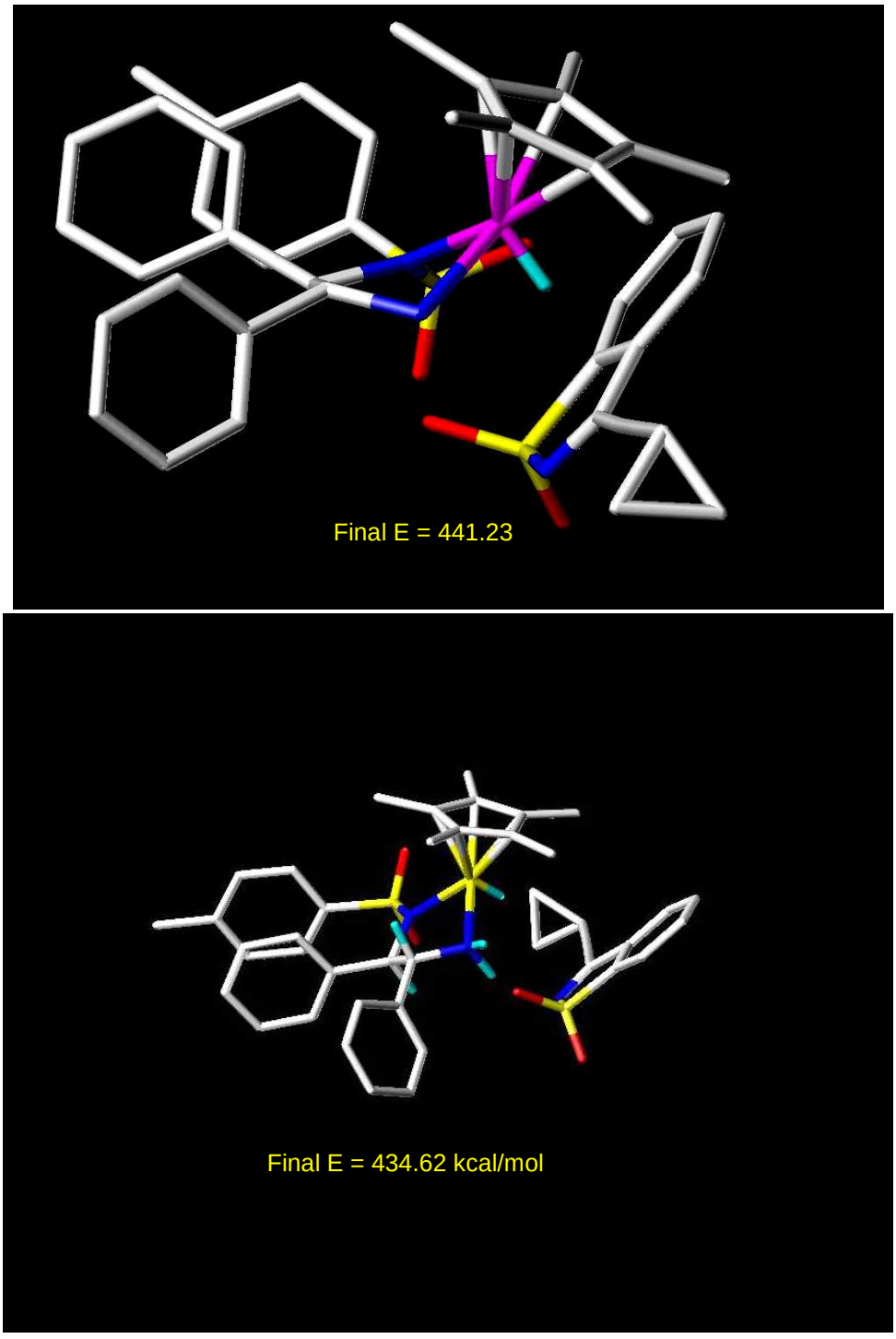

Figure 31. Cyclopropylethynyl imine sultam in catalyst cavity. (A) direct approach; (B) reverse approach.

III. Experimental

Preparation of 3-(chloro)-1,2-benzisothiazole 1,1-dioxide (1)

In a dry round bottom flask equipped with a stir bar and an air condenser were placed 4.05 g (22.1 mmol) of saccharin and 5.88 g (28.6 mmol) of PCl_5. The apparatus was fitted with an inlet nitrogen line and an outlet vent to allow release of gas build up into the fume hood and the mixture was heated to 80 ºC. Once the reaction changed from cloudy to clear, the temperature was raised to 175 ºC for 2 h. At the end of the 2-h period, the reaction mixture was cooled to 100 ºC and a vacuum was applied to remove the $POCl_3$. The reaction was left to cool to room temperature while under vacuum and when at room temperature the vacuum was maintained for another 1 h. A pale yellow solid formed. It was recrystallized from hot toluene to give a white fluffy solid (3.5 g, 79% yield): mp (139-143 ºC; lit. 140–144) ^{1}H-NMR (300 MHz, $CDCl_3$, 25 ºC): δ 7.8–8.4 ppm (m, 4H, aromatic). ^{13}C NMR (300 MHz, $CDCl_3$, 25 ºC): δ 166 (C3), 140.5 (C9), 134.9 (C8), 134.4(C7), 129.8 (C4) 125.1 (C5), 122.5 (C8).

3-Ethynylalkyl 1,2-benzisothizoles 1,1-dioxides

In a dry flask was dissolved 2.0 mmol of the respective alkyne in 6 mL of freshly dried THF. The solution was stirred and cooled to –78 ºC under anhydrous conditions and a nitrogen atmosphere. One equivalent of 2.2 M *n*-BuLi solution in THF (0.9 mL) or 1.6 M MeLi in THF (1.25 mL) were then added via a syringe. The reaction was left to stir for 4 h and then warm to –40 ºC. It was then cooled to –78 ºC, and a solution of 0.643 g (1.5 equiv.) 3-chloro-1,2-benzisothiazole 1,1-dioxide in dry THF was quickly poured into the reaction. The flask was refitted

with a septum and a nitrogen line, and the coupling reaction mixture was left to stir at –78 ºC for 1 h. It was monitored by TLC. After 1 h , 5 mL of satd aq NH_4Cl was added to quench the reaction at –78 ºC. The mixture was left to warm to room temperature overnight, and a white precipitate formed. The biphasic mixture was then filtered and separated. The organic layer was washed with 1.0 M $NaHCO_3$ (2 x 5 mL). It was dried over anhyd. $MgSO_4$, vacuum filtered and rotary evaporated. The desired product was purified using silica gel column chromatography eluting with a gradient solvent system starting with 5% acetone in petroleum ether to 10% acetone in petroleum ether (for the butylethynyl analogues **4** and **5)** or 15% acetone in petroleum ether (for the cyclopropylethnyl analogue **3**).

3-(Cyclopropylethynyl)-1,2-benzisothiazole 1,1-dioxide (3)

Yield: 0.177 g (40% yield). ^{1}H NMR (300 MHz, $CDCl_3$, 25 ºC): δ 7.89–7.73 (m, 4H, CH, ArH), 1.64–1.74 (m, 1H, CH-cyclopropyl), 1.10–1.21 (m, 4H, CH_2-cyclopropyl).

^{13}C NMR (300 MHz, $CDCl_3$, 25 ºC): δ 156.54 (C-3, C=N), 138.71 (C-9, CH, Ar), 133.86 (C-6, Ar), 133.74 (C-7, Ar), 131.36 (C-4, Ar), 125.04 (C-5, Ar), 122.11 (C-8, Ar), 115.77 (C-1', alkyne), 68.79 (C-2', alkyne), 10.97 (C-4',C-5', cyclopropyl), 1.11 (C-3', cyclopropyl). HRMS-APPI (*m/z*): $[M+H]^+$ calcd for $C_{12}H_{10}NO_2S$, 232.0432; found, 232.0424.

3-(*tert*-Butylethynyl)-1,2-benzisothiazole 1,1-dioxide (4)

Yield: 0.140 g (47% yield). ^{1}H NMR (300 MHz, $CDCl_3$, 25 ºC): δ 7.92–7.68 (m, 4H, CH, ArH), 1.46 (s, 9H, CH_3, *t*-butyl). ^{13}C NMR (300 MHz, $CDCl_3$, 25 ºC): δ

156.81 (C-3, C=N), 138.68 (C-9, CH, Ar), 133.97 (C-6,CH, Ar), 133.82 (C-7, CH,Ar), 131.31 (C4,CH, Ar), 125.05 (C-8, Ch, Ar), 122.11 (C-5, CH, Ar, 118.59 (C-2′, C≡C), 71.51 (C-1′, C≡C), 29.95 (3CH_3, *t*-Bu), 28.99 (-$C(CH_3)_3$, *t*-But). HRMS-APPI (*m/z*): $[M+H]^+$ calcd for $C_{13}H_{14}NO_2S$, 248.0745; found, 248.0731.

3-(Cyclobutylethynyl)-1,2-benzisothizoles 1,1-dioxide (5)

Yield: 0.185 g (43% yield). ^1H NMR (300 MHz, $CDCl_3$, 25 ºC): δ 7.9–7.60 (m, 4H, CH, ArH), 3.31–3.29 (m, 1H, CH-cyclobutyl), 2.24–1.80 (m, 6H, CH_2-cyclobutyll). ^{13}C NMR (300 MHz, $CDCl_3$, 25 ºC): δ 157 (C-3, C=N), 138.59 (C-9, CH, Ar), 133.99 (C-6, Ar), 133.89 (C-7, Ar), 131.26 (C-4, Ar), 125.015(C-5, Ar), 122.10 (C-8, Ar), 114.23.77 (C-1', alkyne), 89.01 (C-2', alkyne), 19.42–18.16(C-4',C-5', C-6′, cyclobutyl , 0.97 (C-3', cyclobutyl). HRMS-APPI (*m/z*): $[M+H]^+$calcd for $C_{13}H_{14}NO_2S$, 245.051; found, 245.062.

3-(Cyclopropylethyl)-2,3-dihydrdo-1,2-benzisothiazole 1,1-dioxide (6)

In a dry round-bottom flask equipped with a stirring bar and a nitrogen line was dissolved 1.9 mg of (*R,R*)-[TSDPEN]RhCp* in 1 mL of dry dichloromethane and 0.05 mL of an azeotropic mixture of HCOOH:Et_3N (5:2) . The mixture was stirred for ten min. A solution of 3-(cyclopropylethynyl)-1,2-benzisothiazole 1,1-dioxide (140 mg 0.606 mmol) in 1 mL dry dicholoromethane, and 0.05 mL of azeotrope were added. The reaction was monitored by TLC. After 30 min, no product formation was observed. Another aliquote of the azeotrope (0.1 mL) were added, and the reaction mixture was stirred for another 30 min, and product formation was observed at this time. Over the course of 2 h a total of 0.6 mL of azeotrope was added, and TLC were taken at 15-min intervals. Upon

disappearance of all starting material, the reaction was quenched with 1 M $NaHCO_3$ (aq.). The two layers were separated, and the organic layer was dried over anhyd $MgSO_4$, vacuum filtered and evaporated under reduced pressure to give a dark-red residue. Purification by silica gel column chromatography in a gradient solvent system from 5% acetone in pet ether→15% acetone in pet ether (this concentration was held until the first spot was isolated)→ 20% acetone in pet ether (product eluted with this concentration) gave the desired product in 50% yield (70 mg). ^{1}H NMR (300 MHz, $CDCl_3$, 25 ºC): δ 7.81–7.36 (4H, CH, ArH), 5.45 (1H,s, NH), 5.13 (m,1H, CH, *J* = 3.9, *J* = 9.3, CH), 3.26–3.03 (m, 2H, CH_2(1′), *J* = 3.6 Hz, *J* = 9.6 Hz, J_{gem}= 18 Hz), 1.95 (m, 1H, CH in cycloropyl, *J* = 4.5, *J* = 1.5), 1.15–1.11 (m, 2H, CH_2(2′),*J* = 4.5) 0.99–0.95 (dt, 2H, CH_2 in cyclopropyl, *J* = 3.6, *J* = 4.5), 0.89-0.84 (m, 2H, CH_2 in cyclopropyl). ^{13}C NMR (300 MHz, $CDCl_3$, 25 ºC): δ 138.61 (C-4, CH, Ar), 135.60 (C-9, Ar), 133.11 (C-6, Ar), 129.36 (C-8, Ar), 123.88 (C-5, Ar), 121.55 (C-7, Ar), 52.90 (C-3), 48.95 (C-1′), 21.06 (C-2′), 14 (CH, cyclopropyl), 11.71–11.61 ($2CH_2$, cyclopropyl). HRMS-APPI (*m/z*): $[M+H]^+$ calcd for $C_{12}H_{15}NO_2S$, 238.0902; found, 238.0907.

3-(*tert*-Butylethynyl)-2,3-dihydro-1,2 benzisothiazole 1,1-dioxide (7)

In a dry round-bottom flask equipped with a stirring bar was dissolved 1.6 mg of R,R-[TSDPEN]RhCp* in 1 mL of freshly dried dichloromethane and 0.047 mL of HCOOH:Et_3N azeotrope (1 equiv of formic acid to 1 equiv of catalyst) The mixture was stirred for 10 min at room temperature, then a solution of 3-(*tert*-butylethynyl)-1,2-benzisothizole 1,1-dioxide, 120 mg (0.485 mmol) in 1 mL of CH_2Cl_2 and 0.047 mL of azeotrope were added. The reaction was monitored by

TLC, and after 30 min product was already forming. Over the course of 2.5 h a total of 0.6 mL of azeotrope was added in increments of 0.1 mL at 30 min intervals. TLC were taken every 15 min. At 2.5 h the TLC indicated completion of the reaction. The reaction was quenched with 1 M $NaHCO_3$ (aq). The biphasic mixture was separated, and the organic layer was dried over anhyd $MgSO_4$, vacuum filtered and rotary evaporated to give a dark red-residue. Column chromatography using a gradient solvent system starting with 5% acetone in pet ether → 15% acetone in pet ether (this was held until the first spot was completely eluted)→ 20% acetone in pet ether until the desired product was collected. Rotary evaporation gave the desired product as a white solid in 61% yield (40 mg). ^{1}H NMR (300 MHz, 25 ºC, $CDCl_3$: δ 7.70–7.91 (m, 4H, CH, ArH), 6.2 (s,1H, CH), 1.25 (s, 9H, -C(CH_3)). ^{13}C NMR : δ 151.00 (C-4), 135.42 (C-9), 133.42 (C-6), 133.09 (C-8), 129.92 (C-7), 122.65 (C7), 121.82 (C2′, C≡C), 89.54 (C1′, C≡C), 41.77 (C3), 27.04 (3 CH_3, t-Butl), 0.98 (C3′, *t*-But). HRMS-APPI (*m/z*): $[M-H]^+$ calcd for $C_{13}H_{14}NO_2S$, 248.074; found, 248.072.

3-(Cyclobutylethyl)-2,3-dihydro-1,2benzisothiazole 1,1-dioxide (23)

(*R,R*)-[TSDPEN]RhCp* (1.15 mg, 0.002 mmol) were dissolved in dry dicholoromethane under anhydrous conditions and a nitrogen atmosphere. An azeotropic mixture of HCOOH:Et_3N (5:2) (0.034 mL) was added via a micro syringe. The reaction was stirred for 10 min, then a solution of 3-(cyclobutylethynyl)-1,2-benzisothiazole 1,1-dioxide (**5**) (89 mg, 0.36 mmol) in 1 mL of dichloromethane and 0.034 mL of azeotrope was added. Reaction progress was monitored by TLC, and product started forming around 35 min.

Over the course of 2.5 h 0.1 mL increments were added at 30-min intervals while TLCs were taken every 15 min. Upon disappearance of all starting material, the reaction was quenched with 1 M $NaHCO_3$ (aq). The two layers were then separated, and the organic layer was dried over anhyd $MgSO_4$. It was then vacuum filtered, and the solvent was removed under reduced pressure to give a dark-red residue. Silica gel column chromatography using a gradient solvent system from 5% acetone in petroleum ether to 15% acetone in petroleum ether gave 79 mg (60%) of the desired product. ^{1}H NMR (300 MHz, $CDCl_3$, 25 ºC): δ 7.99–7.24 (4H, CH, ArH), 5.95 (1H,s, NH), 5.20 (m,1H), 3.95–3.1(m, 2H, CH_2(1′), 2.95 (m, 1H, CH in cyclobutyl) 2.1–1.1 (m, 4CH_2, CH_2(2′), 3CH_2 in cyclobutyl). ^{13}C NMR (300 MHz, $CDCl_3$, 25 ºC): δ 138.61 (C-4, CH, Ar), 135.60 (C-9, Ar), 133.10 (C-6, Ar), 129.33 (C-8, Ar), 123.80 (C-5, Ar), 121.45 (C-7, Ar), 56.89 (C-3), 48.95 (C-1′), 21.06 (C-2′), 29.02 (CH, cyclobutyl), 19.42–18.16 (3CH_2, cyclobutyll). HRMS-APPI (*m/z*): $[M+H]^+$ calcd for $C_{13}H_{17}NO_2S$, 251.098; found, 250.969.

3-(Alkylethynyl)-2,3-dihydro-2-methyl 1,1-dioxide

The respective 3-(alkylethynyl)-2,3-dihydro-1,2-benisothiazole 1,1-dioxide was dissolved in dry *N*-*N*-dimethylformamide or dry acetonitrile under anhydrous conditions and a nitrogen atmosphere. Cs_2CO_3 (1.5 equiv) were added, and the reaction mixture was then stirred at room temperature for 1 h. Excess amount of MeI was added via a syringe, and the reaction was then stirred at room temperature for 1 h. It was monitored by TLC (25% acetone in petroleum ether). Upon disappearance of the starting material, the reaction was quenched with

water. The mixture was concentrated under high vacuum to give a yellow oil with a white precipitate. The residue was taken up in 5 mL dichloromethane and washed with water (3 x 5 mL). The organic layer was then dried over anhydrous $MgSO_4$, and vacuum filtered, and the solvent was rotary evaporated under reduced pressure to give a yellow oil. Flash column chromatography with 15%–20% acetone in petroleum ether afforded the desired products in quantitative yields.

3-(Cyclopropylethyl)-2,3-dihydro-2-methyl 1,1-dioxide (9)

Yield: 35 mg, 90% ^{1}H NMR (300 MHz, $CDCl_3$, 25 ºC): δ 7.32–7.8 (m, 4H, CH, ArH), 4.97–4.90 (t, 1H, CH(3)), 3.3-2.96 (m, 2H, CH_2(2′), 2.90 (m, 3H, N–CH_3), 2.0-1.9 (m, 1H, CH in cyclopropyl), 1.2–1.1 (m, 2H, CH_2(2′)), 1.85–0.95 (m, 4H, $2CH_2$ in cyclopropyl). ^{13}C NMR (300 MHz, $CDCl_3$, 25 ºC): δ 138.13 (C-9, CH, Ar), 134.51 (C-6, Ar), 133.01 (C-7, Ar), 129.35 (C-5, Ar), 124.24 (C-4, Ar), 121.35 (C-8, Ar), 58.64 (C-3), 47.46 (N-CH_3), 29.59 (C-1′), 21.37 (C-2′), 18.00 (CH, cyclopropyl), 11.71-11.61 ($2CH_2$, cyclopropyl). HRMS-APPI failed after several trials. Compound would not ionize.

3-(*tert*-Butylethynyl)-2,3-dihydro-2-methyl 1,1-dioxide(10)

Yield: 40 mg, 89% ^{1}H NMR (300 MHz, $CDCl_3$, 25 ºC): δ 9.13-9.12 (d,1H, CH, Ar), 7.86-7.85 (m, 3H, CH, ArH), 6.13 (s,1H, CH(3), 10b), 5.91 (s,1H, CH(3), 10a), 3.21 (s, 3H, N-CH_3, 10b), 3.18 (s,3H,N-CH_3,10b), 1.2 (s, 9H, $3CH_3$, *t*-butyl). ^{13}C NMR (300 MHz, $CDCl_3$, 25 ºC): δ 133.87 (C-9), 133.57 (C-6), 132.17 (C-8), 129.00 (C-7), 122.65 (C7), 99.17 (C2′, C≡C), 94.73 (C1′, C≡C), 41.71 (C3 **10a** or **10b**), 44.21 (C3, **10a** or **10b**), 29.69 (N-CH_3) 27.12 (3 CH_3, t-butyl), 0.98 (C3′, t-

butyl). HR MS-APPI (*m/z*): $[M+H]^+$ Calcd for $C_{14}H_{16}NO_2S$, 262.0902; found 262.0933.

3-(Cyclobutylethynyl)-2,3-dihydro-1,2-benzisothiazole (11).

Yield: 20 mg , 60%. ^1H NMR (300 MHz, $CDCl_3$, 25 ºC): δ 7.80–7.41 (4H, CH, ArH), 5.20 (m,1H), 3.85–3.1(m, 2H, CH_2(1′), 2.95 (m, 1H, CH in cyclobutyl), 2.89 (s, 3H, N-CH_3) 2.1–1.1 (m, 4CH_2, CH_2(2′), 3CH_2 in cyclobutyl). ^{13}C NMR (300 MHz, $CDCl_3$, 25 ºC): δ 137.61 (C-4, CH, Ar), 135.50 (C-9, Ar), 133.20 (C-6, Ar), 129.33(C-8, Ar), 123.80 (C-5, Ar), 121.45 (C-7, Ar), 57.99 (C-3), 48.95 (C-1′), 21.06 (C-2′), 29.02 (CH, cyclobutyl), 19.42–18.16 (3CH_2, cyclobutyll). APPI failed after several attempts. The expected m/z of 280.137 was not observed, the spectrum only had background.

2,3-Dihydro-3,3-dialkylethynyl-1,2-benzisothizoles 1,1-dioxide

Method A.

In a dry flask under anhydrous conditions and a nitrogen atmosphere were dissolved 2.0 mmol of the respective alkyne. 1 equivilant of 2.2 M n-BuLi (0.9 mL) or 1.6 M MeLi (1.25 mL) were added via a syringe at -78 ºC. The reaction was left to stir for four h while it warmed to -40 ºC. 0.9 mmol (0.165 g)of saccharin (0.45 equivalents) were dissolved in dry THF and added dropwise over a period of 30 min. The reaction was then left to warm up to r.t over night. It was then cooled to 0 ºC and quenched with saturated NH_4Cl (aq.). The biphasic mixture was filtered, and the organic layer separated. It was washed with 1 M $NaHCO_3$ (2 x 5 mL) and dried over anhydrous $MgSO_4$. Rotary evaporation afforded the bis-alkylated sultam in low yields (15-30%yield).

Method B.

In a dry flask under anhydrous conditions and a nitrogen atmosphere were dissolved 2.0 mmol of the respective alkyne. 1 equivialnt of 2.2 M n-BuLi (0.9 mL) or of 1.6 M MeLi (1.25 mL) were added via a syringe at -78 ºC. The reaction was left to warm to -40 ºC over the course of four h. A solution of 3-chloro-1,2-benzisothizole 1,1-dioxide in THF (2 mmol, 0.402 g, 1 equivilant), were added slowly over the course of 30-40 min at -78 ºC. The reaction was then left to warm again to -40 ºC. It was then quenched with saturated NH_4Cl (aq); the mixture was filtered then separated. The organic layer was then washed with 1 M $NaHCO_3$ (aq), then dried over anhydrous $MgSO_4$. Vacuum filtration followed by rotary evaporation gave the desired products as crystalline solids in moderate yields.

2,3-Dihydro-3,3-dicyclopropyllethynyl-1,2-benzisothizoles 1,1-dioxide (12)

Yield: 0.130 g, 60%. ^{1}H NMR (300 MHz, $CDCl_3$, 25 ºC): δ 7.74-7.754 (m, 4H, CH, ArH), 5.0 (s, 1H, NH), 1.29-1.2 (m, 2H, 2CH from cyclopropyl), 0.81-0.68 (m, 8H, 4CH_2 from cyclopropyl). ^{13}C NMR (300 MHz, $CDCl_3$, 25 ºC): δ 140.97 (C-9, CH, Ar), 134.26 (C-6, Ar), 133.63 (C-7, Ar), 130.36 (C-5, Ar), 125.21 (C-4, Ar), 121.21 (C-8, Ar), 88.76 (C-2′, C≡C), 72.39 (C-1′, C≡C), 52.27 (C-3), 8.37 (4CH_2 cylopropyl), -0.59 (2CH cyclopropyl). HR MS-APPI (*m/z*): $[M+H]^+$ calcd for $C_{17}H_{16}NO_2S$ 298.0902, found 298.0906.

2,3-Dihydro-3,3-dicyclobutylethynyl-1,2-benzisothizoles 1,1-dioxide (13)

Yield: 0.150 g, 67% ^{1}H NMR (300 MHz, $CDCl_3$, 25 ºC): δ 7.76-7.55 (m, 4H, CH, ArH), 3.09-2.90 (m, 1H, CH from cyclobutyl), 2.26-1.82 (m, 6H, $3CH_2$ from cyclobutyl). ^{13}C NMR (300 MHz, $CDCl_3$, 25 ºC): 140.91 (C9, Ar), 134.03 (C-6, Ar), 133.37 (C-7,Ar), 130.09 (C-5), 124.98 (C-4,Ar), 120.95 (C-8,Ar), 89.09 (C-2′, C≡C), 78.07 (C-1′, C≡C), 52.38 (C-3), 29.28-29.27 ($2CH_2$, cyclobutyl ring), 24.61 (CH, cyclobutyl), 19.13 (CH cyclobutyl). HR MS-APPI (*m/z*): $[M+H]^+$ calcd for $C_{19}H_{20}NO_2S$ 326.1215, found326.1223. $[M-H]^+$ calcd for $C_{19}H_{18}NO_2S$ 324.1058 found, 324.1471.

3,3-(di-*tert*-butylethynyl)-2,3-dihydro-1,2-benistohiazole 1,1-dioxide (14)

Yield: 0.110 9, 70%. ^{1}H NMR (300 MHz, $CDCl_3$, 25 ºC): δ 8.21-7.41 (m, 4H, CH, ArH), 1.26 (s, 9H, *t*-butyl). ^{13}C NMR (300 MHz, $CDCl_3$, 25 ºC): δ 140.31 (C-4), 139.15 (C-9), 132.89 (C-6), 130.28 (C-8), 129.92 (C-5), 129.00 (C-7), 95.15 (C-2′, C≡C), 79.69 (C-1′, C≡C), 66.14 (C-3), 30.29 (CH_3, t-butyl), 27.58 (C-3′, *t*-butyl). HR MS-APPI (*m/z*): $[M+H]^+$ calcld for $C_{19}H_{24}NO_2S$ 330.1528, found 330.1534.

2,3-Dihydro-2-methyl-3,3-(di-*t*-butylethynyl)-1,2-benzisothizoles 1,1-dioxide (15)

In a flame dried flask 0.205 g (0.62 mmol) of (**14**) and 0.303 g (0.93 mmol, 1.5 equiv.) of Cs_2CO_3 were dissolved in freshly dried acetonitrile under anhydrous conditions and a nitrogen atmosphere. The reaction was stirred at r.t. for one hour then excess amount of MeI (0.1 mL, 3 mmol) were added via a syringe. The progress of the reaction was monitored by TLC. Upon disappearance of the starting material, the mixture was concentrated under reduced pressure to give a

yellow oil and a white precipitate. The mixture was suspended in dicholormethane and the organic layer was washed with water (3x 10 mL) and dried over anhydrous $MgSO_4$. Vacuum filtration, followed by rotary evaporation, then high vacuum rotary evaporation gave a pale yellow oil. Flash column chromatography with 15% acetone in petroleum ether afforded the desired product in qualitative yield (0.200 g). ^{1}H NMR (300 MHz, $CDCl_3$, 25 ºC): δ 8.36-7.4 (m, 4H, CH, ArH), 2.9 (s, 3H, N-CH_3), 2.25 (s, 18H, 6CH_3 *t*-butyl). ^{13}C NMR 143.03 (C-9), 137.12 (C-4), 132.41 (C-6), 129.92 (C-8), 129.54 (C-5), 128.55 (C-7), 94.79 (C-2′,C≡C), 79.09 (C-1′,C≡C), 65.62 (C-3), 37.75 (N-CH_3), 30.39 (-$C(CH_3)_3$, 2 *t*-butyl), 27.49 (-$C(CH_3)$). HRMS-APPI (*m/z*): calcd for $C_{20}H_{26}NO_2S$ 343.1606 found

2,3-Dihydro-2-methyl-3,3-(dicyclobutyllethynyl)-1,2-benzisothizoles 1,1-dioxide (16).

In a dry round-bottom flask 83 mg (0.255 mmol) and 125 mg (0.383 mmol , 1.5 equiv.) were dissolved in dry acetonitrile under anhydrous conditions and a nitrogen atmosphere. The mixture was stirred at r.t. for one hour, then an excess amount of MeI (108 mg, 0.048 mL, 3 equiv) were added via a syringe. The reaction was monitored by TLC. Upon disappearance of starting material, it was rotarty evaporated to give a yellow oil and white precipitate. The residue was taken up in 10 mL of dichloromethane and washed with water (3 x 5 mL). The organic layer was then collected, dried over anhydrous $MgSO_4$ and vacuum filtered. It was concentrated under reduced pressure and high vacuum pressure to give a pale yellow crystalline solid. Flash chromatography using 15% acetone

in petroleum ether gave the desired product in quantitative yield as a while crystalline solid (85 mg). ^{1}H NMR (300 MHz, $CDCl_3$, 25 ºC): δ 7.78-7.75 (4H, CH, ArH), 3.07-2.81 (m, 2H, 2CH from cyclobutyl), 2.99 (s, 3H, CH_3), 2.26-1.83 (m, 12H, $3CH_2$) from cyclobutyl). HRMS-APPI(*m/z*): $[M+H]^+$ calculated for $C_{20}H_{22}NO_2S$ 339.1293, found 339.1298

3,3-(Dicyclopropylethynyl)-2,3-dihydro-2-methyl-1,2-benzisothizoles 1,1-dioxide (12)

In a flame dried round-bottom flask 89mg (0.329 mmol) and 161 mg (0.495 mmol , 1.5 equiv.) were dissolved in dry acetonitrile under anhydrous conditions and a nitrogen atmosphere. The mixture was stirred at r.t. for one hour, then an excess amount of MeI (108 mg, 0.048 mL, 3 equiv) were added via a syringe. The reaction was monitored by TLC. Upon disappearance of starting material, it was rotarty evaporated to give a yellow oil and white precipitate. The residue was taken up in 10 mL of dichloromethane and washed with water (3 x 5 mL). The organic layer was then collected, dried over anhydrous $MgSO_4$ and vacuum filtered. It was concentrated under reduced pressure and high vacuum pressure to give a pale yellow crystalline solid. Flash chromatography using 15% acetone in petroleum ether gave the desired product in quantitative yield as a while crystalline solid (160 mg). ^{1}H NMR (300 MHz, $CDCl_3$, 25 ºC): δ 7.64-7.44 (m, 4H, CH, ArH), 2.98 (s, 3H, N-CH_3) ,1.91-1.21 (m, 2H, 2CH from cyclopropyl), 0.81-0.68 (m, 8H, $4CH_2$ from cyclopropyl). ^{13}C NMR (300 MHz, $CDCl_3$, 25 ºC): δ 140.87 (C-9, CH, Ar), 134.16 (C-6, Ar), 133.63 (C-7, Ar), 130.36 (C-5, Ar), 125.11 (C-4, Ar), 121.21 (C-8, Ar), 88.76 (C-2′, C≡C), 72.39 (C-1′, C≡C), 55.27 (C-3),

30.41 (N-CH_3) 8.37 (4CH_2 cylopropyl), -0.59 (2CH cyclopropyl).HRMS-APPI (*m/z)*: $[M+H]^+$ calcd for 340.1293 found 340.1299

IV. Literature Cited

1. PBS Frontline: The Age of Aids. http://www.pbs.org/wgbh/pages/frontline/aids/ (Accessed September 15, 2006).
2. Gallo, R. C., Viewpoint: Historical essay: The early years of HIV/AIDS. *Science (Washington, DC, United States)* **2002,** *298*, 1728-1730.
3. Montagnier, L., Viewpoint: Historical essay. *Science (Washington, DC, United States)* **2002,** *298*, 1727-1728.
4. Kolata, G., FDA approves AZT. *Science* **1987,** *235*, 1570.
5. Balzarini, J., Current status of the non-nucleoside reverse transcriptase inhibitors of human immunodeficiency virus type 1. *Current Topics in Medicinal Chemistry (Sharjah, United Arab Emirates)* **2004,** *4*, 921-944.
6. Sharp, P. M.; Bailes, E.; Gao, F.; Beer, B. E.; Hirsch, V. M.; Hahn, B. H., Origins and evolution of AIDS viruses: estimating the time-scale. *Biochem. Soc. Trans.* **2000,** *28*, 275-282.
7. Gao, F.; Bailes, E.; Robertson, D. L.; Chen, Y.; Rodenburg, C. M.; Michael, S. F.; Cummins, L. B.; Arthur, L. O.; Peeters, M.; Shaw, G. M.; Sharp, P. M.; Hahn, B. H., Origin of HIV-1 in the chimpanzee Pan troglodytes troglodytes. *Nature* **1999,** *397*, 436-41.
8. Chen, Z.; Luckay, A.; Sodora, D. L.; Telfer, P.; Reed, P.; Gettie, A.; Kanu, J. M.; Sadek, R. F.; Yee, J.; Ho, D. D.; Zhang, L.; Marx, P. A., Human immunodeficiency virus type 2 (HIV-2) seroprevalence and characterization of a distinct HIV-2 genetic subtype from the natural range of simian immunodeficiency virus-infected sooty mangabeys. *J. Virol.* **1997,** *71*, 3953-60.

9. Gao, F.; Yue, L.; Robertson, D. L.; Hill, S. C.; Hui, H.; Biggar, R. J.; Neequaye, A. E.; Whelan, T. M.; Ho, D. D.; Shaw, G. M., Genetic diversity of human immunodeficiency virus type 2: evidence for distinct sequence subtypes with differences in virus biology. *J. Virol.* **1994,** *68*, 7433-47.

10. Smith, T. F.; Srinivasan, A.; Schochetman, G.; Marcus, M.; Myers, G., The phylogenetic history of immunodeficiency viruses. *Nature (London, United Kingdom)* **1988,** *333*, 573-5.

11. Mulder, C., Human AIDS virus not from monkeys. *Nature* **1988,** *333*, 396.

12. Morin, P. A.; Moore, J. J.; Chakraborty, R.; Jin, L.; Goodall, J.; Woodruff, D. S., Kin selection, social structure, gene flow, and the evolution of chimpanzees. *Science* **1994,** *265*, 1193-201.

13. Li, W. H.; Tanimura, M.; Sharp, P. M., Rates and dates of divergence between AIDS virus nucleotide sequences. *Molecular biology and evolution* **1988,** *5*, 313-30.

14. Ugolini, S.; Mondor, I.; Sattentau, Q. J., HIV-1 attachment: another look. *Trends in microbiology* **1999,** *7*, 144-9.

15. Kwong, P. D.; Wyatt, R.; Robinson, J.; Sweet, R. W.; Sodroski, J.; Hendrickson, W. A., Structure of an HIV gp120 envelope glycoprotein in complex with the CD4 receptor and a neutralizing human antibody. *Nature (London)* **1998,** *393*, 648-659.

16. Chiou, S. H.; Freed, E. O.; Panganiban, A. T.; Kenealy, W. R., Studies on the role of the V3 loop in human immunodeficiency virus type 1 envelope

glycoprotein function. *AIDS Research and Human Retroviruses* **1992,** *8*, 1611-18.

17. Moore, J. P.; Binley, J., HIV: Envelope's letters boxed into shape. *Nature (London)* **1998,** *393*, 630-631.

18. Este, J. A., Virus entry as a target for anti-HIV intervention. *Current Medicinal Chemistry* **2003,** *10*, 1617-1632.

19. Kwong, P. D.; Wyatt, R.; Majeed, S.; Robinson, J.; Sweet, R. W.; Sodroski, J.; Hendrickson, W. A., Structures of HIV-1 gp120 Envelope Glycoproteins from Laboratory-Adapted and Primary Isolates. *Structure (Cambridge, MA, United States)* **2000,** *8*, 1329-1339.

20. Wyatt, R.; Kwong, P. D.; Desjardins, E.; Sweet, R. G.; Robinson, J.; Hendrickson, W. A.; Sodroski, J. G., The antigenic structure of the HIV gp120 envelope glycoprotein. *Nature (London)* **1998,** *393*, 705-711.

21. Gallaher, W. R., Detection of a fusion peptide sequence in the transmembrane protein of human immunodeficiency virus. *Cell (Cambridge, MA, United States)* **1987,** *50*, 327-8.

22. Weiss Carol, D., HIV-1 gp41: mediator of fusion and target for inhibition. *AIDS reviews* **2003,** *5*, 214-21.

23. Peisajovich, S. G.; Shai, Y., HIV gp41: a viral membrane fusion machine. *Protein Reviews* **2005,** *1*, 35-47.

24. Chan, D. C.; Fass, D.; Berger, J. M.; Kim, P. S., Core structure of gp41 from the HIV envelope glycoprotein. *Cell (Cambridge, Mass.)* **1997,** *89*, 263-273.

25. Caffrey, M.; Cai, M.; Kaufman, J.; Stahl, S. J.; Wingfield, P. T.; Covell, D. G.; Gronenborn, A. M.; Clore, M. G., Three-dimensional solution structure of the 44 kDa ectodomain of SIV gp41. *EMBO J.* **1998,** *17*, 4572-4584.

26. Orloff, G. M.; Kennedy, M. S.; Dawson, C.; McDougal, J. S., HIV-1 binding to CD4 T cells does not induce a calcium influx or lead to activation of protein kinases. *AIDS Research and Human Retroviruses* **1991,** *7*, 587-93.

27. Sattentau, Q. J.; Moore, J. P., Conformational changes induced in the human immunodeficiency virus envelope glycoprotein by soluble CD4 binding. *J. Exp. Med.* **1991,** *174*, 407-15.

28. Melikyan, G. B.; Markosyan, R. M.; Hemmati, H.; Delmedico, M. K.; Lambert, D. M.; Cohen, F. S., Evidence that the transition of HIV-1 gp41 into a six-helix bundle, not the bundle configuration, induces membrane fusion. *J. Cell Biol.* **2000,** *151*, 413-423.

29. Salzwedel, K. W., John T.; Hunter, Eric, A conserved tryptophan-rich motif in the membrane-proximal region of the human immunodeficiency virus type 1 gp41 ectodomain is important for Env-mediated fusion and virus infectivity. . *J. Virol.* **1999,** *73*, 2469-2480.

30. Harrich, D.; Hooker, B., Mechanistic aspects of HIV-1 reverse transcription initiation. *Reviews in Medical Virology* **2002,** *12*, 31-45.

31. Tronchet, J. M. J.; Seman, M., Non-nucleoside inhibitors of HIV-1 reverse transcriptase: From the biology of reverse transcription to molecular

design. *Current Topics in Medicinal Chemistry (Sharjah, United Arab Emirates)* **2003,** *3*, 1496-1511.

32. Rodgers, D. W.; Gamblin, S. J.; Harris, B. A.; Culp, J. S.; Hellmig, B.; Woolf, D. J.; Debouck, C.; Harrison, S. C.; Ray, S., The structure of unliganded reverse transcriptase from the human immunodeficiency virus type 1. *Proc. Natl. Acad. Sci. U. S. A.* **1995,** *92*, 1222-6.

33. Kohlstaedt, L. A.; Wang, J.; Friedman, J. M.; Rice, P. A.; Steitz, T. A., Crystal structure at 3.5 .ANG. resolution of HIV-1 reverse transcriptase complexed with an inhibitor. *Science (Washington, DC, United States)* **1992,** *256*, 1783-90.

34. Sarafianos, S. G.; Das, K.; Tantillo, C.; Clark, A. D., Jr.; Ding, J.; Whitcomb, J. M.; Boyer, P. L.; Hughes, S. H.; Arnold, E., Crystal structure of HIV-1 reverse transcriptase in complex with a polypurine tract RNA:DNA. *EMBO J.* **2001,** *20*, 1449-1461.

35. Das, K.; Ding, J.; Hsiou, Y.; Clark, A. D., Jr.; Moereels, H.; Koymans, L.; Andries, K.; Pauwels, R.; Janssen, P. A. J.; Boyer, P. L.; Clark, P.; Smith, R. H., Jr.; Smith, M. B. K.; Michejda, C. J.; Hughes, S. H.; Arnold, E., Crystal structures of 8-Cl and 9-Cl TIBO complexed with wild-type HIV-1 RT and 8-Cl TIBO complexed with the Tyr181Cys HIV-1 RT drug-resistant mutant. *J. Mol. Biol.* **1996,** *264*, 1085-1100.

36. Das, K.; Lewi, P. J.; Hughes, S. H.; Arnold, E., Crystallography and the design of anti-AIDS drugs: conformational flexibility and positional adaptability are important in the design of non-nucleoside HIV-1 reverse

transcriptase inhibitors. *Progress in Biophysics & Molecular Biology* **2005,** *88*, 209-231.

37. Hopkins, A. L.; Ren, J.; Esnouf, R. M.; Willcox, B. E.; Jones, E. Y.; Ross, C.; Miyasaka, T.; Walker, R. T.; Tanaka, H.; Stammers, D. K.; Stuart, D. I., Complexes of HIV-1 reverse transcriptase with inhibitors of the HEPT series reveal conformational changes relevant to the design of potent non-nucleoside inhibitors. *J. Med. Chem.* **1996,** *39*, 1589-600.

38. Stammers, D. K.; Somers, D. O. N.; Ross, C. K.; Kirby, I.; Ray, P. H.; Wilson, J. E.; Norman, M.; Ren, J. S.; Esnouf, R. M.; et al., Crystals of HIV-1 reverse transcriptase diffracting to 2.2 .ANG. resolution. *J. Mol. Biol.* **1994,** *242*, 586-8.

39. Jacobo-Molina, A.; Ding, J.; Nanni, R. G.; Clark, A. D., Jr.; Lu, X.; Tantillo, C.; Williams, R. L.; Kamer, G.; Ferris, A. L.; et al., Crystal structure of human immunodeficiency virus type 1 reverse transcriptase complexed with double-stranded DNA at 3.0 .ANG. resolution shows bent DNA. *Proc. Natl. Acad. Sci. U. S. A.* **1993,** *90*, 6320-4.

40. Hindmarsh, P.; Leis, J., Retroviral DNA integration. *Microbiology and Molecular Biology Reviews* **1999,** *63*, 836-843.

41. Craigie, R., HIV integrase, a brief overview from chemistry to therapeutics. *J. Biol. Chem.* **2001,** *276*, 23213-23216.

42. Engelman, A.; Mizuuchi, K.; Craigie, R., HIV-1 DNA integration: mechanism of viral DNA cleavage and DNA strand transfer. *Cell (Cambridge, MA, United States)* **1991,** *67*, 1211-21.

43. Chiu, T. K.; Davies, D. R., Structure and function of HIV-1 integrase. *Current Topics in Medicinal Chemistry (Sharjah, United Arab Emirates)* **2004,** *4*, 965-977.

44. Cai, M.; Zheng, R.; Caffrey, M.; Craigie, R.; Clore, G. M.; Gronenborn, A. M., Solution structure of the N-terminal zinc binding domain of HIV-1 integrase. *Nature Structural Biology* **1997,** *4*, 567-577.

45. Cai, M.; Huang, Y.; Caffrey, M.; Zheng, R.; Craigie, R.; Clore, G. M.; Gronenborn, A. M., Solution structure of the His12 -> Cys mutant of the N-terminal zinc binding domain of HIV-1 integrase complexed to cadmium. *Protein Science* **1998,** *7*, 2669-2674.

46. Eijkelenboom, A. P. A. M.; Van Den Ent, F. M. I.; Vos, A.; Doreleijers, J. F.; Hard, K.; Tullius, T. D.; Plasterk, R. H. A.; Kaptein, R.; Boelens, R., The solution structure of the amino-terminal HHCC domain of HIV-2 integrase: a three-helix bundle stabilized by zinc. *Current Biology* **1997,** *7*, 739-746.

47. Lodi, P. J.; Ernst, J. A.; Kuszewski, J.; Hickman, A. B.; Engelman, A.; Craigie, R.; Clore, G. M.; Gronenborn, A. M., Solution Structure of the DNA Binding Domain of HIV-1 Integrase. *Biochemistry* **1995,** *34*, 9826-33.

48. Dyda, F.; Hickman, A. B.; Jenkins, T. M.; Engelman, A.; Craigie, R.; Davies, D. R., Crystal structure of the catalytic domain of HIV-1 integrase: similarity to other polynucleotidyl transferases. *Science (Washington, D. C.)* **1994,** *266*, 1981-6.

49. Goldgur, Y.; Dyda, F.; Hickman, A. B.; Jenkins, T. M.; Craigie, R.; Davies, D. R., Three new structures of the core domain of HIV-1 integrase: an active site that binds magnesium. *Proc. Natl. Acad. Sci. U. S. A.* **1998,** *95*, 9150-9154.

50. Rodriguez-Barrios, F.; Gago, F., HIV protease inhibition: Limited recent progress and advances in understanding current pitfalls. *Current Topics in Medicinal Chemistry (Sharjah, United Arab Emirates)* **2004,** *4*, 991-1007.

51. Yamazaki, T.; Nicholson, L. K.; Wingfield, P.; Stahl, S. J.; Kaufman, J. D.; Eyermann, C. J.; Hodge, C. N.; Lam, P. Y. S.; Torchia, D. A.; et al., NMR and X-ray Evidence That the HIV Protease Catalytic Aspartyl Groups Are Protonated in the Complex Formed by the Protease and a Non-Peptide Cyclic Urea-Based Inhibitor. *J. Am. Chem. Soc.* **1994,** *116*, 10791-2.

52. Smith, R.; Brereton, I. M.; Chai, R. Y.; Kent, S. B., Ionization states of the catalytic residues in HIV-1 protease. *Nature structural biology* **1996,** *3*, 946-50.

53. Vermeire, K.; Zhang, Y.; Princen, K.; Hatse, S.; Samala, M. F.; Dey, K.; Choi, H.-J.; Ahn, Y.; Sodoma, A.; Snoeck, R.; Andrei, G.; De Clercq, E.; Bell, T. W.; Schols, D., CADA Inhibits Human Immunodeficiency Virus and Human Herpesvirus 7 Replication by Down-modulation of the Cellular CD4 Receptor. *Virology* **2002,** *302*, 342-353.

54. Vermeire, K.; Bell, T. W.; Choi, H.-J.; Jin, Q.; Samala, M. F.; Sodoma, A.; De Clercq, E.; Schols, D., The anti-HIV potency of

cyclotriazadisulfonamide analogs is directly correlated with their ability to down-modulate the CD4 receptor. *Mol. Pharmacol.* **2003,** *63*, 203-210.

55. Vermeire, K.; Princen, K.; Hatse, S.; de Clercq, E.; Dey, K.; Bell, T. W.; Schols, D., CADA, a novel CD4-targeted HIV inhibitor, is synergistic with various anti-HIV drugs in vitro. *AIDS (London, United Kingdom)* **2004,** *18*, 2115-2125.

56. Balzarini, J.; Hatse, S.; Vermeire, K.; Princen, K.; Aquaro, S.; Perno, C.-F.; de Clercq, E.; Egberink, H.; Vanden Mooter, G.; Peumans, W.; van Damme, E.; Schols, D., Mannose-specific plant lectins from the Amaryllidaceae family qualify as efficient microbicides for prevention of human immunodeficiency virus infection. *Antimicrob. Agents Chemother.* **2004,** *48*, 3858-3870.

57. Balzarini, J.; van Laethem, K.; Hatse, S.; Vermeire, K.; de Clercq, E.; Peumans, W.; van Damme, E.; Vandamme, A.-M.; Boehlmstedt, A.; Schols, D., Profile of resistance of human immunodeficiency virus to mannose-specific plant lectins. *J. Virol.* **2004,** *78*, 10617-10627.

58. Boyd, M. R.; Gustafson, K. R.; McMahon, J. B.; Shoemaker, R. H.; O'Keefe, B. R.; Mori, T.; Gulakowski, R. J.; Wu, L.; Rivera, M. I.; Laurencot, C. M.; Currens, M. J.; Cardellina, J. H., 2nd; Buckheit, R. W., Jr.; Nara, P. L.; Pannell, L. K.; Sowder, R. C., 2nd; Henderson, L. E., Discovery of cyanovirin-N, a novel human immunodeficiency virus-inactivating protein that binds viral surface envelope glycoprotein gp120:

potential applications to microbicide development. *Antimicrob. Agents Chemother.* **1997,** *41*, 1521-30.

59. Mori, T.; Boyd, M. R., Cyanovirin-N, a potent human immunodeficiency virus-inactivating protein, blocks both CD4-dependent and CD4-independent binding of soluble gp120 (sgp120) to target cells, inhibits sCD4-induced binding of sgp120 to cell-associated CXCR4, and dissociates bound sgp120 from target cells. *Antimicrob. Agents Chemother.* **2001,** *45*, 664-672.

60. Botos, I.; Wlodawer, A., Cyanovirin-N: a sugar-binding antiviral protein with a new twist. *Cellular and Molecular Life Sciences* **2003,** *60*, 277-287.

61. Wang, S.; York, J.; Shu, W.; Stoller, M. O.; Nunberg, J. H.; Lu, M., Interhelical interactions in the gp41 core: Implications for activation of HIV-1 membrane fusion. *Biochemistry* **2002,** *41*, 7283-7292.

62. Guo, Q.; Ho, H.-T.; Dicker, I.; Fan, L.; Zhou, N.; Friborg, J.; Wang, T.; McAuliffe, B. V.; Wang, H.-g. H.; Rose, R. E.; Fang, H.; Scarnati, H. T.; Langley, D. R.; Meanwell, N. A.; Abraham, R.; Colonno, R. J.; Lin, P.-f., Biochemical and genetic characterizations of a novel human immunodeficiency virus type 1 inhibitor that blocks gp120-CD4 interactions. *J. Virol.* **2003,** *77*, 10528-10536.

63. Lin, P.-F.; Blair, W.; Wang, T.; Spicer, T.; Guo, Q.; Zhou, N.; Gong, Y.-F.; Wang, H. G. H.; Rose, R.; Yamanaka, G.; Robinson, B.; Li, C.-B.; Fridell, R.; Deminie, C.; Demers, G.; Yang, Z.; Zadjura, L.; Meanwell, N.; Colonno, R., A small molecule HIV-1 inhibitor that targets the HIV-1

envelope and inhibits CD4 receptor binding. *Proc. Natl. Acad. Sci. U. S. A.* **2003,** *100*, 11013-11018.

64. De Clercq, E., Timeline: The bicyclam AMD3100 story. *Nature Reviews Drug Discovery* **2003,** *2*, 581-587.

65. De Clercq, E., New Approaches toward Anti-HIV Chemotherapy. *J. Med. Chem.* **2005,** *48*, 1297-1313.

66. Baba, M.; Nishimura, O.; Kanzaki, N.; Okamoto, M.; Sawada, H.; Iizawa, Y.; Shiraishi, M.; Aramaki, Y.; Okonogi, K.; Ogawa, Y.; Meguro, K.; Fujino, M., A small-molecule, nonpeptide CCR5 antagonist with highly potent and selective anti-HIV-1 activity. *Proc. Natl. Acad. Sci. U. S. A.* **1999,** *96*, 5698-703.

67. Dragic, T.; Trkola, A.; Thompson, D. A.; Cormier, E. G.; Kajumo, F. A.; Maxwell, E.; Lin, S. W.; Ying, W.; Smith, S. O.; Sakmar, T. P.; Moore, J. P., A binding pocket for a small molecule inhibitor of HIV-1 entry within the transmembrane helices of CCR5. *Proc. Natl. Acad. Sci. U. S. A.* **2000,** *97*, 5639-44.

68. Strizki, J. M.; Xu, S.; Wagner, N. E.; Wojcik, L.; Liu, J.; Hou, Y.; Endres, M.; Palani, A.; Shapiro, S.; Clader, J. W.; Greenlee, W. J.; Tagat, J. R.; McCombie, S.; Cox, K.; Fawzi, A. B.; Chou, C. C.; Pugliese-Sivo, C.; Davies, L.; Moreno, M. E.; Ho, D. D.; Trkola, A.; Stoddart, C. A.; Moore, J. P.; Reyes, G. R.; Baroudy, B. M., SCH-C (SCH 351125), an orally bioavailable, small molecule antagonist of the chemokine receptor CCR5,

is a potent inhibitor of HIV-1 infection in vitro and in vivo. *Proc. Natl. Acad. Sci. U. S. A.* **2001,** *98*, 12718-23.

69. Tsamis, F.; Gavrilov, S.; Kajumo, F.; Seibert, C.; Kuhmann, S.; Ketas, T.; Trkola, A.; Palani, A.; Clader, J. W.; Tagat, J. R.; McCombie, S.; Baroudy, B.; Moore, J. P.; Sakmar, T. P.; Dragic, T., Analysis of the mechanism by which the small-molecule CCR5 antagonists SCH-351125 and SCH-350581 inhibit human immunodeficiency virus type 1 entry. *J. Virol.* **2003,** *77*, 5201-5208.

70. Hale, J. J.; Budhu, R. J.; Holson, E. B.; Finke, P. E.; Oates, B.; Mills, S. G.; MacCoss, M.; Gould, S. L.; DeMartino, J. A.; Springer, M. S.; Siciliano, S.; Malkowitz, L.; Schleif, W. A.; Hazuda, D.; Miller, M.; Kessler, J.; Danzeisen, R.; Holmes, K.; Lineberger, J.; Carella, A.; Carver, G.; Emini, E., 1,3,4-Trisubstituted pyrrolidine CCR5 receptor antagonists. Part 2: lead optimization affording selective, orally bioavailable compounds with potent Anti-HIV activity. *Bioorg. Med. Chem. Lett.* **2001,** *11*, 2741-2745.

71. Veazey, R. S.; Klasse, P. J.; Ketas, T. J.; Reeves, J. D.; Piatak, M., Jr.; Kunstman, K.; Kuhmann, S. E.; Marx, P. A.; Lifson, J. D.; Dufour, J.; Mefford, M.; Pandrea, I.; Wolinsky, S. M.; Doms, R. W.; DeMartino, J. A.; Siciliano, S. J.; Lyons, K.; Springer, M. S.; Moore, J. P., Use of a small molecule CCR5 inhibitor in macaques to treat simian immunodeficiency virus infection or prevent simian-human immunodeficiency virus infection. *J. Exp. Med.* **2003,** *198*, 1551-1562.

72. Lalezari, J.; Henry, K.; O'Hearn, M.; Montaner, J. S. G.; Piliero, P. J.; Trottier, B.; Walmsley, S.; Cohen, C.; Kuritzkes, D. R.; Eron, J. J., Jr.; Chung, J.; DeMasi, R.; Donatacci, L.; Drobnes, C.; Belehanty, J.; Salgo, M.; Farthing, C.; Graham, E.; Packard, M.; Ngo, L.; Lederman, M.; Baum, J.; Pollard, R.; Rauf, S.; Silkowski, W.; Thompson, M.; Rucker, A.; Harris, M.; Larsen, G.; Preston, S.; Cunningham, D.; Guimaraes, D.; Bertasso, A.; Kinchelow, T.; Myers, R.; Casimir, B.; Skolnik, P. R.; Adams, B.; Leite, O. H. M.; Oliveira, M.; Lefebvre, E.; Gomez, B.; Foy, K. B.; Lampiris, H.; Charles, S.; Dobkin, J.; Crawford, M.; Slom, T.; Murphy, R.; Mikaitis, T.; Witek, J.; Anthony, R.; Richmond, G.; Appleby, V. F.; Smaill, F.; Kelleher, L.; Nieto, L.; Trevino, S.; Schechter, M.; Fonseca, B.; DeJesus, E.; Ortiz, R.; Wheat, J.; Goldman, M.; O'Connor, D. K.; Sierra-Madero, J. G.; Nino-Oberto, S.; Gallant, J. E.; Apuzzo, L.; Bosgoz, N.; Habeeb, K.; Alpert, P.; Thomas, S.; Miller, T.; Kempner, T.; Wolfe, P. R.; Bautista, J.; Martin, H. L.; Morton, M. E.; Henry, D.; Kilcoyne, S.; Glutzer, E.; Rivera-Vazquez, C.; Pomales, Z.; Bellos, N.; Hoffman, L. A.; Olmscheid, B.; Klein, O.; Miller, M.; Steinhart, C. R.; Liebmann, A.; Williams, S.; Springate, L.; Logue, K.; Smiley, L.; Miralles, G. D.; Haubrich, R.; Nuffer, K.; Beatty, G.; O'Leary, S.; Rouleau, D.; Dufresne, S.; Kilby, J. M.; Saag, M.; Upton, K.; Feinberg, J.; Kohler, P.; Campbell, T. B.; Putnam, B. A.; Riddler, S. A.; Rosener, R. R.; Barnett, B. J.; Hansen, I.; Collier, A. C.; Royer, B. A.; Haas, D. W.; Morgan, M.; Sathasivam, K.; Hersch, J., Enfuvirtide, an HIV-1 fusion

inhibitor, for drug-resistant HIV infection in North and South America. *New England Journal of Medicine* **2003,** *348*, 2175-2185.

73. Ketas, T. J.; Klasse, P. J.; Spenlehauer, C.; Nesin, M.; Frank, I.; Pope, M.; Strizki, J. M.; Reyes, G. R.; Baroudy, B. M.; Moore, J. P., Entry inhibitors SCH-C, RANTES, and T-20 block HIV Type 1 replication in multiple cell types. *AIDS Research and Human Retroviruses* **2003,** *19*, 177-186.

74. Orner, B. P.; Ernst, J. T.; Hamilton, A. D., Toward proteomimetics: terphenyl derivatives as structural and functional mimics of extended regions of an alpha-helix. *J. Am. Chem. Soc.* **2001,** *123*, 5382-3.

75. Hazuda, D. J.; Felock, P.; Witmer, M.; Wolfe, A.; Stillmock, K.; Grobler, J. A.; Espeseth, A.; Gabryelski, L.; Schleif, W.; Blau, C.; Miller, M. D., Inhibitors of strand transfer that prevent integration and inhibit HIV-1 replication in cells. *Science (Washington, D. C.)* **2000,** *287*, 646-650.

76. Pluymers, W.; Pais, G.; Van Maele, B.; Pannecouque, C.; Fikkert, V.; Burke, T. R., Jr.; De Clercq, E.; Witvrouw, M.; Neamati, N.; Debyser, Z., Inhibition of human immunodeficiency virus type 1 integration by diketo derivatives. *Antimicrob. Agents Chemother.* **2002,** *46*, 3292-3297.

77. Fikkert, V.; Van Maele, B.; Vercammen, J.; Hantson, A.; Van Remoortel, B.; Michiels, M.; Gurnari, C.; Pannecouque, C.; De Maeyer, M.; Engelborghs, Y.; De Clercq, E.; Debyser, Z.; Witvrouw, M., Development of resistance against diketo derivatives of human immunodeficiency virus type 1 by progressive accumulation of integrase mutations. *J. Virol.* **2003,** *77*, 11459-11470.

78. Gong, Y.-F.; Robinson, B. S.; Rose, R. E.; Deminie, C.; Spicer, T. P.; Stock, D.; Colonno, R. J.; Lin, P.-F., In vitro resistance profile of the human immunodeficiency virus type 1 protease inhibitor BMS-232632. *Antimicrob. Agents Chemother.* **2000,** *44*, 2319-2326.

79. Colonno, R. J.; Thiry, A.; Limoli, K.; Parkin, N., Activities of atazanavir (BMS-232632) against a large panel of human immunodeficiency virus type 1 clinical isolates resistant to one or more approved protease inhibitors. *Antimicrob. Agents Chemother.* **2003,** *47*, 1324-1333.

80. Ren, J.; Stammers, D. K., HIV reverse transcriptase structures: designing new inhibitors and understanding mechanisms of drug resistance. *Trends Pharmacol. Sci.* **2005,** *26*, 4-7.

81. Larder, B. A.; Kemp, S. D., Multiple mutations in HIV-1 reverse transcriptase confer high-level resistance to zidovudine (AZT). *Science* **1989,** *246*, 1155-8.

82. James, J. S., ddI: FDA approves once-daily dosing. Food and Drug Administration. *AIDS treatment news* **1999**, 1.

83. De Clercq, E., Toward Improved Anti-HIV Chemotherapy: Therapeutic Strategies for Intervention with HIV Infections. *J. Med. Chem.* **1995,** *38*, 2491-517.

84. De Clercq, E., The role of non-nucleoside reverse transcriptase inhibitors (NNRTIs) in the therapy of HIV-1 infection. *Antiviral Research* **1998,** *38*, 153-179.

85. De Clercq, E., Non-nucleoside reverse transcriptase inhibitors (NNRTIs): past, present, and future. *Chemistry & Biodiversity* **2004,** *1*, 44-64.

86. Pani, A.; Musiu, C.; Loi, A. G.; Mai, A.; Loddo, R.; La Colla, P.; Marongiu, M. E., DABOs as candidates to prevent mucosal HIV transmission. *Antiviral Chemistry & Chemotherapy* **2001,** *12*, 51-59.

87. Ren, J.; Esnouf, R.; Hopkins, A.; Ross, C.; Jones, Y.; Stammers, D.; Stuart, D., The structure of HIV-1 reverse transcriptase complexed with 9-chloro-TIBO: lessons for inhibitor design. *Structure (London)* **1995,** *3*, 915-26.

88. Schaefer, W.; Friebe, W. G.; Leinert, H.; Mertens, A.; Poll, T.; Von der Saal, W.; Zilch, H.; Nuber, B.; Ziegler, M. L., Non-nucleoside inhibitors of HIV-1 reverse transcriptase: molecular modeling and x-ray structure investigations. *J. Med. Chem.* **1993,** *36*, 726-32.

89. De Clercq, E., What can be expected from non-nucleoside reverse transcriptase inhibitors (NNRTIs) in the treatment of human immunodeficiency virus type 1 (HIV-1) infections? *Reviews in Medical Virology* **1996,** *6*, 97-117.

90. Howard, K. J.; Frank, K. B.; Sim, I. S.; Le Grice, S. F., Reconstitution and properties of homologous and chimeric HIV-1.HIV-2 p66.p51 reverse transcriptase. *The Journal of biological chemistry* **1991,** *266*, 23003-9.

91. Shih, C. K.; Rose, J. M.; Hansen, G. L.; Wu, J. C.; Bacolla, A.; Griffin, J. A., Chimeric human immunodeficiency virus type 1/type 2 reverse

transcriptases display reversed sensitivity to non-nucleoside analog inhibitors. *Proc. Natl. Acad. Sci. U. S. A.* **1991,** *88*, 9878-82.

92. Yang, G.; Song, Q.; Charles, M.; Drosopoulos, W. C.; Arnold, E.; Prasad, V. R., Use of chimeric human immunodeficiency virus types 1 and 2 reverse transcriptases for structure-function analysis and for mapping susceptibility to non-nucleoside inhibitors. *Journal of Acquired Immune Deficiency Syndromes and Human Retrovirology* **1996,** *11*, 326-33.

93. Hizi, A.; Tal, R.; Shaharabany, M.; Currens, M. J.; Boyd, M. R.; Hughes, S. H.; McMahon, J. B., Specific inhibition of the reverse transcriptase of human immunodeficiency virus type 1 and the chimeric enzymes of human immunodeficiency virus type 1 and type 2 by non-nucleoside inhibitors. *Antimicrob. Agents Chemother.* **1993,** *37*, 1037-42.

94. Isaka, Y.; Sato, A.; Kawauchi, S.; Suyama, A.; Miki, S.; Hayami, M.; Fujiwara, T., Construction of the chimeric reverse transcriptase of simian immunodeficiency virus sensitive to non-nucleoside reverse transcriptase inhibitor. *Microbiol. Immunol.* **1998,** *42*, 195-202.

95. Ahgren, C.; Backro, K.; Bell, F. W.; Cantrell, A. S.; Clemens, M.; Colacino, J. M.; Deeter, J. B.; Engelhardt, J. A.; Hogberg, M.; et al., The PETT series, a new class of potent non-nucleoside inhibitors of human immunodeficiency virus type 1 reverse transcriptase. *Antimicrob. Agents Chemother.* **1995,** *39*, 1329-35.

96. Goldman, M. E.; Nunberg, J. H.; O'Brien, J. A.; Quintero, J. C.; Schleif, W. A.; Freund, K. F.; Gaul, S. L.; Saari, W. S.; Wai, J. S.; et al., Pyridinone

derivatives: specific human immunodeficiency virus type 1 reverse transcriptase inhibitors with antiviral activity. *Proc. Natl. Acad. Sci. U. S. A.* **1991,** *88*, 6863-7.

97. Kleim, J. P.; Bender, R.; Billhardt, U. M.; Meichsner, C.; Riess, G.; Rosner, M.; Winkler, I.; Paessens, A., Activity of a novel quinoxaline derivative against human immunodeficiency virus type 1 reverse transcriptase and viral replication. *Antimicrob. Agents Chemother.* **1993,** *37*, 1659-64.

98. Debyser, Z.; Pauwels, R.; Andries, K.; De Clercq, E., Specific HIV-1 reverse transcriptase inhibitors. *Journal of enzyme inhibition* **1992,** *6*, 47-53.

99. White, E. L.; Buckheit, R. W., Jr.; Ross, L. J.; Germany, J. M.; Andries, K.; Pauwels, R.; Janssen, P. A.; Shannon, W. M.; Chirigos, M. A., A TIBO derivative, R82913, is a potent inhibitor of HIV-1 reverse transcriptase with heteropolymer templates. *Antiviral research* **1991,** *16*, 257-66.

100. Wu, J. C.; Warren, T. C.; Adams, J.; Proudfoot, J.; Skiles, J.; Raghavan, P.; Perry, C.; Potocki, I.; Farina, P. R.; Grob, P. M., A novel dipyridodiazepinone inhibitor of HIV-1 reverse transcriptase acts through a nonsubstrate binding site. *Biochemistry* **1991,** *30*, 2022-6.

101. Frank, K. B.; Noll, G. J.; Connell, E. V.; Sim, I. S., Kinetic interaction of human immunodeficiency virus type 1 reverse transcriptase with the antiviral tetrahydroimidazo[4,5,1-jk]-[1,4]-benzodiazepine-2-(1H)-thione compound, R82150. *The Journal of biological chemistry* **1991,** *266*, 14232-6.

102. Auwerx, J.; Stevens, M.; Van Rompay, A. R.; Bird, L. E.; Ren, J.; De Clercq, E.; Oeberg, B.; Stammers, D. K.; Karlsson, A.; Balzarini, J., The phenylmethylthiazolylthiourea non-nucleoside reverse transcriptase (RT) inhibitor MSK-076 selects for a resistance mutation in the active site of human immunodeficiency virus type 2 RT. *J. Virol.* **2004,** *78*, 7427-7437.

103. Buckheit, R. W., Jr.; Watson, K.; Fliakas-Boltz, V.; Russell, J.; Loftus, T. L.; Osterling, M. C.; Turpin, J. A.; Pallansch, L. A.; White, E. L.; Lee, J. W.; Lee, S. H.; Oh, J. W.; Kwon, H. S.; Chung, S. G.; Cho, E. H., SJ-3366, a unique and highly potent non-nucleoside reverse transcriptase inhibitor of human immunodeficiency virus type 1 (HIV-1) that also inhibits HIV-2. *Antimicrob. Agents Chemother.* **2001,** *45*, 393-400.

104. Shen, L.; Shen, J.; Luo, X.; Cheng, F.; Xu, Y.; Chen, K.; Arnold, E.; Ding, J.; Jiang, H., Steered molecular dynamics simulation on the binding of NNRTI to HIV-1 RT. *Biophys. J.* **2003,** *84*, 3547-3563.

105. Esnouf, R.; Ren, J.; Ross, C.; Jones, Y.; Stammers, D.; Stuart, D., Mechanism of inhibition of HIV-1 reverse transcriptase by non-nucleoside inhibitors. *Nature Structural Biology* **1995,** *2*, 303-8.

106. Esnouf, R. M.; Ren, J.; Hopkins, A. L.; Ross, C. K.; Jones, E. Y.; Stammers, D. K.; Stuart, D. I., Unique features in the structure of the complex between HIV-1 reverse transcriptase and the bis(heteroaryl)piperazine (BHAP) U-90152 explain resistance mutations for this non-nucleoside inhibitor. *Proc. Natl. Acad. Sci. U. S. A.* **1997,** *94*, 3984-3989.

107. Nanni, R. G.; Ding, J.; Jacobo-Molina, A.; Hughes, S. H.; Arnold, E., Review of HIV-1 reverse transcriptase three-dimensional structure: Implications for drug design. *Perspectives in Drug Discovery and Design* **1993,** *1*, 129-50.

108. Smerdon, S. J.; Jager, J.; Wang, J.; Kohlstaedt, L. A.; Chirino, A. J.; Friedman, J. M.; Rice, P. A.; Steitz, T. A., Structure of the binding site for non-nucleoside inhibitors of the reverse transcriptase of human immunodeficiency virus type 1. *Proc. Natl. Acad. Sci. U. S. A.* **1994,** *91*, 3911-15.

109. Spence, R. A.; Kati, W. M.; Anderson, K. S.; Johnson, K. A., Mechanism of inhibition of HIV-1 reverse transcriptase by non-nucleoside inhibitors. *Science (Washington, D. C.)* **1995,** *267*, 988-93.

110. Deng, B.-L.; Cullen, M. D.; Zhou, Z.; Hartman, T. L.; Buckheit, R. W.; Pannecouque, C.; De Clercq, E.; Fanwick, P. E.; Cushman, M., Synthesis and anti-HIV activity of new alkenyldiarylmethane (ADAM) non-nucleoside reverse transcriptase inhibitors (NNRTIs) incorporating benzoxazolone and benzisoxazole rings. *Bioorganic & Medicinal Chemistry* **2006,** *14*, 2366-2374.

111. Medina-Franco, J. L.; Rodriguez-Morales, S.; Juarez-Gordiano, C.; Hernandez-Campos, A.; Jimenez-Barbero, J.; Castillo, R., Flexible docking of pyridinone derivatives into the non-nucleoside inhibitor binding site of HIV-1 reverse transcriptase. *Bioorganic & Medicinal Chemistry* **2004,** *12*, 6085-6095.

112. De Martino, G.; La Regina, G.; Di Pasquali, A.; Ragno, R.; Bergamini, A.; Ciaprini, C.; Sinistro, A.; Maga, G.; Crespan, E.; Artico, M.; Silvestri, R., Novel 1-[2-(Diarylmethoxy)ethyl]-2-methyl-5-nitroimidazoles as HIV-1 Non-Nucleoside Reverse Transcriptase Inhibitors. A Structure-Activity Relationship Investigation. *J. Med. Chem.* **2005,** *48*, 4378-4388.

113. Udier-Blagovic, M.; Tirado-Rives, J.; Jorgensen, W. L., Structural and Energetic Analyses of the Effects of the K103N Mutation of HIV-1 Reverse Transcriptase on Efavirenz Analogues. *J. Med. Chem.* **2004,** *47*, 2389-2392.

114. Mager, P. P., A check on rational drug design: molecular simulation of the allosteric inhibition of HIV-1 reverse transcriptase. *Med. Res. Rev.* **1997,** *17*, 235-276.

115. Seki, M.; Sadakata, Y.; Yuasa, S.; Baba, M., Isolation and characterization of human immunodeficiency virus type-1 mutants resistant to the non-nucleotide reverse transcriptase inhibitor MKC-442. *Antiviral Chemistry & Chemotherapy* **1995,** *6*, 73-9.

116. Young, S. D.; Britcher, S. F.; Tran, L. O.; Payne, L. S.; Lumma, W. C.; Lyle, T. A.; Huff, J. R.; Anderson, P. S.; Olsen, D. B.; et al., L-743,726 (DMP-266): a novel, highly potent non-nucleoside inhibitor of the human immunodeficiency virus type 1 reverse transcriptase. *Antimicrob. Agents Chemother.* **1995,** *39*, 2602-5.

117. Gussio, R.; Pattabiraman, N.; Zaharevitz, D. W.; Kellogg, G. E.; Topol, I. A.; Rice, W. G.; Schaeffer, C. A.; Erickson, J. W.; Burt, S. K., All-Atom

Models for the Non-Nucleoside Binding Site of HIV-1 Reverse Transcriptase Complexed with Inhibitors: A 3D QSAR Approach. *J. Med. Chem.* **1996,** *39*, 1645-50.

118. Watanabe, H.; Gay, R. L.; Hauser, C. R., Ortho metalation of N-substituted benzenesulfonamides by excess N-butyllithium. Condensation with carbonyl compounds. Cyclizations. *J. Org. Chem.* **1968,** *33*, 900-3.

119. Baker, D. C.; Mayasundari, A.; Mao, J.; Johnson, S. C.; Yan, S. Methods of synthesizing sultams and anti-viral compositions. 99-US16240 2000004004, 19990716., 2000.

120. Baker, D. C.; Mayasundari, A.; Mao, J.; Johnson, S. C.; Yan, S. Preparation of sultams having antiviral and especially anti-HIV-1 activity. 99-353900, 6562850, 19990715., 2003.

121. Mashima, K.; Abe, T.; Tani, K., Asymmetric transfer hydrogenation of ketonic substrates catalyzed by (h5-C5Me5)MCl complexes (M = Rh and Ir) of (1S,2S)-N-(p-toluenesulfonyl)-1,2-diphenylethylenediamine. *Chem. Lett.* **1998**, 1199-1200.

122. Mao, J.; Baker, D. C., A Chiral Rhodium Complex for Rapid Asymmetric Transfer Hydrogenation of Imines with High Enantioselectivity. *Organic Letters* **1999,** *1*, 841-843.

123. Clark, M.; Cramer, R. D., III; Van Opdenbosch, N., Validation of the general purpose Tripos 5.2 force field. *J. Comput. Chem.* **1989,** *10*, 982-1012.

124. Vinter, J. G.; Davis, A.; Saunders, M. R., Strategic approaches to drug design. I. An integrated software framework for molecular modelling. *Journal of Computer-Aided Molecular Design* **1987,** *1*, 31-51.

125. Motoc, I.; Dammkoehler, R. A.; Mayer, D.; Labanowski, J., Three-dimensional quantitative structure-activity relationships. I. General approach to the pharmacophore model validation. *Quantitative Structure-Activity Relationships* **1986,** *5*, 99-105.

126. Purcell, W. P.; Singer, J. A., A brief review and table of semiempirical parameters used in the Hueckel molecular orbital method. *J. Chem. Eng. Data* **1967,** *12*, 235-46.

127. Marsili, M.; Gasteiger, J., p Charge distribution from molecular topology and p orbital electronegativity. *Croat. Chem. Acta* **1981,** *53*, 601-14.

128. Gasteiger, J.; Marsili, M., Iterative partial equalization of orbital electronegativity: a rapid access to atomic charges. *Tetrahedron* **1980,** *36*, 3219-22.

129. Berthod, H.; Pullman, A., Calculation of the s structure of conjugated molecules. *J. Chim. Phys. Phys.-Chim. Biol.* **1965,** *62*, 942-6.

130. Berthod, H.; Giessner-Prettre, C.; Pullman, A., Role of s and p electrons on the properties of halogens-substituted conjugated molecules. Application to the study of uracil and fluorouracil. *Theoret. Chim. Acta* **1967,** *8*, 212-22.

131. Judson, R., Genetic algorithms and their use in chemistry. *Reviews in Computational Chemistry* **1997,** *10*, 1-73.

132. Lindberg, J.; Sigurosson, S.; Lowgren, S.; Andersson, H. O.; Sahlberg, C.; Noreen, R.; Fridborg, K.; Zhang, H.; Unge, T., Structural basis for the inhibitory efficacy of efavirenz (DMP-266), MSC194 and PNU142721 towards the HIV-1 RT K103N mutant. *Eur. J. Biochem.* **2002,** *269*, 1670-1677.

133. Ren, J.; Nichols, C.; Bird, L.; Chamberlain, P.; Weaver, K.; Short, S.; Stuart, D. I.; Stammers, D. K., Structural Mechanisms of Drug Resistance for Mutations at Codons 181 and 188 in HIV-1 Reverse Transcriptase and the Improved Resilience of Second Generation Non-nucleoside Inhibitors. *J. Mol. Biol.* **2001,** *312*, 795-805.

134. Schafer, W., Rational design of inhibitors of HIV-1 reverse transcriptase. *Methods and Principles in Medicinal Chemistry* **1998,** *6*, 121-127.

135. Sudbeck, E. A.; Mao, C.; Vig, R.; Venkatachalam, T. K.; Tuel-Ahlgren, L.; Uckun, F. M., Structure-based design of novel dihydroalkoxybenzyloxopyrimidine derivatives as potent non-nucleoside inhibitors of the human immunodeficiency virus reverse transcriptase. *Antimicrob. Agents Chemother.* **1998,** *42*, 3225-33.

136. Zhou, Z.; Madrid, M.; Evanseck, J. D.; Madura, J. D., Effect of a Bound Non-Nucleoside RT Inhibitor on the Dynamics of Wild-Type and Mutant HIV-1 Reverse Transcriptase. *J. Am. Chem. Soc.* **2005,** *127*, 17253-17260.

137. Rodriguez-Barrios, F.; Balzarini, J.; Gago, F., The Molecular Basis of Resilience to the Effect of the Lys103Asn Mutation in Non-Nucleoside

HIV-1 Reverse Transcriptase Inhibitors Studied by Targeted Molecular Dynamics Simulations. *J. Am. Chem. Soc.* **2005,** *127*, 7570-7578.

138. Rodriguez-Barrios, F.; Gago, F., Understanding the Basis of Resistance in the Irksome Lys103Asn HIV-1 Reverse Transcriptase Mutant through Targeted Molecular Dynamics Simulations. *J. Am. Chem. Soc.* **2004,** *126*, 15386-15387.

139. Abramovitch, R. A.; Shinkai, I.; Mavunkel, B. J.; More, K. M.; O'Connor, S.; Ooi, G. H.; Pennington, W. T.; Srinivasan, P. C.; Stowers, J. R., New ring systems from 1,2-benzisothiazole-1,1-dioxides and related compounds. *Tetrahedron* **1996,** *52*, 3339-54.

140. Davis, F. A.; Towson, J. C.; Vashi, D. B.; ThimmaReddy, R.; McCauley, J. P., Jr.; Harakal, M. E.; Gosciniak, D. J., Chemistry of oxaziridines. 13. Synthesis, reactions, and properties of 3-substituted 1,2-benzisothiazole 1,1-dioxide oxides. *J. Org. Chem.* **1990,** *55*, 1254-61.

141. Meadow, J. R.; Reid, E. E., Pseudosaccharin chloride, a reagent for the identification of alcohols. *J. Am. Chem. Soc.* **1943,** *65*, 457-8.

142. Dopp, D.; Lauterfeld, P.; Schneider, M.; Schneider, D.; Henkel, G.; El Sayed Issac, Y. A.; Elghamry, I., Photoisomerization of sultams derived from saccharin; part 4: generation of cyclic sulfine hydroxamic acids. *Synthesis* **2001**, 1228-1235.

143. Mao, J.; Baker, D. C. Preparation of arylsultams as HIV reverse transcriptase inhibitors. 2000-US7892 2000056332, 20000324., 2000.

144. Hagemann, H.; Dulak, M.; Wesolowski, T. A.; Chapuis, C.; Jurczak, J., Comparative infrared, Raman, and natural-bond-orbital analyses of King's sultam. *Helv. Chim. Acta* **2004,** *87*, 1748-1766.

145. Noyori, R.; Hashiguchi, S., Asymmetric Transfer Hydrogenation Catalyzed by Chiral Ruthenium Complexes. *Acc. Chem. Res.* **1997,** *30*, 97-102.

146. Imai, H.; Nishiguchi, T.; Fukuzumi, K., Transfer hydrogenation and transfer hydrogenolysis. IX. Hydrogen transfer from organic compounds to aldehydes and ketones catalyzed by dihydridotetrakis(triphenylphosphine)ruthenium(II). *J. Org. Chem.* **1976,** *41*, 665-71.

147. Mueller, D.; Umbricht, G.; Weber, B.; Pfaltz, A., C2-Symmetric 4,4',5,5'-tetrahydrobi(oxazoles) and 4,4',5,5'-tetrahydro-2,2'-methylenebis[oxazoles] as chiral ligands for enantioselective catalysis. *Helv. Chim. Acta* **1991,** *74*, 232-40.

148. Genet, J. P.; Ratovelomanana-Vidal, V.; Pinel, C., Asymmetric hydrogen transfer reaction of aryl ketones with chiral diphosphine-ruthenium(II) catalysts. *Synlett* **1993**, 478-80.

149. Gamez, P.; Fache, F.; Lemaire, M., Asymmetric catalytic reduction of carbonyl compounds using C2 symmetric diamines as chiral ligands. *Tetrahedron: Asymmetry* **1995,** *6*, 705-18.

150. Evans, D. A.; Nelson, S. G.; Gagne, M. R.; Muci, A. R., A chiral samarium-based catalyst for the asymmetric Meerwein-Ponndorf-Verley reduction. *J. Am. Chem. Soc.* **1993,** *115*, 9800-1.

151. Noyori, R.; Takaya, H., BINAP: an efficient chiral element for asymmetric catalysis. *Acc. Chem. Res.* **1990,** *23*, 345-50.

152. Yang, Q.; Shang, G.; Gao, W.; Deng, J.; Zhang, X., A highly enantioselective, Pd-TangPhos catalyzed hydrogenation of N-tosylimines. *Angewandte Chemie, International Edition* **2006,** *45*, 3832-3835.

153. Bragg, M. T. Structural and spectroscopic studies of transition metal organometallic and coordination complexes with reference to catalysis. 2005.

154. Yamakawa, M.; Ito, H.; Noyori, R., The Metal-Ligand Bifunctional Catalysis: A Theoretical Study on the Ruthenium(II)-Catalyzed Hydrogen Transfer between Alcohols and Carbonyl Compounds. *J. Am. Chem. Soc.* **2000,** *122*, 1466-1478.

155. Yamakawa, M.; Yamada, I.; Noyori, R., CH/p attraction: The origin of enantioselectivity in transfer hydrogenation of aromatic carbonyl compounds catalyzed by chiral h6-arene-ruthenium(II) complexes. *Angewandte Chemie, International Edition* **2001,** *40*, 2818-2821.

V. Appendix

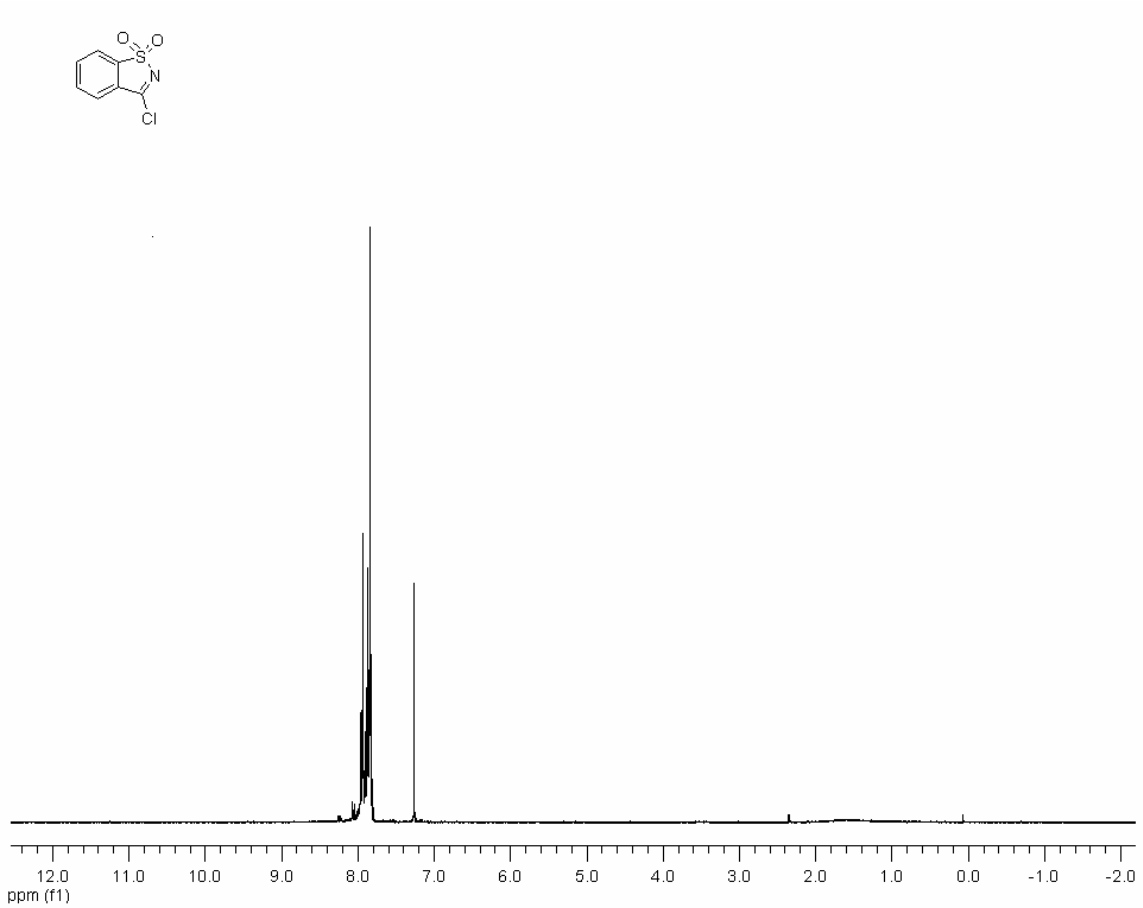

^{1}H NMR of 3-chloro-1.2-benzisothiazole 1.1-dioxide

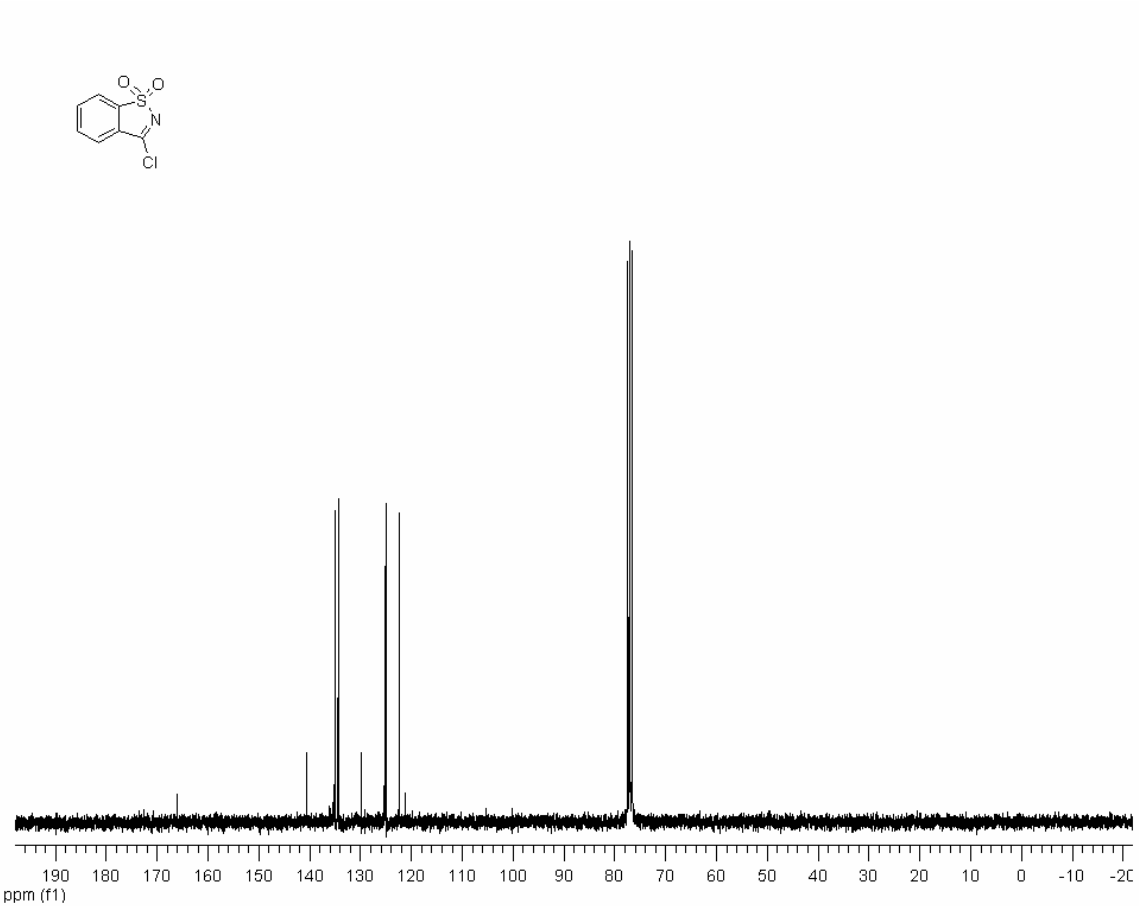

^{13}C NMR of 3-chloro-1,2-benzisothiazole 1,1-dioxide

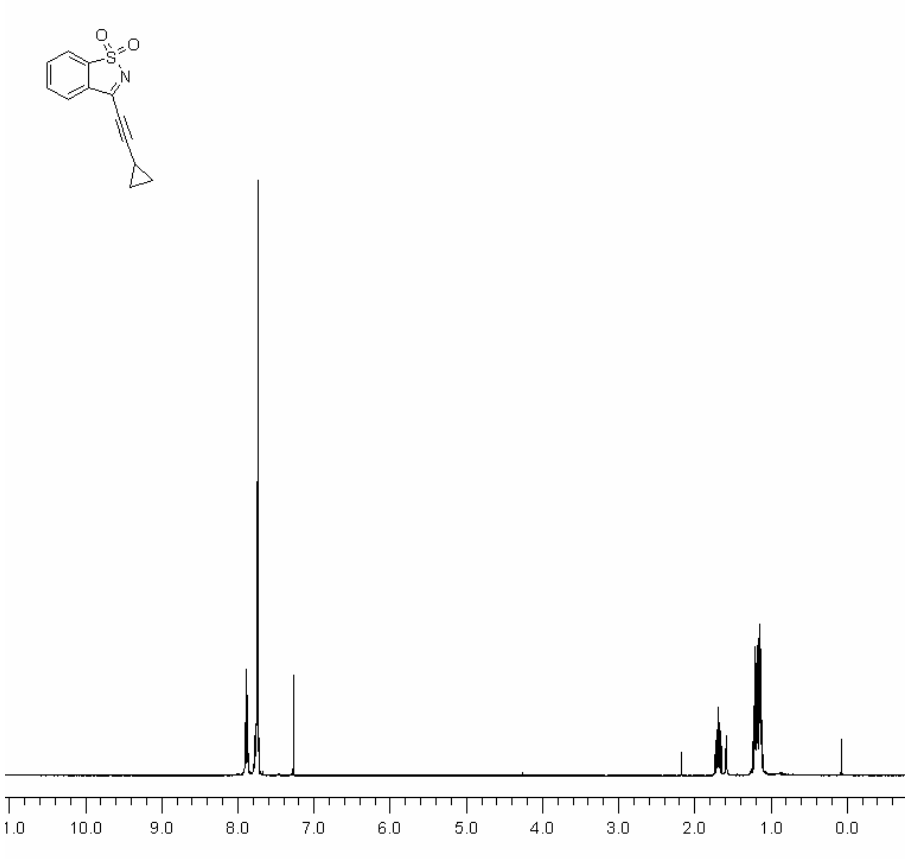

^{1}H NMR of 3-(cyclopropylethynyl)-1,2-benzisothiazole 1,1-dioxide

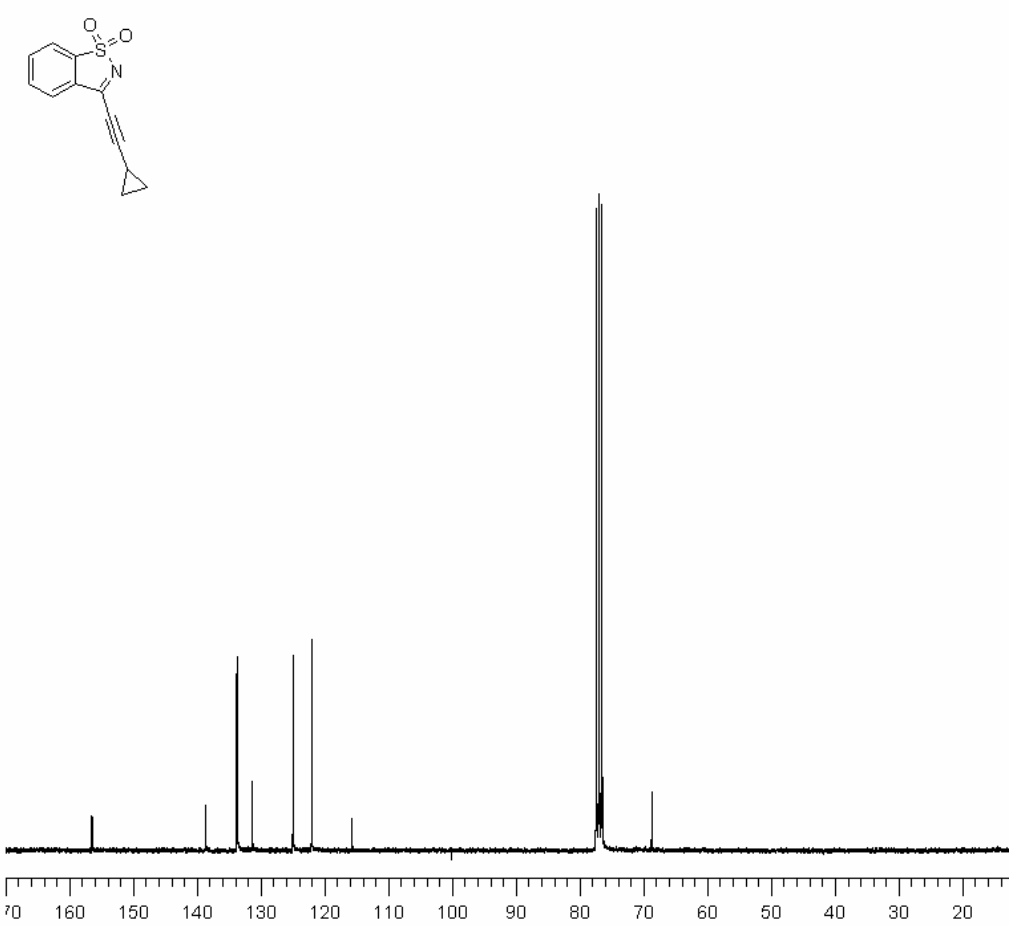

^{13}C NMR of 3-(cyclopropylethynyl)-1,2-benzisothiazole 1,1-dioxide

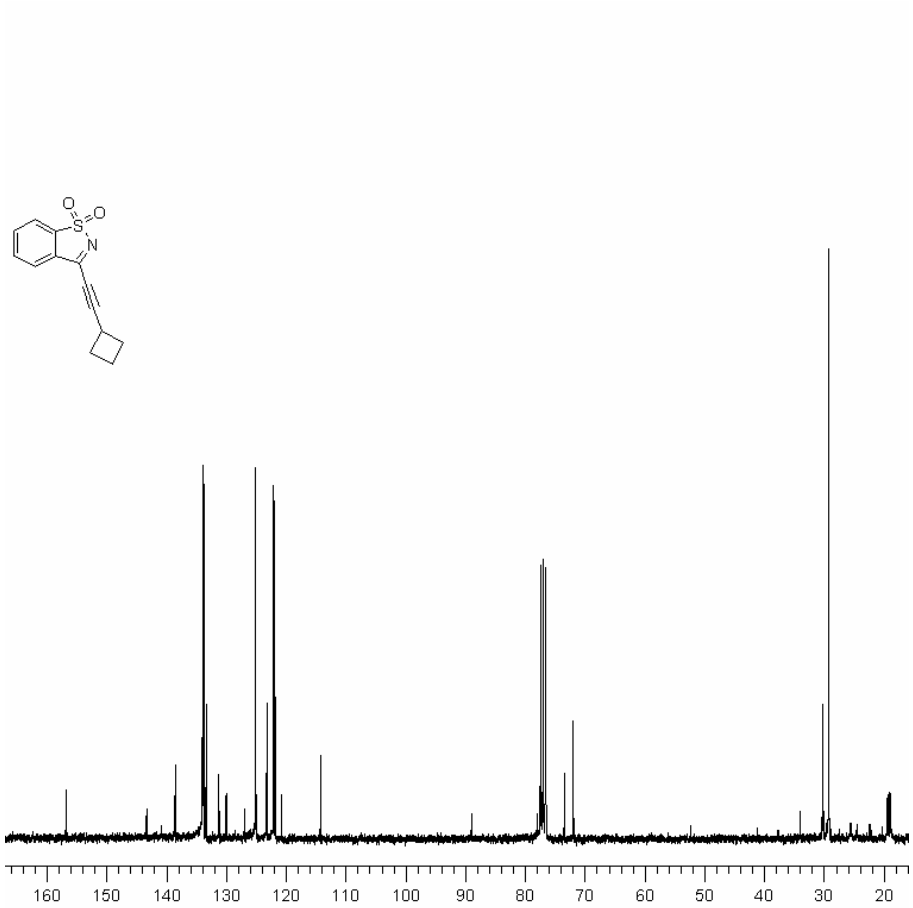

^{13}C NMR of 3-(cyclobutylethynyl)-1,2-benzisothiazole 1,1-dioxide

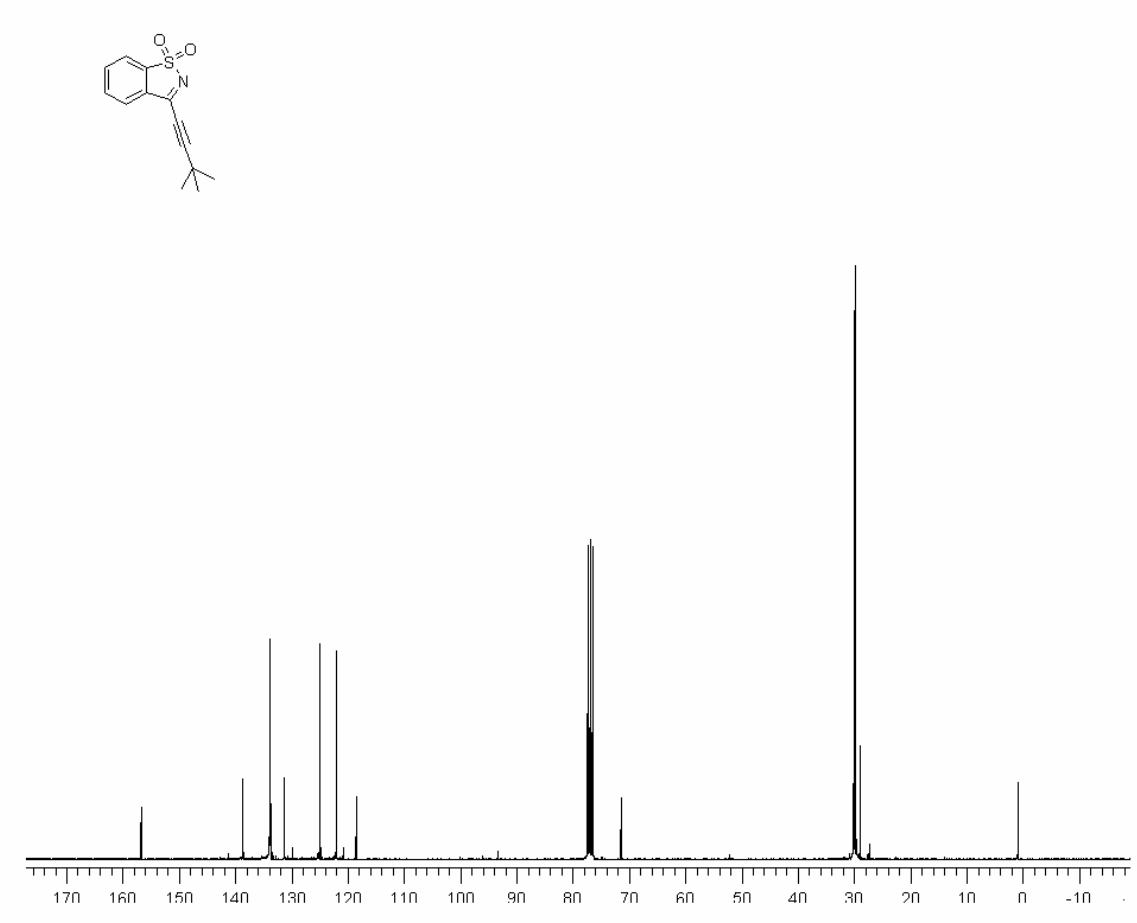

^{13}C NMR of 3-(*tert*-butylethynyl)-1,2-benzisothiazole 1,1-dioxide

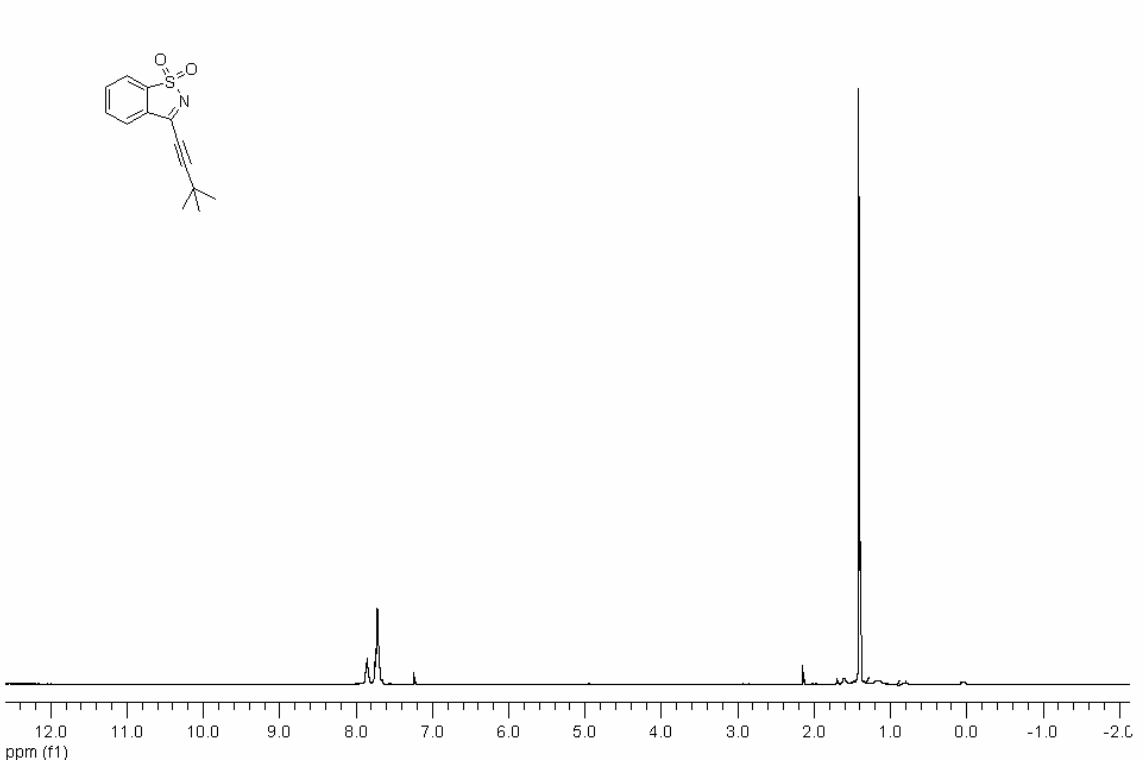

^{1}H NMR of 3-(*tert*-butylethynyl)-1,2-benzisothiazole 1,1-dioxide

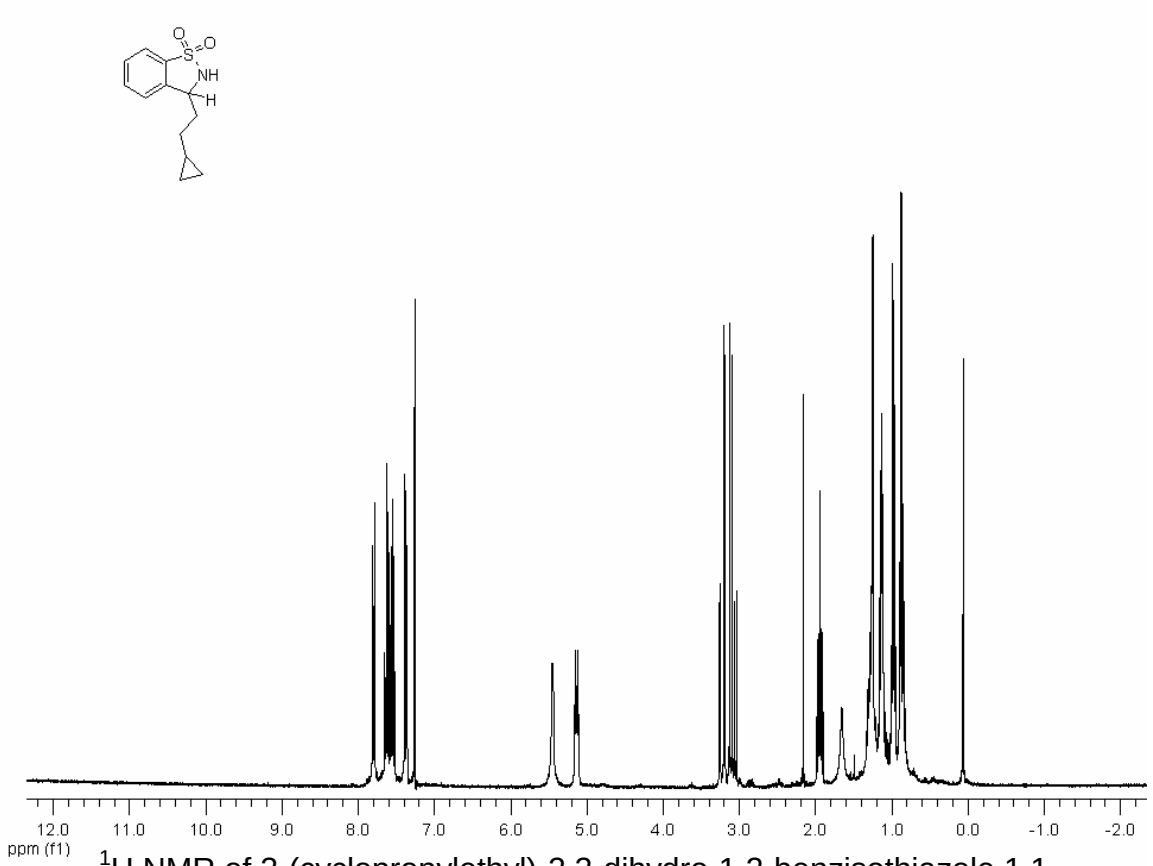

^{1}H NMR of 3-(cyclopropylethyl)-2,3-dihydro-1,2-benzisothiazole 1,1 dioxide

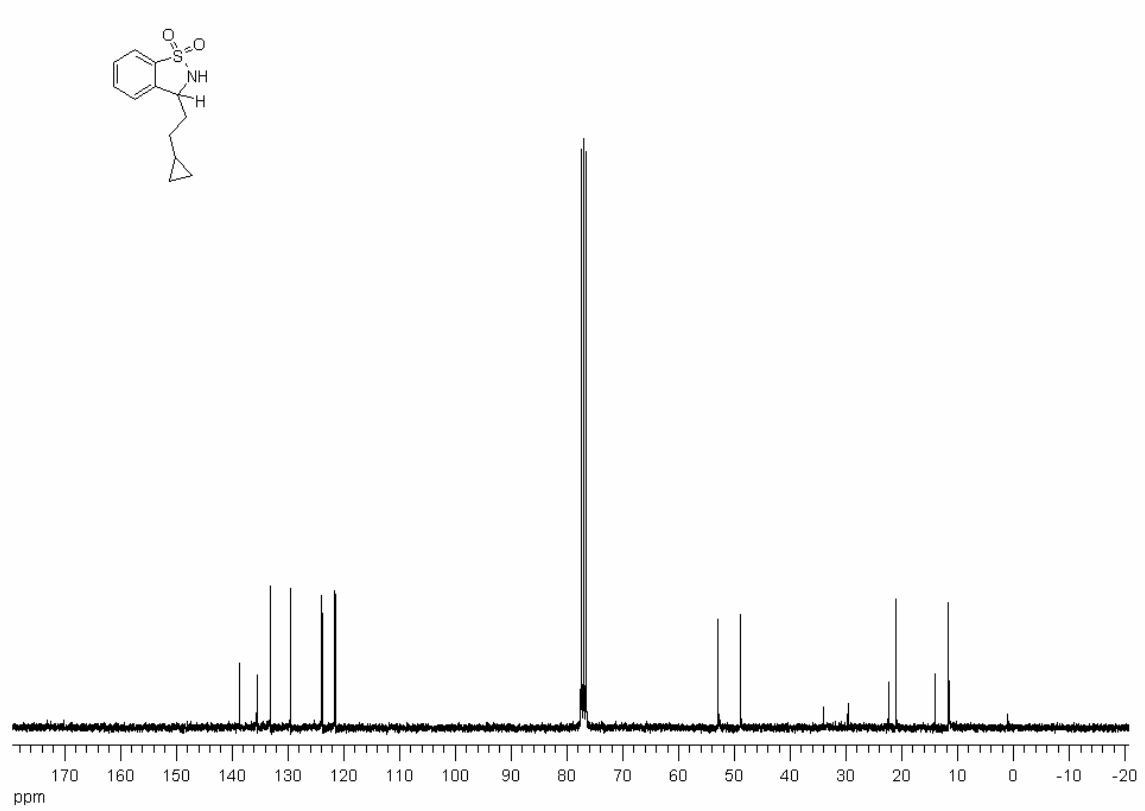

^{13}C NMR of 3-(cyclopropylethyl)-2,3-dihydro-1,2-benzisothiazole 1,1 dioxide

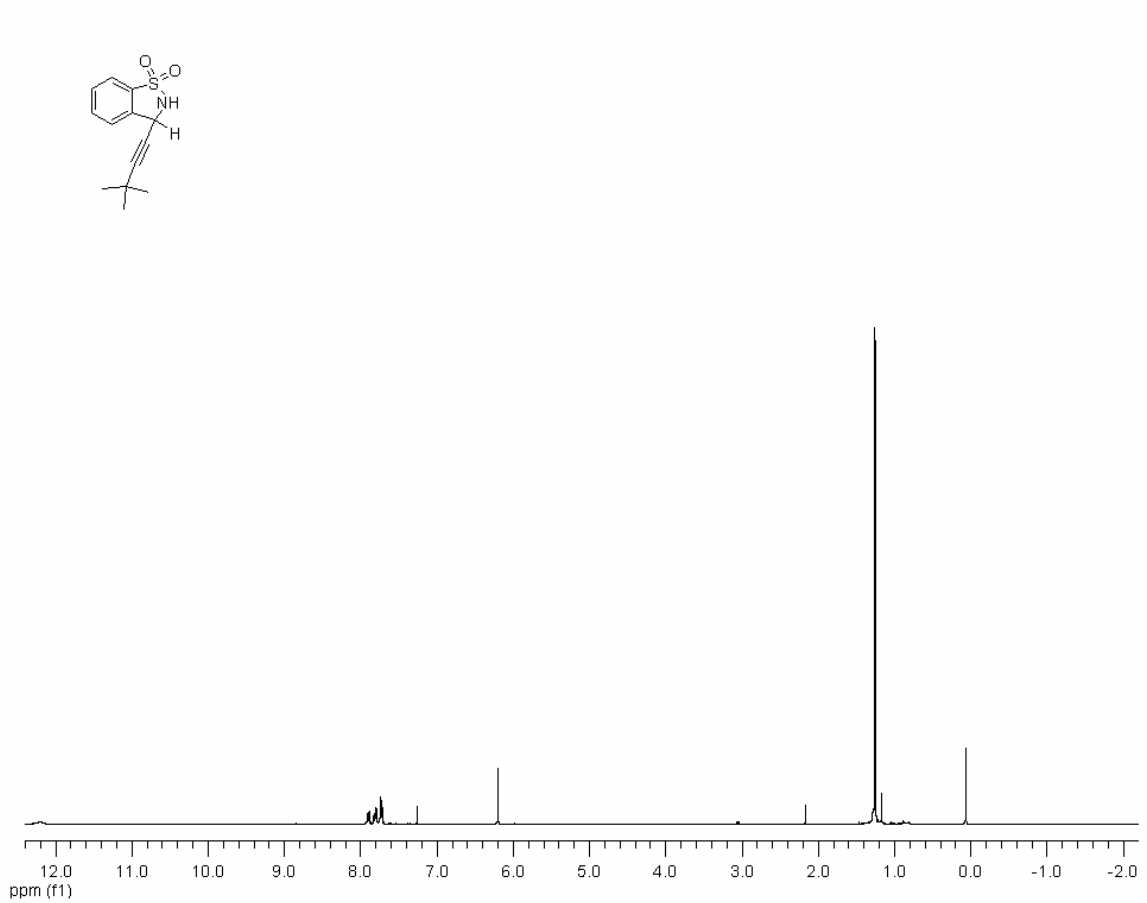

^{1}H NMR of 3-(*tert*-butylethynyl)-2,3-dihydro-1,2-benzisothiazole 1,1 dioxide

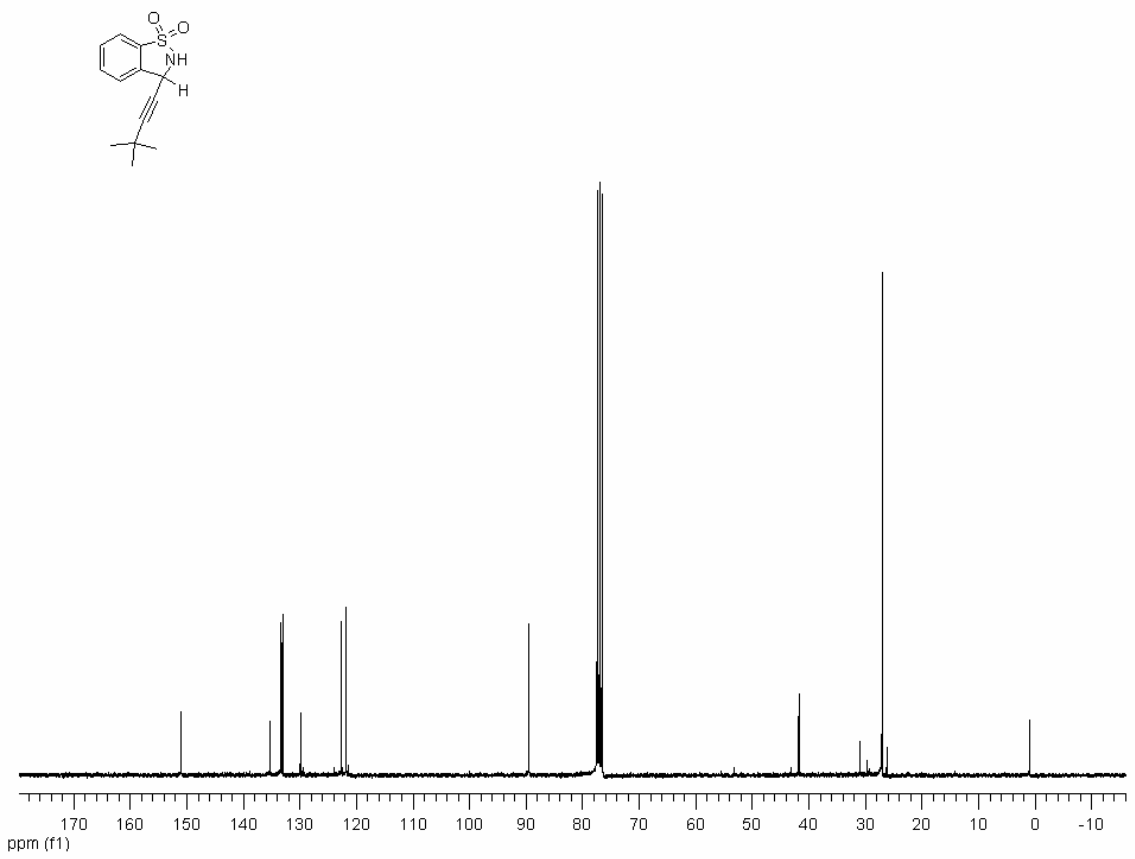

^{13}C NMR of 3-(*tert*-butyl)-2,3-dihydro-1,2-benzisothiazole 1,1 dioxide

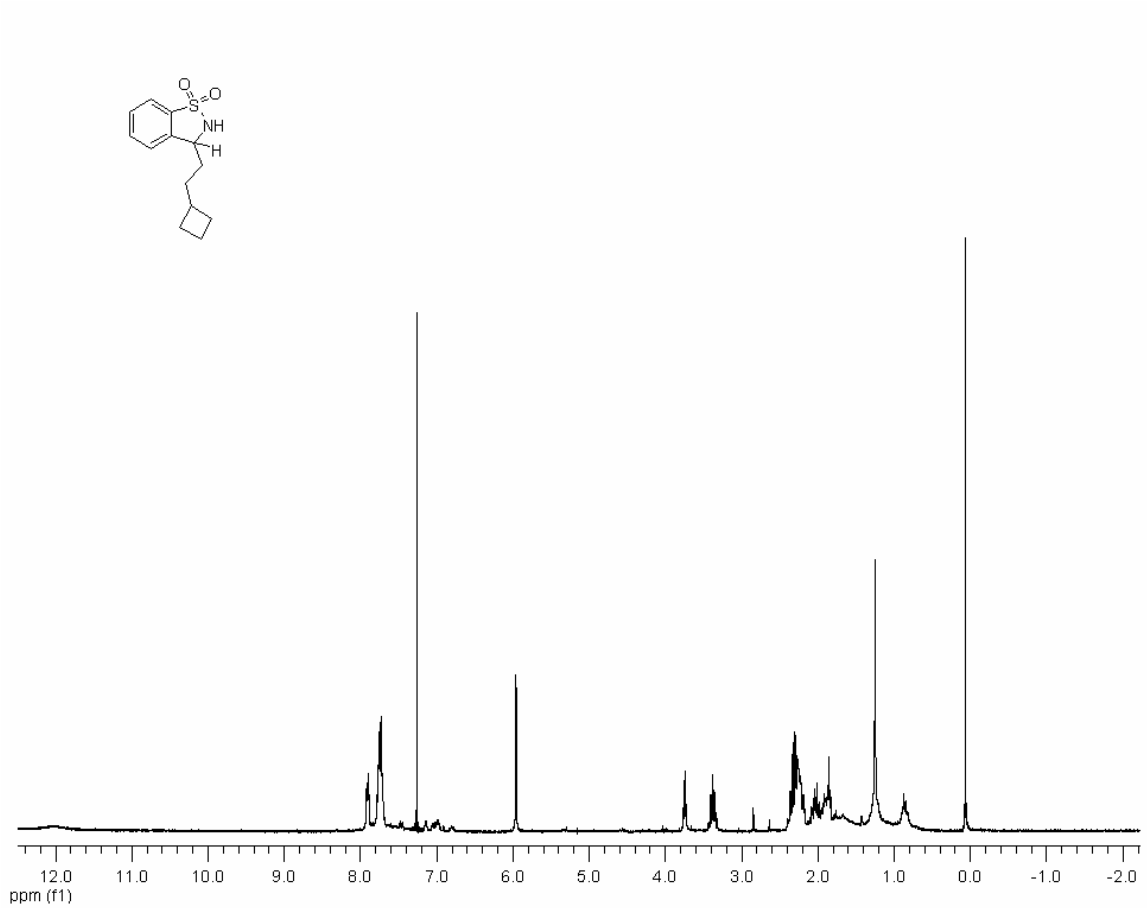

^{1}H NMR of 3-(cyclobutylethyl)-2,3-dihydro-1,2-benzisothiazole 1,1 dioxide

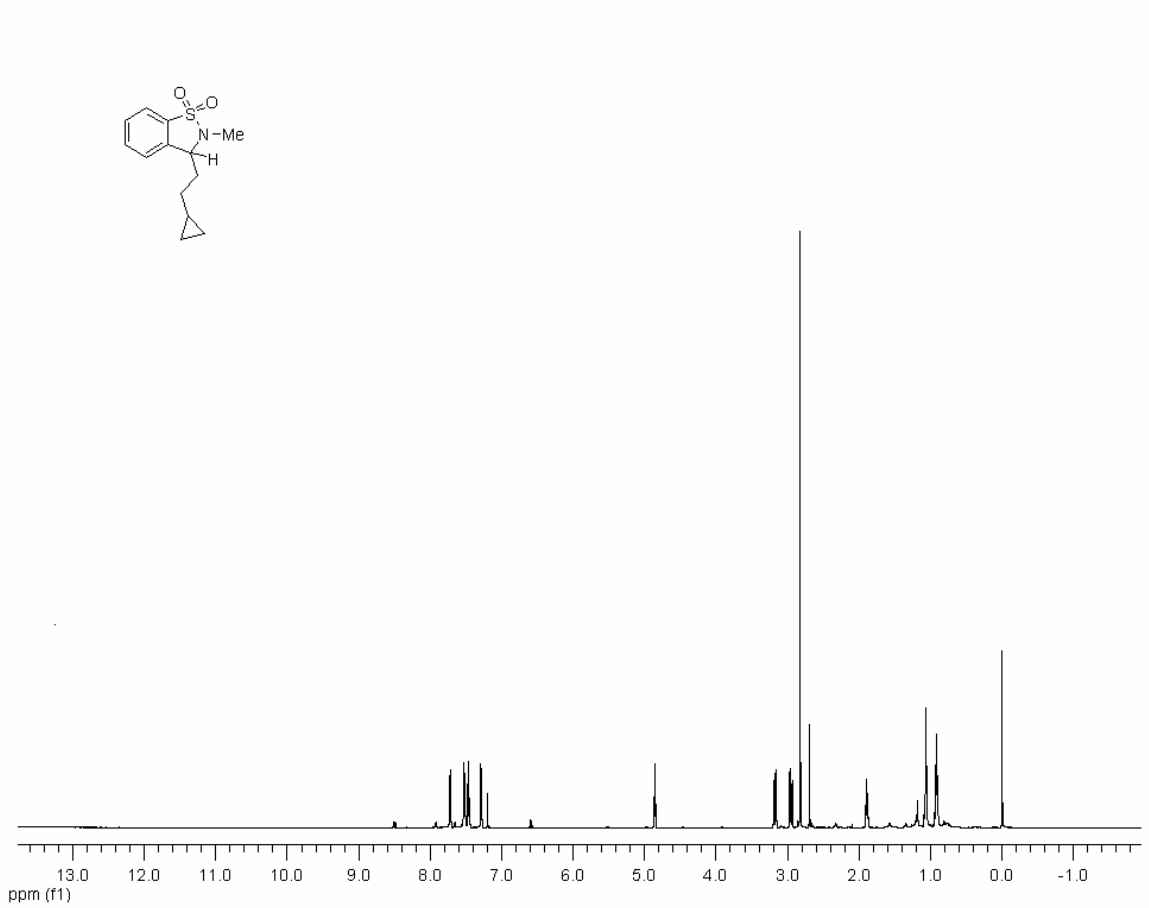

^{1}H NMR of 3-(cyclopropylethyl)-2,3-dihydro-2-methyl-1,2-benzisothiazole 1,1 dioxide

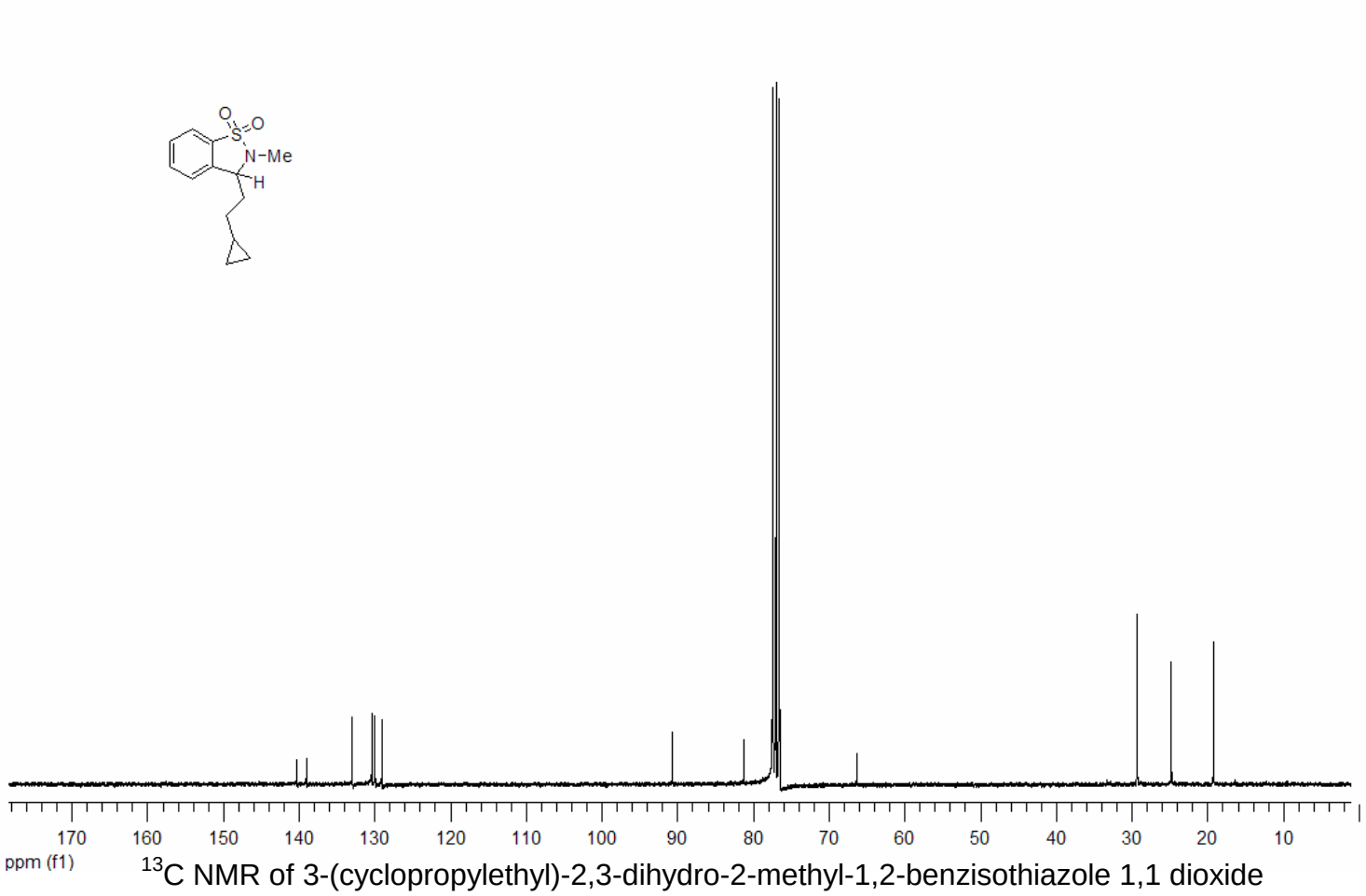

^{13}C NMR of 3-(cyclopropylethyl)-2,3-dihydro-2-methyl-1,2-benzisothiazole 1,1 dioxide

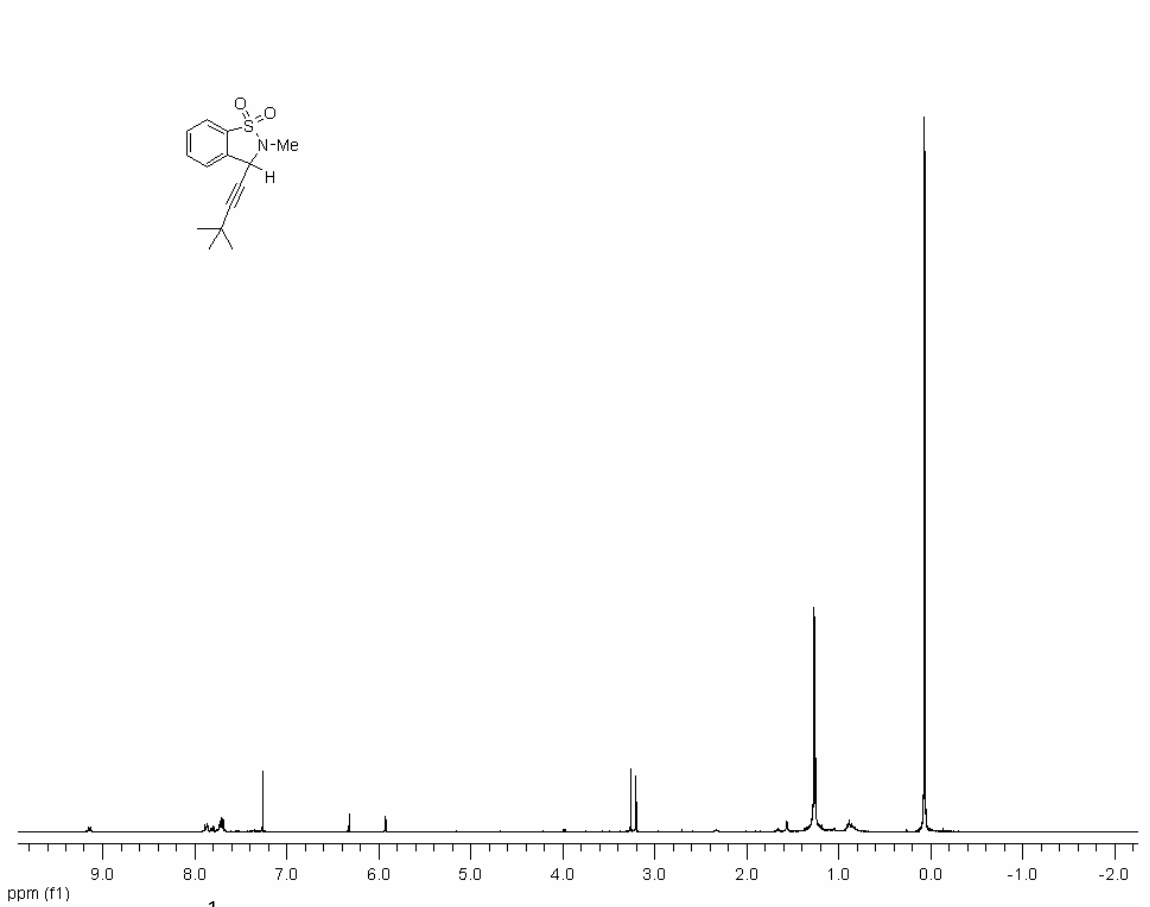

^{1}H NMR of 3-(*tert*-butylethynyl)-2,3-dihydro-2-methyl-1,2-benzisothiazole 1,1 dioxide

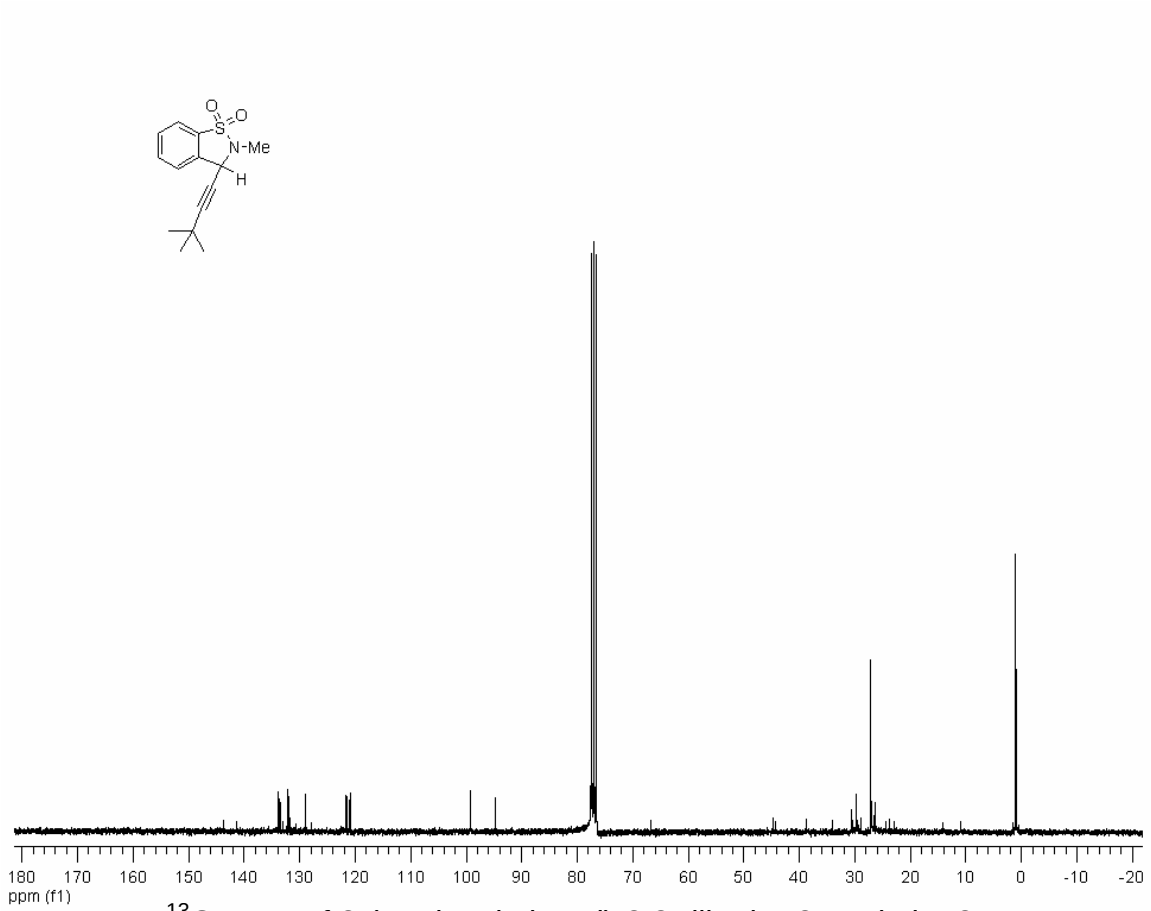

^{13}C NMR of 3-(*tert*-butylethynyl)-2,3-dihydro-2-methyl-1,2-benzisothiazole 1,1 dioxide

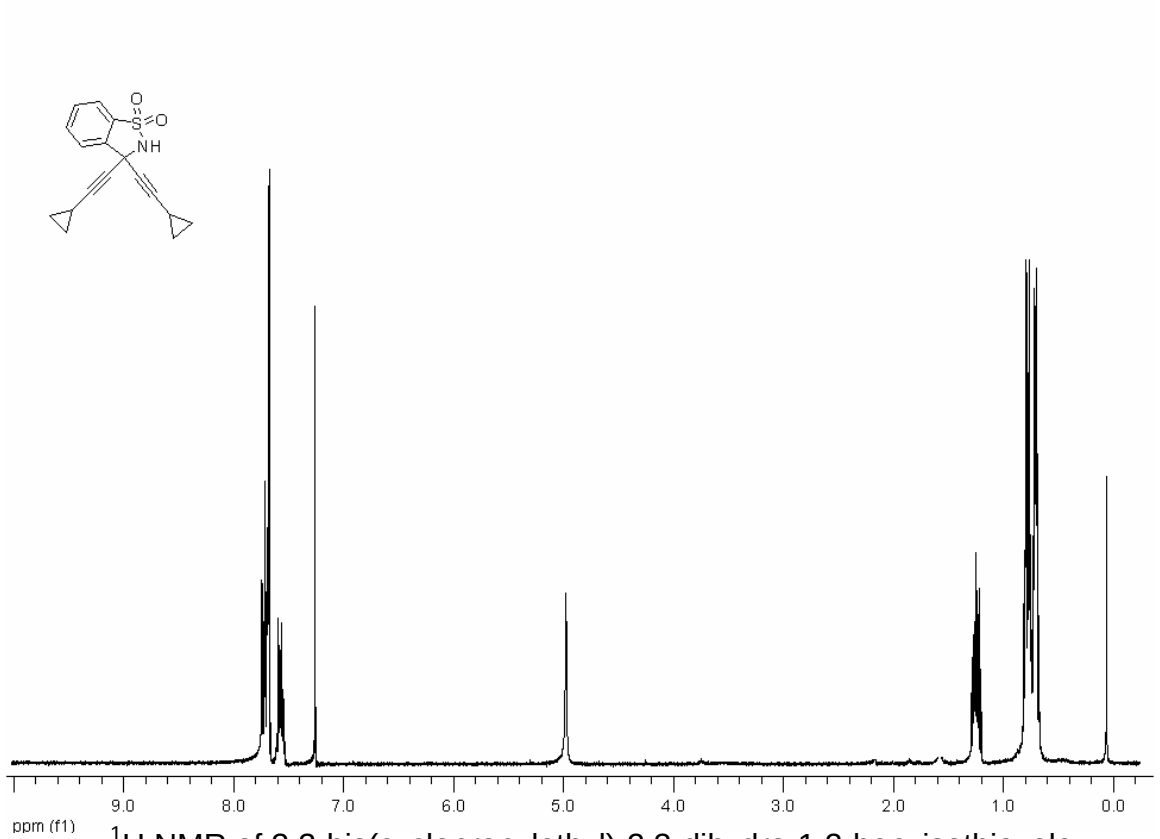

^{1}H NMR of 3,3-bis(cyclopropylethyl)-2,3-dihydro-1,2-benzisothiazole 1,1 dioxide

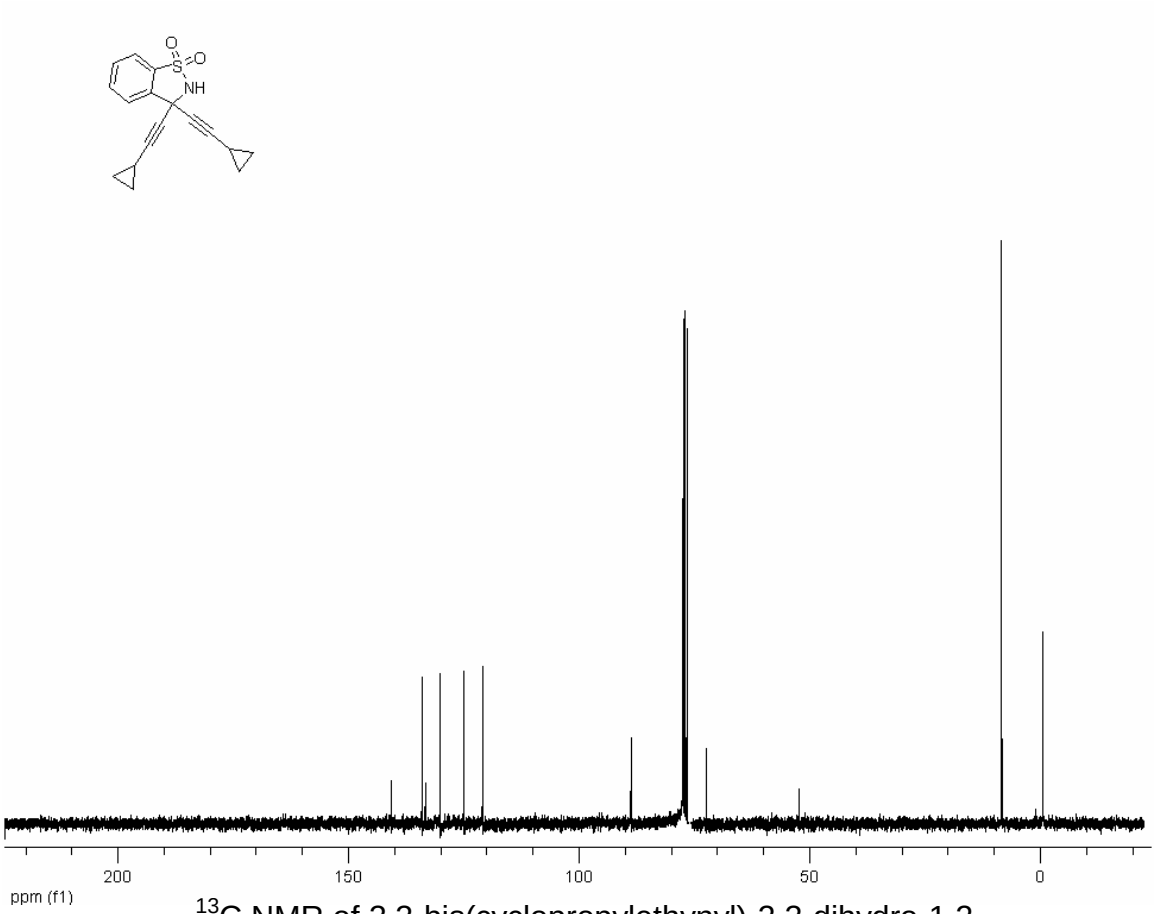

^{13}C NMR of 3,3-bis(cyclopropylethynyl)-2,3-dihydro-1,2-benzisothiazole 1,1 dioxide

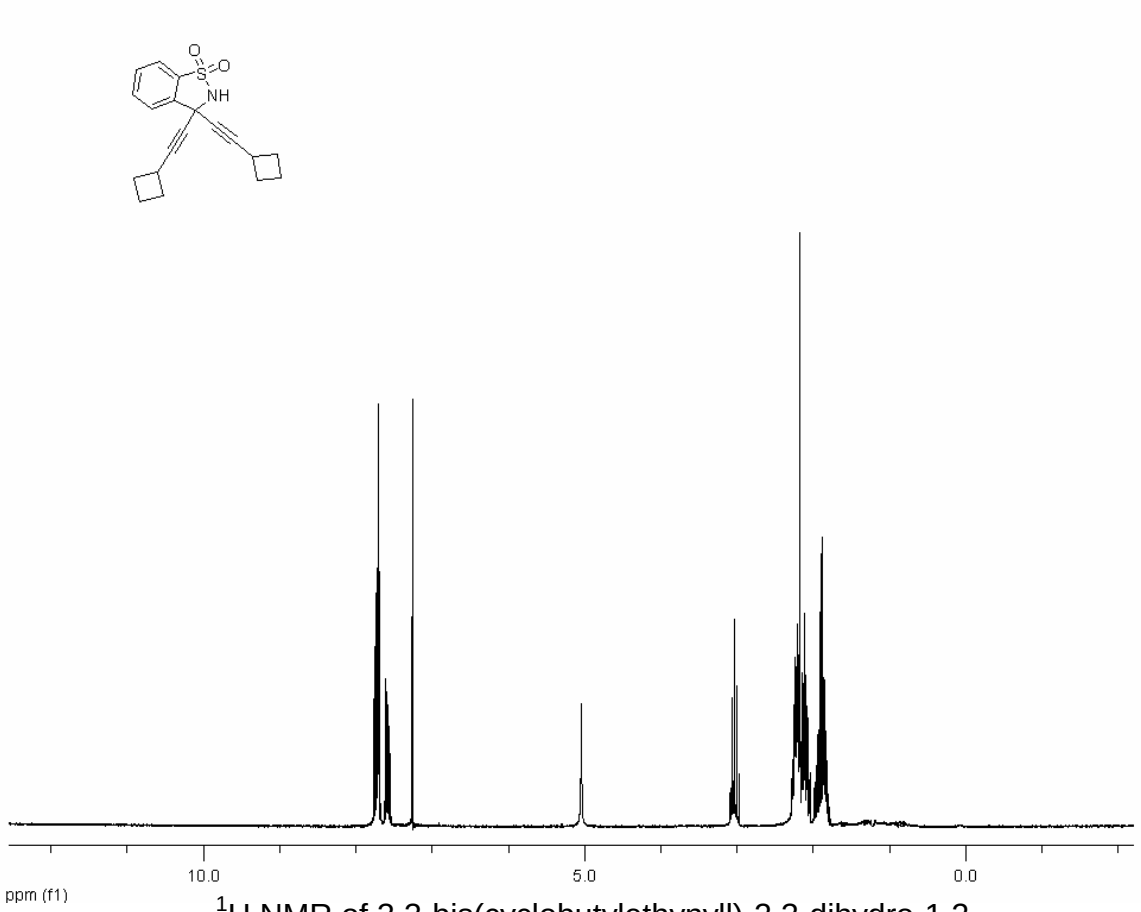

^{1}H NMR of 3,3-bis(cyclobutylethynyll)-2,3-dihydro-1,2-benzisothiazole 1,1 dioxide

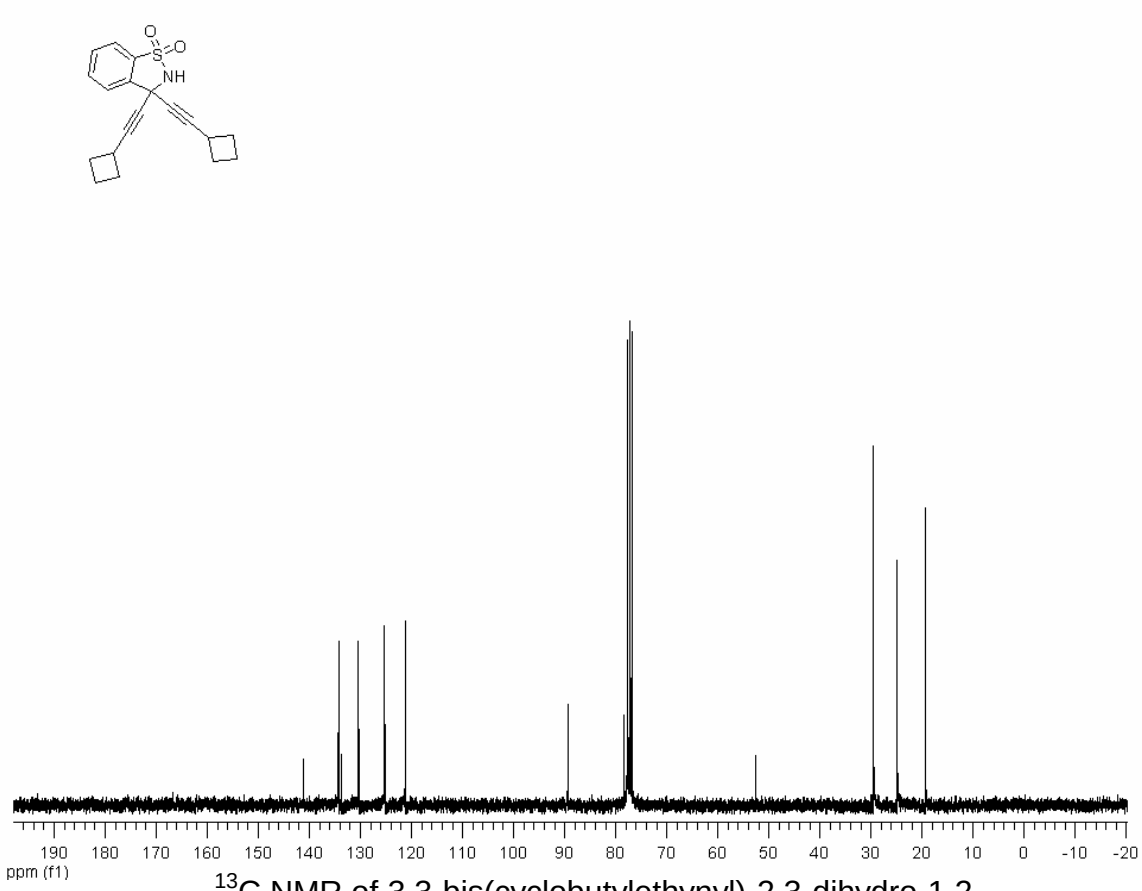

^{13}C NMR of 3,3-bis(cyclobutylethynyl)-2,3-dihydro-1,2-benzisothiazole 1,1 dioxide

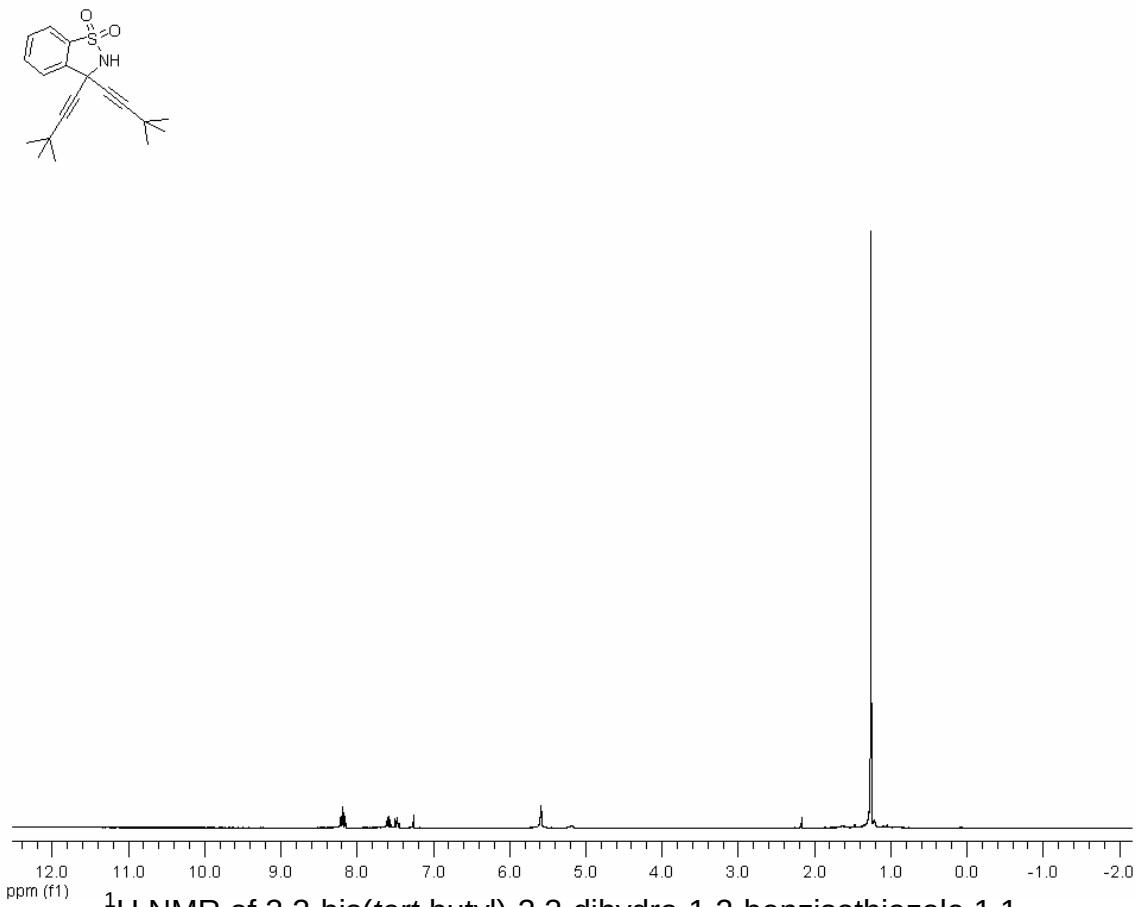

^{1}H NMR of 3,3-bis(*tert*-butyl)-2,3-dihydro-1,2-benzisothiazole 1,1 dioxide

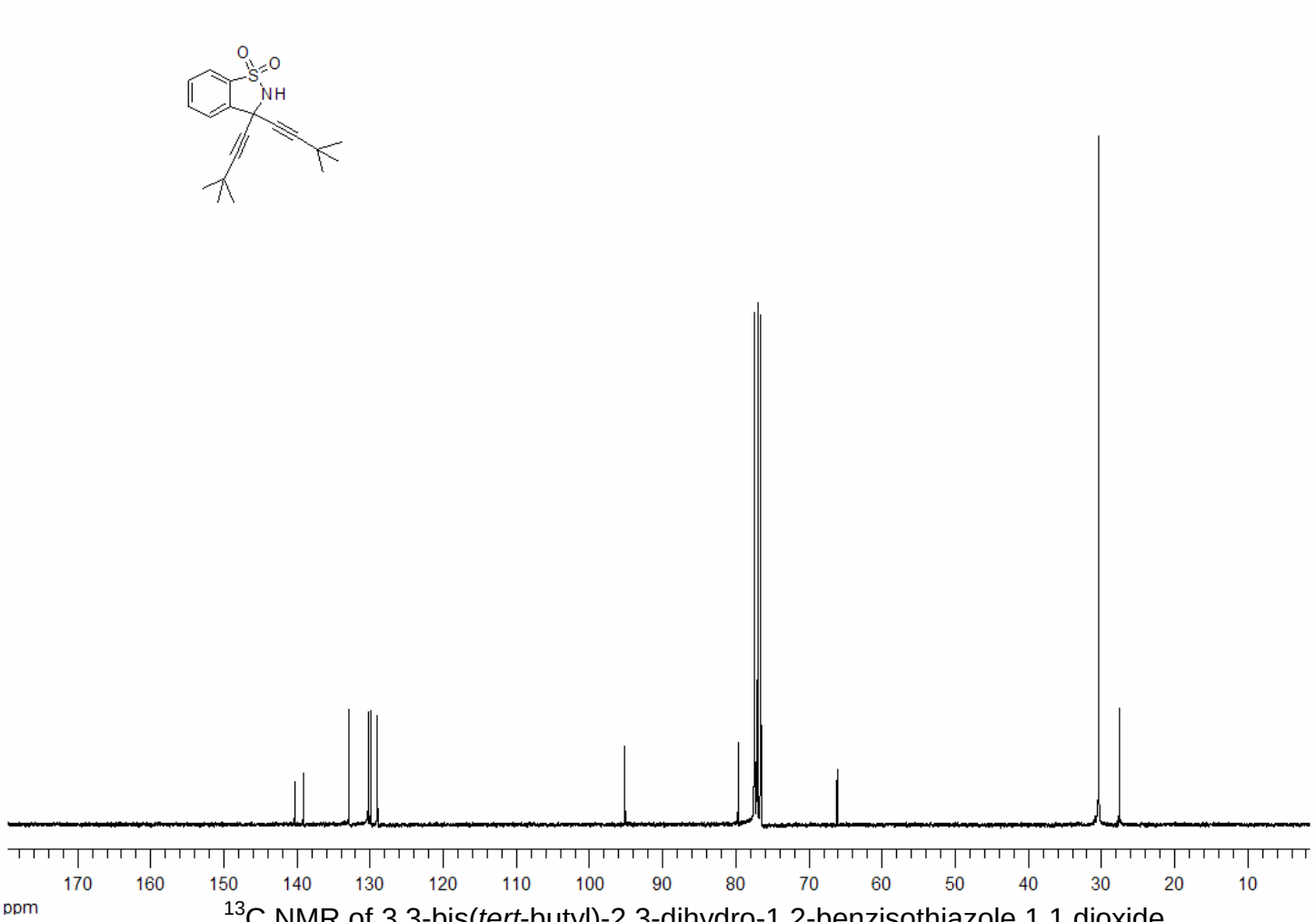

^{13}C NMR of 3,3-bis(*tert*-butyl)-2,3-dihydro-1,2-benzisothiazole 1,1 dioxide

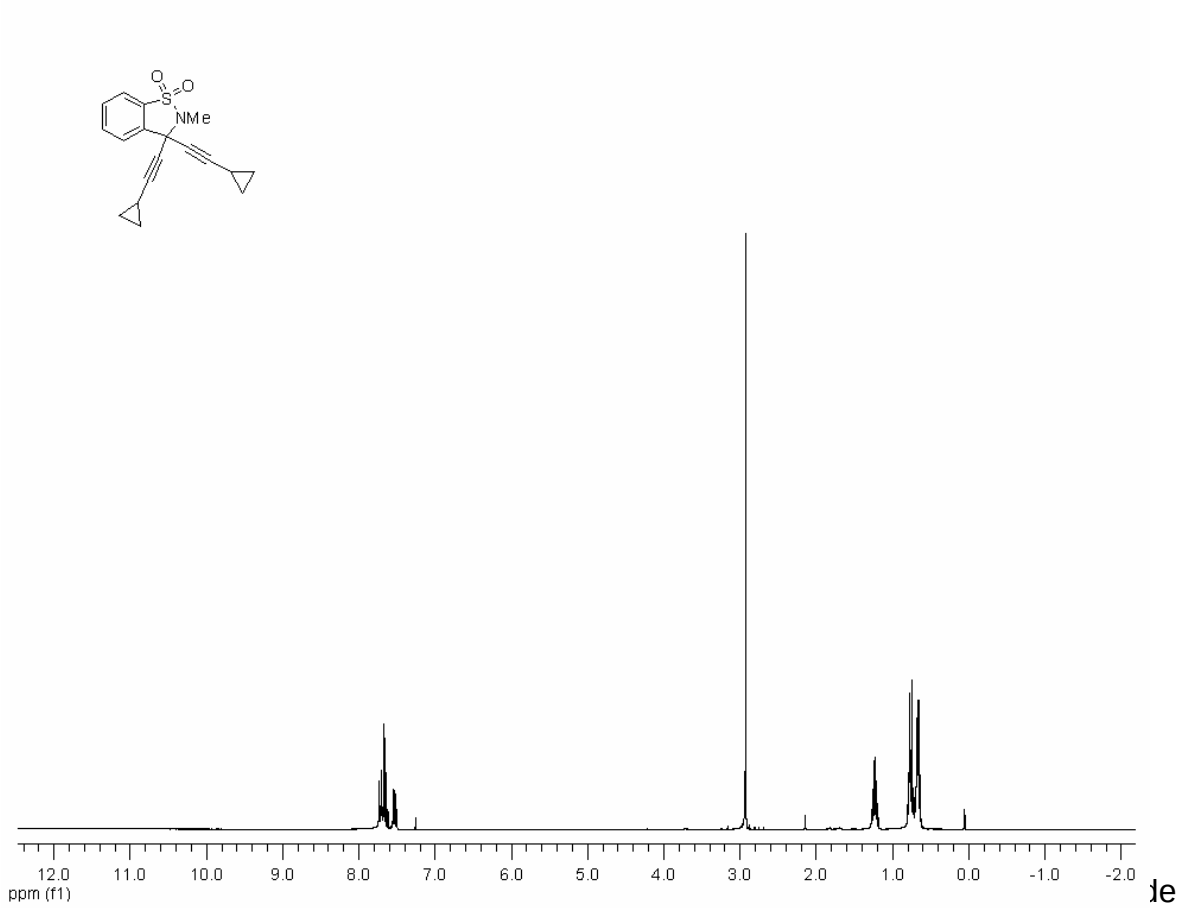

^{1}H NMR of 3,3-bis(cyclopropylethynyl)-2,3-dihydro-2-methyl-1,2-benzisothiazole 1,1 dioxide

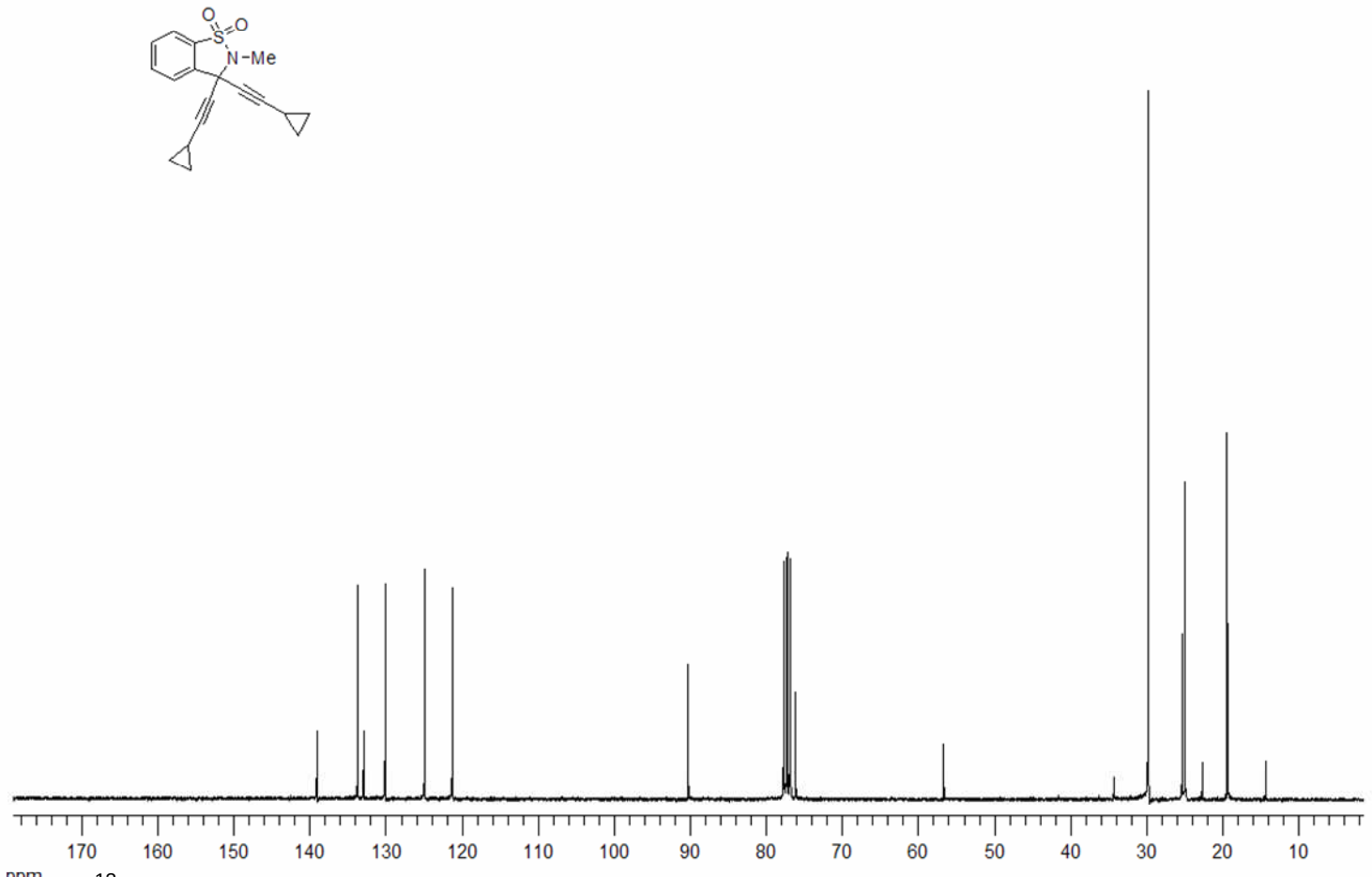

^{13}C NMR of 3,3-bis(cyclopropylethynyl)-2,3-dihydro-2-methyl-1,2-benzisothiazole 1,1 dioxide

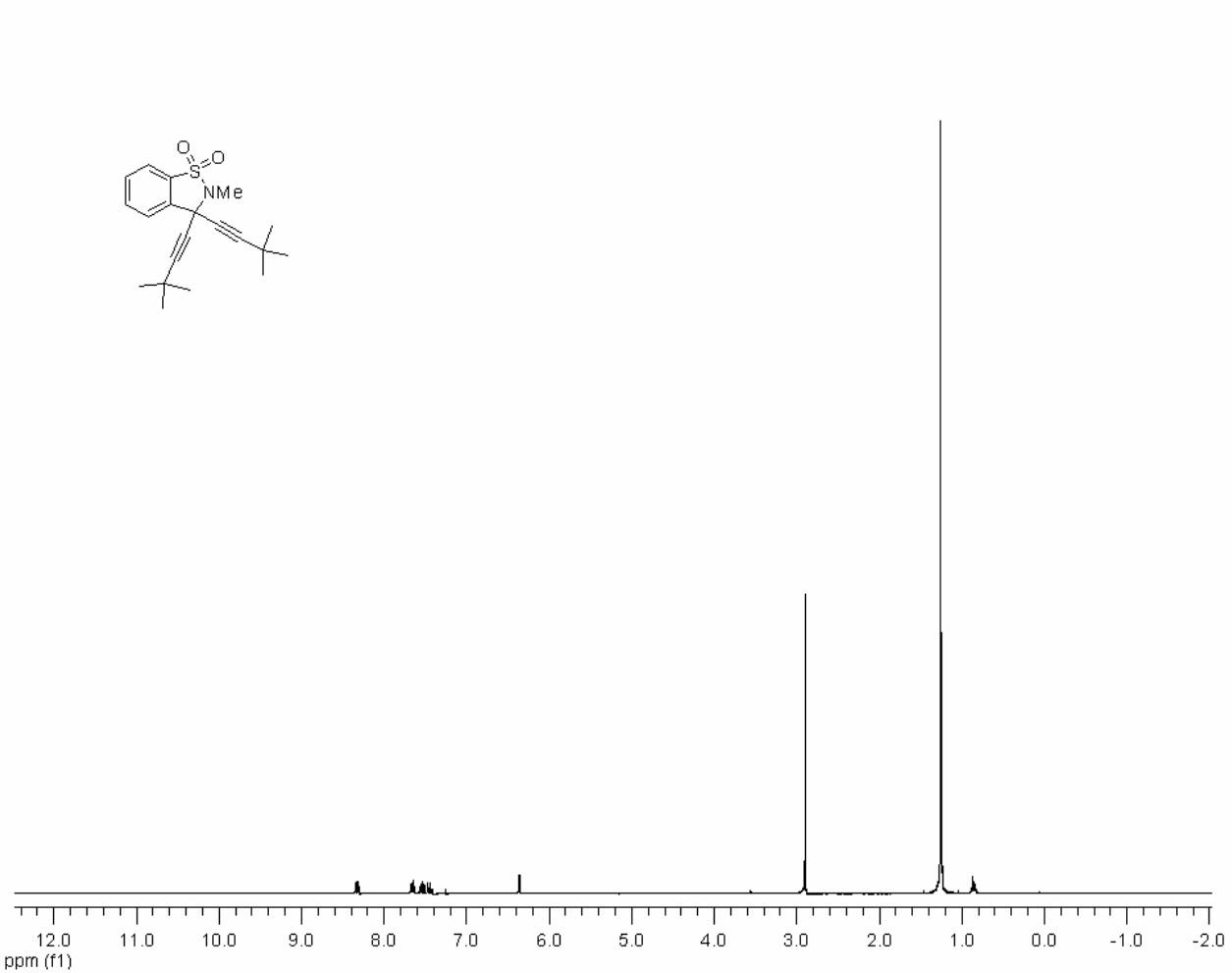

^{1}H NMR of 3,3-bis(tert-butylethynyl)-2,3-dihydro-2-methyl-1,2-benzisothiazole 1,1 dioxide

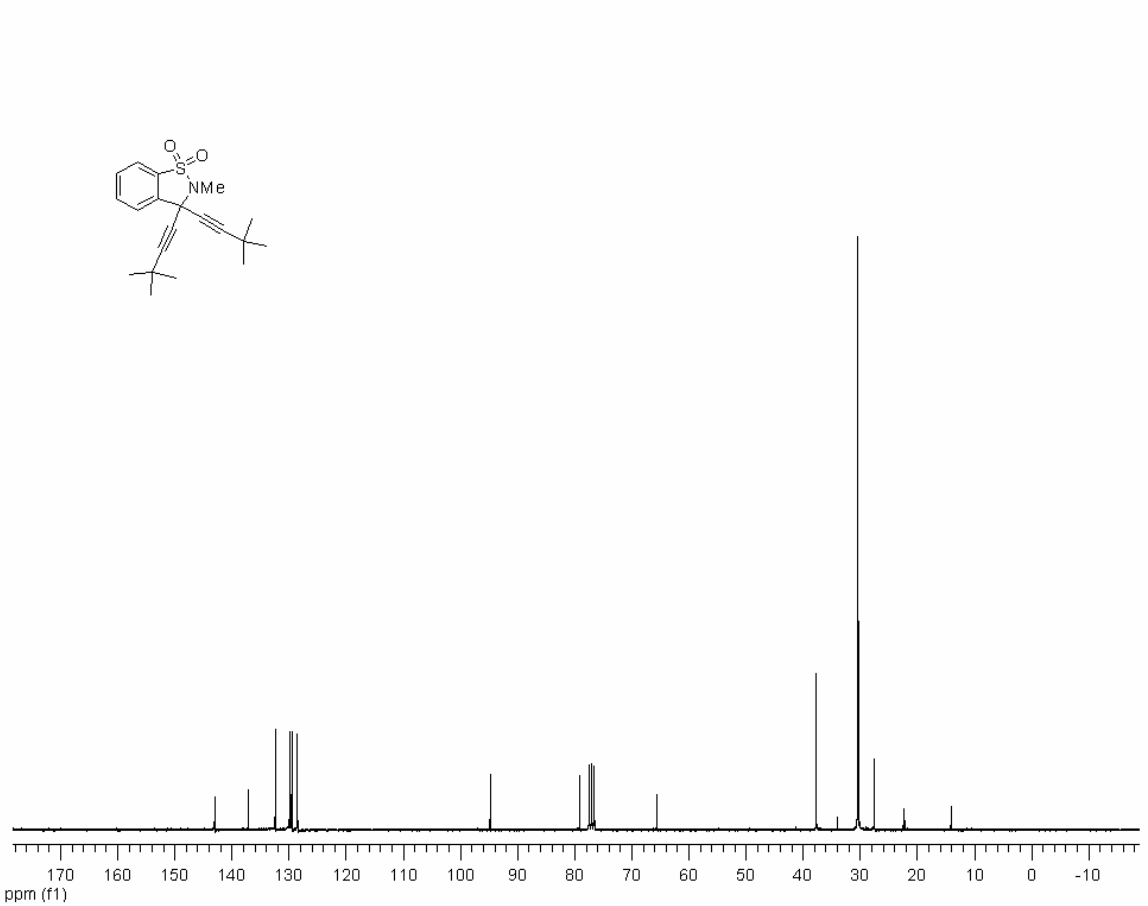

^{1}H NMR of 3,3-bis(*tert*-butylethynyl)-2,3-dihydro-2-methyl-1,2-benzisothiazole 1,1 dioxide

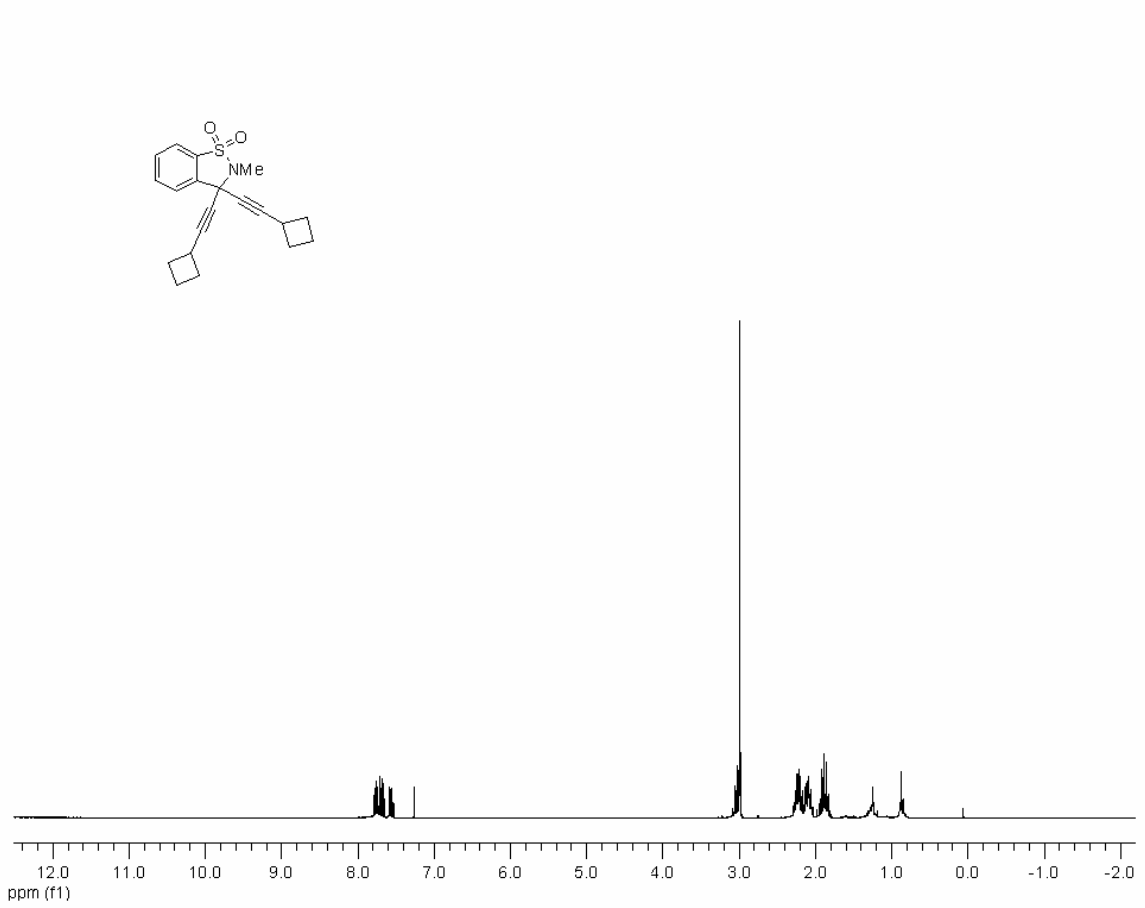

^{1}H NMR of 3,3-bis(cyclobutylethynyl)-2,3-dihydro-2-methyl-1,2-benzisothiazole 1,1 dioxide

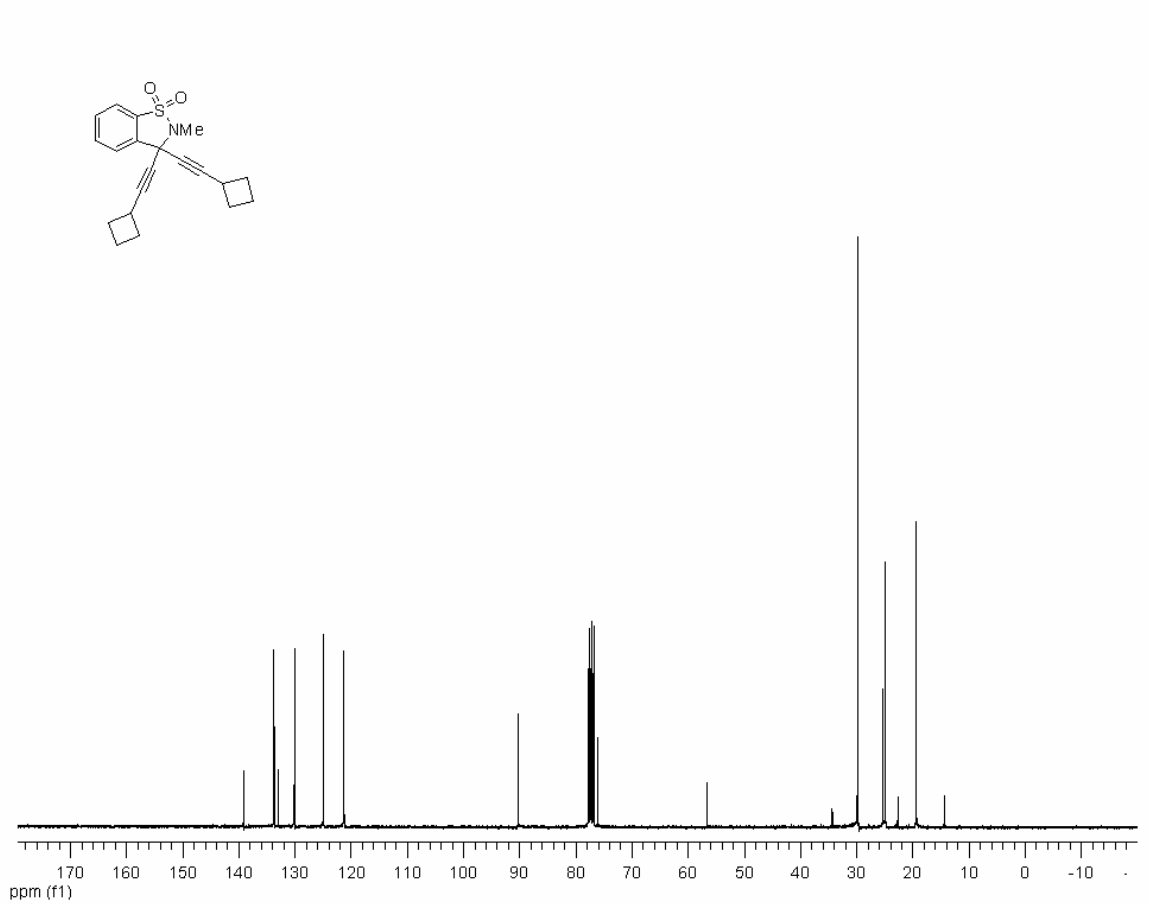

^{13}C NMR of 3,3-bis(cyclobutylethynyl)-2,3-dihydro-2-methyl-1,2-benzisothiazole 1,1 dioxide

VITA

Riyam Kafri was born in Amman Jordan ion October 18, 1978. She attended theRamallah Friends Schools in Ramallah, Palestine where she graduated high school in June 1996. During eleventh grade, Riyam's class covered a large portion of organic chemistry with Mr. Jiryes Abu El-Etham. A year later Riyam was accepted at Earlham College, Richmond, IN for her bachelors studies. She was awarded a full tuition scholarship for four years at Earlham. Riyam's second and most important exposure to organic chemistry came on the hands of Professor Thomas Ruttledge, her organic chemistry professor at Earlham College. Riyam took several classes with Professor Ruttledge including organic courses, toxicology and biochemistry to name a few. She then took a Howard Hughes summer research position with Professor Ruttledge working on natural product isolation and characterization. Upon graduation in May 2000, she enrolled in graduate school at the University of Tennessee, Knoxville and joined Professor David C. Baker's group to work on drug design and discovery of anti HIV reverse transcriptase inhibitors. Riyam completed the doctorate requirement in December 2006 and officially received her diploma in May 2007.